การศึกษาคุณลักษณะของไอออนออกโซเนียม (H_3O^+) ที่ซอลเวตในสารละลายน้ำ โดยการจำลองพลวัตเชิงโมเลกุลที่ผสมผสานกลศาสตร์ควอนตัมและกลศาสตร์โมเลกุล

นายธนวัชร์ สมตัว

วิทยานิพนธ์นี้เป็นส่วนหนึ่งของการศึกษาตามหลักสูตรปริญญาวิทยาศาสตรดุษฎีบัณฑิต
สาขาวิชาเคมี
มหาวิทยาลัยเทคโนโลยีสุรนารี
ปีการศึกษา 2554

CHARACTERISTICS OF H_3O^+ SOLVATED IN AQUEOUS SOLUTION: A COMBINED QM/MM MD SIMULATIONS STUDY

Thanawat Somtua

A Thesis Submitted in Partial Fulfillment of the Requirements for the

Degree of Doctor of Philosophy in Chemistry

Suranaree University of Technology

Academic Year 2011

CHARACTERISTICS OF H_3O^+ SOLVATED IN AQUEOUS SOLUTION: A COMBINED QM/MM MD SIMULATIONS STUDY

Suranaree University of Technology has approved this thesis submitted in partial fulfillment of the requirements for the Degree of Doctor of Philosophy.

Thesis Examining Committee

_____
(Asst. Prof. Dr. Kunwadee Rangsriwatananon)
Chairperson

_____
(Assoc. Prof. Dr. Anan Tongraar)
Member (Thesis Advisor)

_____
(Prof. Dr. Kritsana Sagarik)
Member

_____
(Asst. Prof. Dr. Viwat Vchirawongkwin)
Member

_____
(Assoc. Prof. Dr. Albert Schulte)
Member

_____	_____
(Prof. Dr. Sukit Limpijumnong)	(Assoc. Prof. Dr. Prapun Manyum)
Vice Rector for Academic Affairs	Dean of Institute of Science

ธนวัชร์ สมตัว : การศึกษาคุณลักษณะของไอออนออกโซเนียม (H_3O^+) ที่ซอลเวตในสารละลายน้ำ โดยการจำลองพลวัตเชิงโมเลกุลที่ผสมผสานกลศาสตร์ควอนตัมและกลศาสตร์โมเลกุล (CHARACTERISTICS OF H_3O^+ SOLVATED IN AQUEOUS SOLUTION: A COMBINED QM/MM MD SIMULATIONS STUDY)
อาจารย์ที่ปรึกษา : รองศาสตราจารย์ ดร.อนันต์ ทองระอา, 121 หน้า.

งานวิจัยนี้ได้ทำการศึกษาสมบัติเชิงโครงสร้างและเชิงพลวัตของไอออนออกโซเนียม (H_3O^+) ที่ซอลเวตอยู่ในสารละลายน้ำ โดยในส่วนแรก ได้ทำการจำลองพลวัตเชิงโมเลกุลที่ผสมผสานกลศาสตร์ควอนตัมและกลศาสตร์โมเลกุล (QM/MM MD) 2 แบบ ได้แก่การจำลอง B3LYP/MM และ MP2/MM เพื่อศึกษาอิทธิพลจากผลของสหสัมพันธ์อิเล็กตรอน (Electron Correlation) ที่มีต่อโครงสร้างและพลวัตของออกโซเนียมไฮเดรต ซึ่งเมื่อเปรียบเทียบกับข้อมูลที่ได้จากการจำลอง HF/MM ที่ได้รับการตีพิมพ์ไปแล้ว พบว่า ผลที่ได้จากการจำลอง B3LYP/MM และ MP2/MM แสดงให้เห็นว่า พันธะไฮโดรเจนระหว่างไอออนออกโซเนียมกับน้ำมีความแข็งแรงมากขึ้น ซึ่งส่งผลให้โครงสร้างออกโซเนียมไฮเดรตยึดเหนี่ยวกันแข็งแรงมากขึ้นด้วย อย่างไรก็ตาม ในส่วนของการจำลอง B3LYP/MM นั้น แม้ว่าจะให้รายละเอียดเกี่ยวกับโครงสร้างที่ใกล้เคียงกับข้อมูลที่ได้จากการจำลอง MP2/MM ก็ตาม ได้ให้รายละเอียดเกี่ยวกับสมบัติเชิงพลวัตที่ช้าผิดธรรมชาติของน้ำในซอลเวชันชั้นแรก ซึ่งอธิบายได้ว่า เป็นผลจากการเกิดสารเชิงซ้อนซุนเดล (Zundel complex, $H_5O_2^+$) ที่มีช่วงชีวิตที่ค่อนข้างนาน นอกจากนี้แล้ว สืบเนื่องจากการที่เทคนิคการจำลองพลวัตเชิงโมเลกุลที่ผสมผสานกลศาสตร์ควอนตัมและกลศาสตร์โมเลกุลแบบดั้งเดิมนั้น มีข้อจำกัดบางประการ งานวิจัยในส่วนที่สองจึงได้ดำเนินการจำลองพลวัตเชิงโมเลกุลที่ผสมผสานกลศาสตร์ควอนตัมและกลศาสตร์โมเลกุลบนพื้นฐานของวิธีโอเนียม-เอ็กซ์เอสด้วย โดยมีวัตถุประสงค์เพื่อศึกษาประสิทธิภาพและความน่าเชื่อถือของเทคนิคการจำลองแบบดั้งเดิมดังกล่าว โดยในส่วนของกลศาสตร์ควอนตัมจะใช้การคำนวณในระดับ HF เท่านั้น (เนื่องจากใช้เวลานาน) ผลการเปรียบเทียบ พบว่า การจำลองพลวัตเชิงโมเลกุลที่ผสมผสานกลศาสตร์ควอนตัมและกลศาสตร์โมเลกุลบนพื้นฐานของวิธีโอเนียม-เอ็กซ์เอสให้ผลการศึกษาที่แตกต่างจากผลที่ได้จากการจำลองแบบดั้งเดิมอย่างมีนัยสำคัญ โดยเฉพาะอย่างยิ่ง พบว่า พันธะไฮโดรเจนระหว่างไอออนออกโซเนียมกับน้ำในซอลเวชันชั้นแรกจะอ่อนกว่าและยึดกันอย่างหลวมๆ (เปรียบเทียบกับผลการศึกษาที่ได้จากการจำลองโดยวิธีแบบดั้งเดิม) อย่างไรก็ตาม ในประเด็นนี้ เนื่องจากผลของสหสัมพันธ์อิเล็กตรอนมีผลต่อสมบัติเชิงโครงสร้างและเชิงพลวัตของระบบที่ศึกษา ดังนั้น จึงเสนอแนะว่า การจำลองพลวัตเชิงโมเลกุลที่ผสมผสานกลศาสตร์ควอนตัมและกลศาสตร์โมเลกุล

บนพื้นฐานของวิธีโอเนียม-เอ็กซ์เอสนั้น ควรจะดำเนินการควบคู่กับการคำนวณกลศาสตร์ควอนตัมที่รวมผลของสหสัมพันธ์อิเล็กตรอนเข้าไปด้วย (เช่น วิธี MP2) เพื่อให้ได้ผลการจำลองที่มีความถูกต้องน่าเชื่อถือมากขึ้น

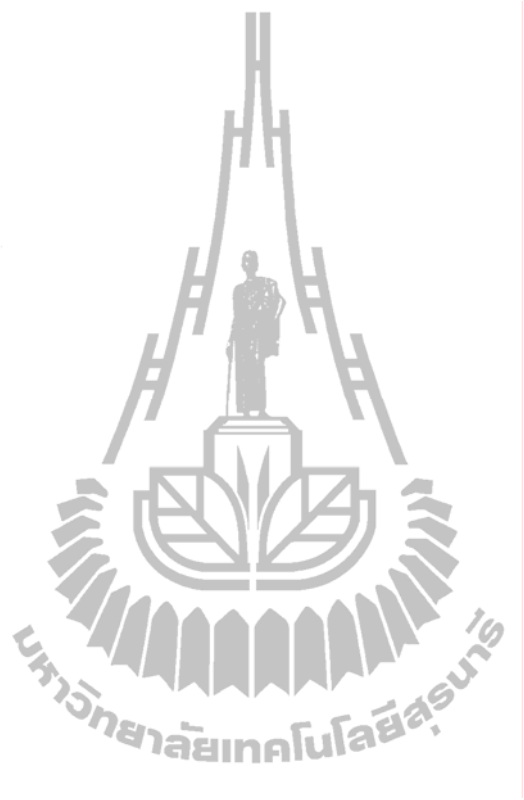

สาขาวิชาเคมี ลายมือชื่อนักศึกษา_____

ปีการศึกษา 2554 ลายมือชื่ออาจารย์ที่ปรึกษา_____

THANAWAT SOMTUA : CHARACTERISTICS OF H_3O^+ SOLVATED IN AQUEOUS SOLUTION: A COMBINED QM/MM MD SIMULATIONS STUDY. THESIS ADVISOR : ASSOC. PROF. ANAN TONGRAAR, Ph.D. 121 PP.

OXONIUM/HYDROGEN BOND /PROTON TRANSFER/ONIOM-XS

The solvation structure and dynamics of H_3O^+ in aqueous solution have been investigated by means of combined quantum mechanics/molecular mechanics (QM/MM) molecular dynamics (MD) simulations. For the first part, two QM/MM MD simulations, namely B3LYP/MM and MP2/MM, have been performed to investigate the possible influence of electron correlation on the structure and dynamics of H_3O^+ hydrate. In comparison to the previously published HF/MM results, both B3LYP/MM and MP2/MM simulations clearly reveal stronger H_3O^+-water hydrogen bond interactions, which are reflected in a slightly greater compactness of the H_3O^+ hydrate. However, the B3LYP/MM simulation, although providing structural details very close to the MP2/MM data, shows an artificially slow dynamics nature of some first shell waters as a consequence of the formation of a long-lived H_3O^+---H_2O hydrogen bonding structure.

For the second part, according to some unsolved problems in the QM/MM scheme, a more sophisticated QM/MM MD based on ONIOM-XS method has been applied for studying such system. Due to the limit of CPU time, the HF method has been used for describing all interactions within the QM region. As compared to the conventional HF/MM results, the HF/MM MD simulation based on ONIOM-XS

method provides remarkable different data, both in the structure and dynamics of the H_3O^+ hydrate. In particular, the ONIOM-XS simulation predicts relatively weak H_3O^+-water hydrogen bonds as compared to the conventional HF/MM results, which corresponds to the observed lower MRT values of water molecules at each of H_3O^+ hydrogens. The observed differences clearly indicate the deficiency of the conventional QM/MM scheme for the treatment of such system. In this respect, however, since the effects of electron correlation have been shown to play an important role in the structure and dynamics of the H_3O^+ hydrate, it is recommended that the QM/MM MD simulation based on ONIOM-XS method should be carried out in conjunction with the correlated methods, such as MP2, in order to obtain a more accurate description of this hydrated ion.

School of Chemistry Student's Signature_____

Academic Year 2011 Advisor's Signature_____

ACKNOWLEDGEMENTS

First and foremost, I would like to express my sincere gratitude to my advisor, Assoc. Prof. Dr. Anan Tongraar for his continuously support of my Ph.D. study and research, for his encouragements and inspiration. Furthermore, I deeply thank for his kind advices, valuable suggestions for my thesis work and life. I am thankful to all of thesis examining committee for their useful comments and suggestions.

I am grateful to Prof. Dr. Christopher J. Cramer, University of Minnesota, USA, who provided me new and worthy research experiences. I would also like to thank my colleagues in the Cramer's group for their helpful. Lastly, I would like to thank Mr. Eugene Allred and his wife, my family in USA, who provided me a warm house and comfortable life in Minnesota. Special thanks to all my friends in School of Chemistry, SUT, for their friendship and kind assistance in work and life.

I would like to acknowledge the financial support by the Thailand Research Fund under the Royal Golden Jubilee Ph.D. scholarship program (TRF, Contract number PHD/0185/2548). I would like to thank School of Chemistry, SUT, for powerful research facilities.

Finally, I would like to take this opportunity to express my special gratitude to my parents and my family for their love, deep understanding and encouragement. My apologies to others I have not mentioned here, I am indebted to them for everything they have helped.

Thanawat Somtua

CONTENTS

CONTENTS (Continued)

CONTENTS (Continued)

LIST OF TABLES

LIST OF FIGURES

LIST OF FIGURES (Continued)

LIST OF FIGURES (Continued)

LIST OF ABBREVIATIONS

IR	=	Infrared
XRD	=	X-ray diffraction
ND	=	Neutron diffraction
NMR	=	Nuclear magnetic resonance
XAFS	=	X-ray absorption fine structure
XANES	=	X-ray absorption near edge structure
MC	=	Monte Carlo
MD	=	Molecular Dynamics
H_2O	=	Water
H_3O^+	=	Oxonium ion
IUPAC	=	International Union of Pure and Applied Chemistry
$H_5O_2^+$	=	Zundel complex
$H_9O_4^+$	=	Eigen complex
PT	=	Proton transfer
C_{3v}	=	Symmetry of C_{3v} point group (rotation around C_{3v} axis)
HB	=	Hydrogen bond
CP	=	Car and Parrinello
GGA	=	Generalized gradient approximation
DFT	=	Density functional theory
DNA	=	Deoxyribonucleic acid

LIST OF ABBREVIATIONS (Continued)

MP2	=	Second-order Møller-Plesset perturbation theory
QM	=	Quantum mechanics
MM	=	Molecular mechanics
QM/MM	=	Combined quantum mechanical/molecular mechanical method
B3LYP	=	Beck three-parameters hybrid functional combined with Lee-Yang-Parr correlation function
HF	=	Hartree-Fock
CASSCF	=	Complete active space self-consistent field
CASPT2	=	Complete active space with second-order perturbation theory
ONIOM	=	Own N-layered integrated molecular orbital and molecular mechanics
ONIOM-XS	=	ONIOM-extension to solvation
BJH	=	Flexible water model developed by Bopp, Jancsó and Heinzinger
CF2	=	Central force model version 2
RDF	=	Radial distribution function
ADF	=	Angular distributions function
MRT	=	Mean residence times
$\hat{H}$	=	Hamiltonian operator
Ψ	=	Wavefunction
m	=	Mass
m_e	=	Mass of electron

LIST OF ABBREVIATIONS (Continued)

m_k	=	Mass of nucleus
$\hbar$	=	Plank's constant
e	=	Electron charge
Z	=	Atomic number
r_{ab}	=	Distance between particles a and b
∇^2	=	Laplacian operator
$\hat{T}$	=	Kinetic energy operator
$\hat{V}$	=	Potential energy operator
Φ	=	Trial wave function
E_i	=	Expectation energy
E_0	=	Ground state energy
etc	=	et cetera
MO	=	Molecular orbital
AO	=	Atomic orbital
LCAO-MO	=	Linear combination of atomic orbitals to molecular orbitals
STO	=	Slater-type orbital
GTO	=	Gaussian-type orbital
SZ	=	Single-zeta basis set
SV	=	Split-valence basis set
DZ	=	Double-zeta basis set
TZ	=	Triple-zeta basis set
QZ	=	Quadruple-zeta basis set

LIST OF ABBREVIATIONS (Continued)

DZP	=	Double-zeta plus polarization
cc-pVDZ	=	Correlation-consistent polarized valence double-zeta basis set
cc-pVTZ	=	Correlation-consistent polarized valence triple-zeta basis set
cc-pVQZ	=	Correlation-consistent polarized valence quadruple-zeta basis set
cc-pV5Z	=	Correlation-consistent polarized valence quintuple-zeta basis set
aug-cc-pVDZ	=	Additional diffuse basis function and correlation consistent polarized valence double zeta
$\chi_i(i)$	=	Spin orbital of the *i-th* electron
SCF	=	Self-consistent field
RHF	=	Restricted Hartree-Fock
$\hat{F}$	=	Fock operator
$\hat{J}$	=	Coulomb operator
$\hat{K}$	=	Exchange operator
$E_{molecule}$	=	Total energy of molecule
E_{elec}	=	Electronic energy
E_{nuc}	=	Nuclear repulsion energy
E_{corr}	=	Correlation energy
E_{exact}	=	Exact energy (ground stat energy)
E_{HF}	=	Hatree-Fock energy
CI	=	Configuration interaction

LIST OF ABBREVIATIONS (Continued)

MBPT	=	Many-body perturbation theory
CC	=	Coupled cluster
KS	=	Kohn-Sham
E_T	=	Kinetic energy
E_V	=	Potential energy
E_J	=	Coulomb energy
E_{xc}	=	Exchange/correlation energy
$\left\|\psi_i(r)\right\|^2$	=	Spatial distribution of an electron
BP	=	Becke-Perdew correlation function
BLYP	=	Becke-Lee-Yang-Parr correlation function
EDF1	=	Empirical Density Functional 1
$\hat{H}_o$	=	Ground-state Hamiltonian
λ	=	Wavelength
MP	=	Møller-Plesset perturbation theory
$\langle A \rangle_{ensemble}$	=	Ensemble average
$\langle A \rangle_{time}$	=	Time average
V_{total}	=	System's interactions
V_{pair}	=	Pair interaction
r_{cut}	=	Cut-off distance
r_m	=	Distance characterizing the end of QM region
E_{tot}	=	Total interaction energy
E_{MM}	=	Interactions within MM region

LIST OF ABBREVIATIONS (Continued)

$E_{QM\text{-}MM}$	=	Interactions between QM and MM regions
$\langle \Psi_{QM} \lvert \hat{H} \rvert \Psi_{QM} \rangle$	=	Interactions within QM region
F_i	=	Forces acting on each particle
$S_m(r)$	=	Smoothing function
F_{QM}	=	QM force
F_{MM}	=	MM force
r_1	=	Distance characterizing the start of QM region
r_0	=	Distance characterizing the end of QM region
BSSE	=	Basis set superposition error
MP2	=	Second-order Møller-Plesset perturbation theory
MP4	=	Møller-Plesset perturbation theory to fourth order
CID	=	Configuration interaction with all double substitutions
CCD	=	Coupled cluster with doubles excitations
CPU	=	Central processing unit
kcal mol^{-1}	=	Kilocalorie per mole
Å	=	Angstrom
°	=	Degree
fs	=	Femtosecond
ps	=	Picosecond
CN	=	Coordination number
t_{sim}	=	Simulation time

LIST OF ABBREVIATIONS (Continued)

N_{ex}	=	Number of exchange event
t^*	=	Time for observing the number of exchange water molecules
K	=	Kelvin
NVT	=	Canonical ensemble
ox	=	Oxonium
w	=	Water
i.e.	=	Id est
e.g.	=	Exempli gratia
τ	=	Mean residence time

CHAPTER I

INTRODUCTION

1.1 Investigations of H_3O^+ in water

The behavior of ions solvated in an aqueous electrolyte solution has long been an interesting subject for scientists in order to understand the role and reactivity of these ions in chemical and biological processes. (Kielland, 1937; Kim, Vercauteren, Welti, Chin, and Clementi, 1985; Mackay, Berens, Wilson, and Hagler, 1984; Ohtaki, 2001; Sagnella and Voth, 1996; Tongraar and Rode, 2004). The proton (H^+) is one of the most interesting ions and has been widely investigated for centuries. One particularly interesting issue comes from the anomalously high mobility of proton in aqueous solution, *i.e.*, around 5-8 times greater than other cations (Koneshan, Rasaiah, Lynden-Bell, and Lee, 1998; Tuckerman, Laasonen, Sprik, and Parrinello, 1995a). Consequently, a number of experimental and theoretical techniques have been employed in order to elucidate such details. In terms of experiments, infrared (IR), X-ray Diffraction (XRD), Neutron Diffraction (ND), Nuclear Magnetic Resonance (NMR) spectroscopy, X-ray Absorption Fine Structure (XAFS) and X-ray Absorption Near-Edge Structure (XANES) spectroscopy (Begemann, Gudeman, Pfaff, and Saykally, 1983; Botti, Bruni, Ricci, and Soper, 2006; Douberly, Walters, Cui, Jordan, and Duncan, 2010; Falk and Giguère, 1957; Fulton and Balasubramanian, 2010; Giguère and Turrell, 1976; Kakiuchi, Shono, and Komatsu, 1951; Mancinelli, Sodo, Bruni, Ricci, and Soper, 2009; Mizuse, Fujii, and Mikami, 2007; Stoyanov, Sto

yanovea, and Reed, 2011; Triolo and Narten, 1975) have been employed to analyze and describe such fast proton mobility. However, the characteristics of the hydrated proton have still not yet been identified unambiguously, since it is rather difficult to prepare the protonated water clusters. Recently, the solvation structure of oxonium (H_3O^+) in water has been examined experimentally using ND with hydrogen isotope substitution (Botti, Bruni, Imberti, Ricci, and Soper, 2005; Botti, Bruni, Ricci, and Soper, 2006). In this work, according to the IUPAC nomenclature of organic and inorganic chemistry, it should be noted that the appropriate nomenclature of H_3O^+ is oxonium (systematic: *oxidanium*). Thus, the name "*oxonium*" was used throughout this work, *i.e.*, instead of the alternative phase "*hydronium*". In aqueous solution, it has been demonstrated that each H^+ is part of a quite stable H_3O^+ ion which preferentially hydrogen-bonds to three nearest-neighbor water molecules. Of particular interest, the fourth water molecule was observed near the oxygen side of H_3O^+, exhibiting strong orientational correlations with the ion.

In terms of theoretical investigations, the *ab initio* (MP2, CASSCF, CASPT2) and density functional theory (DFT/B3LYP) calculations have been carried out to explore the structure as well as the electronic and vibrational spectra of H_3O^+-$(H_2O)_n$ clusters (Sobolewski and Domcke, 2002). Overall, the results for the protonated water clusters revealed that two theoretical methods, DFT/B3LYP and MP2, are mutually consistent. Despite the small quantitative differences in the optimized geometries and in IR absorption spectra obtained by two methods, it has been demonstrated that the picture of the behavior of an excess proton in small water clusters is independent of the applied method (Sobolewski and Domcke, 2002). For the treatment of ions in an aqueous solution, the computer simulations by means of Monte Carlo (MC) and

molecular dynamics (MD) have become a powerful tool to elucidate such details, in particular at the molecular level. In this respect, H_3O^+ has been widely used as a model system for studying proton migration in liquid water (Agmon, 1995; Brancato and Tuckerman, 2005; Brodskaya, Lyubartsev, and Laaksonen, 2002; Day, Soudackov, Čuma, Schmitt, and Voth, 2002; Hermida-Ramón and Karlström, 2004; Intharathep, Tongraar, and Sagarik, 2006; James and Wales, 2005; Karlström, 1988; Kim, Schmitt, Gruetzmacher, Voth, and Scherer, 2002; Kochanski, 1985; Lapid, Agmon, Petersen, and Voth, 2005; Lobaugh and Voth, 1996; Marx, Tuckerman, Hutter, and Parrinello, 1999; Sagnella and Tuckerman, 1998; Schmitt and Voth, 1998; Schmitt and Voth, 1999; Tuckerman, Laasonen, Sprik, and Parrinello, 1995a; Tuckerman, Laasonen, Sprik, and Parrinello, 1995b; Tuckerman, Marx, Klein, and Parrinello, 1997; Voth, 2006; Vuilleumier and Borgis, 1997; Vuilleumier and Borgis, 1998a; Vuilleumier and Borgis, 1998b; Vuilleumier and Borgis, 1999a; Vuilleumier and Borgis, 1999b; Wang and Voth, 2005; Wei and Salahub, 1994).

In general, the mobility of protons in water has been regarded as a combination of rapid protons jumping between different water molecules, known as the Grotthuss mechanism (Grotthuss, 1806; Voth, 2006), and the diffusion of the entire protonated water complexes through the hydrogen bond network, *i.e.*, in a way similar to other simple ions. Based on the theoretical investigations (Berkelbach, Lee, and Tuckerman, 2009; Botti, Bruni, Imberti, Ricci, and Soper, 2005; Brancato and Tuckerman, 2005; Hermida-Ramón and Karlström, 2004; Intharathep, Tongraar, and Sagarik, 2006; James and Wales, 2005; Lapid, Agmon, Petersen, and Voth, 2005; Markovitch and Agmon, 2007; Voth, 2006; Wang and Voth, 2005; Woutersen and Bakker, 2006), it has been proposed that the Eigen cation ($H_3O^+ \cdot (H_2O)_3$ or $H_9O_4^+$

complex) (Eigen, 1964) and Zundel cation ($[H_2O{\cdots}H{\cdots}OH_2]^+$ or $H_5O_2^+$ complex) (Zundel, 1970) are the primarily important species in the aqueous proton transfer (PT) mechanism. According to recent computer simulations (Lapid, Agmon, Petersen, and Voth, 2005) and experiments (Winter *et al.*, 2006; Woutersen and Bakker, 2006), it has been suggested that the PT process occurs on extremely fast time scale, *i.e.*, about 100 fs or less. The $H_9O_4^+$ is formed when the three hydrogen atoms in H_3O^+ are equivalently hydrated (C_{3v} trihydrated H_3O^+ ion), forming three analogous hydrogen bonds with the three nearest-neighbor water molecules, while the $H_5O_2^+$ is formed when one hydrogen atom of the H_3O^+ ion is symmetrically shared with its hydrogen bonding water molecule. These complexes are continuously interconverted, which constituted the PT in water. According to most recent studies, it has been demonstrated that H_3O^+ is more stable (longer living) than $H_5O_2^+$ (Day, Soudackov, Čuma, Schmitt, and Voth, 2002; Kirchner, 2007; Marx, Tuckerman, Hutter, and Parrinello, 1999; Schmitt and Voth, 1999; Winter *et al.*, 2006; Wu, Chen, Wang, Paesani, and Voth, 2008; Zahn and Brickmann, 1999), and that the mechanism for the PT in water involves a concerted single PT event, *i.e.*, the more stable H_3O^+ is converted into the less stable $H_5O_2^+$ and *vice versa.* In this respect, the calculated ratios between Eigen and Zundel cations of 65:35 (Likholyot, Lemke, Hovey, and Seward, 2007; Voth, 2006) and 75:25 (Botti, Bruni, Ricci, and Soper, 2006) have been reported. Several MD simulations suggested that this interconversion is driven by specific fluctuations in the second shell of the hydrogen bond (HB) network around H_3O^+ (Berkelbach, Lee, and Tuckerman, 2009; Lapid, Agmon, Petersen, and Voth, 2005; Markovitch and Agmon, 2007; Tuckerman, Laasonen, Sprik, and Parrinello, 1995a; Tuckerman, Laasonen, Sprik, and Parrinello, 1995b), *i.e.*, the

breakage of a HB of water molecules in the second solvation shell of H_3O^+ and so excess proton advance towards a neighboring water molecule and form the Zundel transient structure. Consequently, it has been demonstrated that the rate-limiting step for the aqueous PT mechanism was the hydrogen bond cleavage, rather than water cluster growth or proton motion.

In terms of quantum-mechanics-based simulations, Car-Parrinello (CP) MD technique has been employed for studying the excess proton in water, providing a reasonable chemical rearrangement of the Grotthuss mechanism (Marx, Tuckerman, Hutter, and Parrinello, 1999; Tuckerman, Laasonen, Sprik, and Parrinello, 1995a; Tuckerman, Laasonen, Sprik, and Parrinello, 1995b; Tuckerman, Marx, Klein, and Parrinello, 1997). By means of the CP-MD technique, however, some methodical drawbacks come from the use of a relatively small system size, as well as from the use of simple generalized gradient approximation (GGA) density functionals. Regarding to earlier CP-MD studies (Tuckerman, Laasonen, Sprik, and Parrinello, 1995a; Vuilleumier and Borgis, 1999), the stability of the $H_5O_2^+$ complex is rather overestimated, which reflects in the coexistence of the $H_9O_4^+$ and $H_5O_2^+$ formation. Recently, the use of simple density functionals in the CP-MD scheme was also found to give poor structural and dynamical data even for the underlying liquid water (Grossman, Schwegler, Draeger, Gygi, and Galli, 2004; Schmidt *et al.*, 2009; Yoo, Zeng, and Xantheas, 2009). Consequently, this leads to serious issues on the accuracy and reliability of the DFT in describing such hydrogen bond systems, since it is known that the hydrogen bonds in water are constantly breaking and forming and that these hydrogen bond dynamics are coupled to the process of proton mobility in water. Moreover, for some particular systems, such as DNA base interactions, the results

suggest that the DFT method is not suitable to study such base-base interactions due to a strong overestimation of the electron correlation, which resulted in too short bonds (Šponer, Leszczynski, and Hobza, 1996)

Besides the CP-MD technique, an alternative approach is to apply a so-called combined quantum mechanical/molecular mechanical (QM/MM) approach (Singh and Kollman, 1986; Warshell and Levitt, 1976). By the QM/MM technique, the system is partitioned into two parts, namely QM and MM region. The QM region, *i.e.*, a sphere which includes the ion and its surrounding solvent molecules, is treated quantum mechanically, while the MM region (*i.e.*, the rest of the system) is described by classical MM potentials. In the past several years, the QM/MM technique has been successfully applied to study various condensed-phase systems (Åqvist and Warshel, 1993; Bash, Ho, Mackerell, Levine, and Hallstrom, 1996; Bernardi, Olivucci, and Robb, 1992; Cummins and Gready, 1997; Curutchet *et al.*, 2009; Field, Bash, and Karplus, 1990; Gao, 1996; Stanton, Hartspugh, and Merz, 1995). Recently, a HF/MM MD simulation has been performed for the H_3O^+ in an aqueous solution (Intharathep, Tongraar, and Sagarik, 2006), providing more insights into the structure and dynamics of this hydrated ion. With regard to the previous HF/MM MD study, however, it is known that the HF method takes into account the interactions between electrons only in an average way. In this respect, it could be expected that the effects of "electron correlation" may affect the structural and dynamical properties of the H_3O^+ hydrate.

In addition, according to the QM/MM technique, some unsolved problems still exist. First, only the exchanging particles are treated by the smoothing function when they are crossing the QM/MM boundary. This is not realistic since immediate addition or deletion of a particle in the QM region, due to the solvent exchange also

affects the forces acting on the remaining QM particles. As a consequence, this may result in the numerical instability of the QM/MM performance whenever there are solvent exchanges between the QM and MM subsystem, sometimes even causing the program to halt. Second, the original QM/MM scheme cannot clearly define the appropriate energy expression during the solvent exchange process.

To solve those problems, a more sophisticated QM/MM technique based on ONIOM-XS method has been proposed (Kerdcharoen and Morokuma, 2002; Kerdcharoen and Morokuma, 2003). The ONIOM method, originally developed by Morokuma *et al.* (Svensson, Humbel, Froese, Matsubara, Sieber, and Morokuma, 1996) can handle not only the QM + MM combinations (which is implemented in the conventional QM/MM scheme), but also the QM + QM combinations. Interestingly, this technique allows forces on all QM particles to be smoothed during particle exchange, and thus, clearly defines the system's energy expression.

1.2 Research objectives

1. To investigate the effects of electron correlation on the solvation structure and dynamics of H_3O^+ in an aqueous solution. In this work, the results obtained by the present B3LYP/MM and MP2/MM MD simulations were compared and discussed with respect to the previous HF/MM MD study (Intharathep, Tongraar, and Sagarik, 2006).
2. To investigate the reliability and accuracy of the QM/MM MD approach for the treatment of such system. In this work, a more sophisticated HF/MM MD simulation based on ONIOM-XS method was performed, and

the results were compared to those obtained by the conventional HF/MM MD approach.

1.3 Scope and limitation of the study

In this work, the investigations were divided into two parts. In the first part, two conventional QM/MM MD simulations, namely B3LYP/MM and MP2/MM, were performed in order to investigate the effects of electron correlation on the structure and dynamics of H_3O^+ embedded in an aqueous solution. The results obtained by the present B3LYP/MM and MP2/MM MD simulations were compared and discussed with respect to the results obtained by the previous HF/MM MD study (Intharathep, Tongraar, and Sagarik, 2006). In this work, since the B3LYP/MM and MP2/MM MD simulations are rather time-consuming, a relatively small QM size with diameter of 7.6 Å was used, *i.e.*, the same QM size as employed in the previous HF/MM MD simulation (Intharathep, Tongraar, and Sagarik, 2006). For the second part of this work, a more sophisticated HF/MM MD simulation based on ONIOM-XS method, abbreviated throughout this work as "ONIOM-XS MD", was applied for studying the H_3O^+ in an aqueous solution, and the results were compared to those obtained by the conventional HF/MM MD approach. In this work, since the performance of the ONIOM-XS MD simulation is relatively more expensive than the conventional QM/MM scheme, the HF method is then the only possible choice for the description of all interactions within the QM region. To improve the quality of the results, both conventional HF/MM and ONIOM-XS MD simulations were carried out using a larger QM size with diameter of 8.4 Å. Comparing to the conventional HF/MM MD simulation, the results obtained by the present ONIOM-XS MD

simulation can be expected to provide more reliable details regarding the solvation structure and dynamics of this hydrated ion, leading to further understanding of PT process take places in aqueous solution.

By the QM/MM technique, the system consists of a "high-level" QM sphere which contains H_3O^+ ion and its nearest-neighbor water molecules floating inside a cube of "low-level" MM solvent molecules. All interactions inside the QM region are treated quantum mechanically (HF, B3LYP and MP2), while the rest of the system is described by means of classical pair potentials. A flexible BJH-CF2 model, which describes inter- (Stillinger and Rahman, 1978) and intramolecular (Bopp, Jancsó and Heinzinger, 1983) interactions was employed for water. The pair potential functions for describing the H_3O^+-H_2O interactions were employed from the reference (Intharathep, Tongraar and Sagarik, 2006). The structural details of H_3O^+ in aqueous solution were characterized through radial distribution functions (RDFs) and their corresponding integration numbers, as well as by the detailed analysis on angular distribution functions (ADFs) and orientations of water molecules surrounding the ion. The corresponding dynamics details were analyzed with respect to mean residence times (MRTs), of water molecules as well as to water exchange processes at the ion. The results obtained by the present study were discussed and compared to previous theoretical studies, as well as to available experimental observations.

CHAPTER II

THEORETICAL AND COMPUTATIONAL METHODS

2.1 Quantum mechanics

Before 19th century, scientists believed that classical mechanics can be described entire natural phenomena including matter and energy. The classical mechanics, which is governed by the Newton's law of motion and Maxwell's law of electromagnetism, have been used to define and predict the motion of macroscopic objects and energy. Until the end of nineteen century, the classical mechanics were found not able to explain famous experimental phenomena, such as black body radiations, photoelectric effect and optical line spectra. Consequently, a modern theory, namely quantum mechanics (QM), was proposed and developed in order to explain and predict the behavior of the particles in atomic and sub-atomic level, including electron, protons, neutron, atomic nuclei, atom and molecules, as well as photon. The idea of QM is that the microscopic systems can be described by wavefunctions which completely characterize all of the physical properties of the system, *i.e.*, describing molecules in terms of interaction among nuclei and electrons, and molecular geometry in terms of minimum energy arrangements of nuclei. According to the QM theory, the solution for a given wavefunction can be obtained by solving Schrödinger equation (Schrödinger, 1926). The solution to the Schrödinger equation is the properties of matter in terms of motions of electrons, which in turn

leads directly to molecular structure and energy, as well as to information about bonding.

2.1.1 Schrödinger equation

The formulations of QM were devised by the time-independent Schrödinger equation. The Schrödinger equation for a multinuclear, multi-electron system can be written as

$$\hat{H}\Psi = E\Psi, \tag{2.1}$$

where $\hat{H}$, Ψ and E denote the Hamiltonian operator, the wavefunction and the energy, respectively. By means of mathematics, this equation is called an eigen equation. Consequently, Ψ is then called the eigenfuntion and E an eigenvalue. The operator and eigen function can be a matrix and vector, respectively. The wavefunction Ψ is a function of the electron and nuclear position. In this respect, the wave function must be continuous, single-valued, normalizable and antisymmetric with respect to the interchange of electron.

When the Hamiltonian operator $\hat{H}$ in equation (2.1) operates on a wavefunction, it returns the wavefunction multiplied by the energy. The $\hat{H}$ notation can be written as

$$\hat{H} = -\sum_i \frac{\hbar_i^2}{2m_e}\nabla_i^2 + \sum_k \frac{\hbar^2}{2m_k}\nabla_k^2 - \sum_i \sum_k \frac{e^2 Z_k}{r_{ik}} + \sum_{i<j} \frac{e^2}{r_{ij}} + \sum_{k<l} \frac{e^2 Z_k Z_l}{r_{kl}}, \tag{2.2}$$

where i and j run over electron, k and l run over nuclei, $\hbar$ is Planck's constant divided by 2π, m_e is the mass of the electron, m_k is the mass of nucleus k, ∇^2 is the Laplacian operator, e is the charge on the electron, Z is an atomic number, and r_{ab} is the distance between particle a and b. The Laplacian operator in Cartesian coordinates is in the form of

$$\nabla_i^2 = \frac{\partial^2}{\partial x_i^2} + \frac{\partial^2}{\partial y_i^2} + \frac{\partial^2}{\partial z_i^2}. \tag{2.3}$$

According to equation (2.2), the Hamiltonian operator can be divided into two parts, namely kinetic and potential energy operators. The first two terms refer to the kinetic energy operator for each electron and nucleus, respectively, and the last three terms represent the potential energy operator for each electron-nucleus pair, each electron pair and each nucleus pair, respectively. The kinetic energy operator can be written as

$$\hat{T}(i) = -\frac{\hbar^2}{2m_i}\nabla^2(i), \tag{2.4}$$

which can be calculated with respect to the coordinates of the i particle. The potential energy operator can be written in the form of

$$\hat{V}(i,j) = -\frac{q_i q_j}{r_{ij}}, \tag{2.5}$$

where q defines the charge of each particle and r is the distance between the two particles.

In practice, many-electron Schrödinger equation cannot be solved exactly, even for a simple two electron system such as helium atom or hydrogen molecule. Therefore, some approximations were introduced to provide practical use of this method.

2.1.2 Born-Oppenheimer approximation

One way to simplify the Schrödinger equation for molecular system is separating the nuclear and electron motion by assuming that the nuclei do not move, *i.e.*, due to be much heavier. In this respect, the electron distribute in a field of fixed nuclei depending only on the position of nuclei. Consequently, the kinetic energy operator for each nucleus is zero and the potential energy operator for each nucleus pair, which depends only on the molecular geometry, can be treated as constant value. This is called the Born-Oppenheimer approximation, leading to an electronic Schrödinger equation of

$$\hat{H}_{elec}\,\Psi_{elec} = E_{elec}\,\Psi_{elec}, \tag{2.6}$$

where $\hat{H}_{elec}$ is and electronic Hamiltonian and Ψ_{elec} is a function of electron coordinates. The Hamiltonian for a molecule with stationary nuclei is

$$\hat{H}_{elec} = -\sum_{i}^{electrons}\frac{\hbar_i^2}{2m_e}\nabla_i^2 - \sum_{i}^{electrons}\sum_{k}^{nuclei}\frac{e^2 Z_k}{r_{ik}} + \sum_{i<j}^{electrons}\frac{e^2}{r_{ij}}, \tag{2.7}$$

which can be simplified by changing in atomic units,

$$\hat{H}_{elec} = -\sum_{i}^{electrons} \frac{1}{2}\nabla_i^2 - \sum_{i}^{electrons}\sum_{k}^{nuclei} \frac{Z_k}{r_{ik}} + \sum_{i<j}^{electrons} \frac{1}{r_{ij}}, \quad (2.8)$$

where the first term is the kinetic energy of the electron, the second term is the attraction of electrons to nuclei and the last term is the repulsion between electrons. In this regard, the repulsion between nuclei is added onto the energy at the end of the calculation.

2.1.3 Variation principle

According to equation (2.7), the last term on the right hand side is known as the many-body contributions. Since it is not possible to solve the Schrödinger equation exactly for a many-body system, one strategy in the QM calculation is to guess a suitable form of Ψ and then optimize using the Variation principle. By means of the variation principle, a trial wavefunction, Φ, is a function of the appropriate electronic and nuclear coordinates to be operated upon by the Hamiltonian. In this respect, the set of orthonormal wavefunctions Ψ_i must be completely defined, and the function Φ can be written in terms of a linear combination of the Ψ_i,

$$\Phi = \sum_i c_i \Psi_i. \quad (2.9)$$

By this scheme, it should be noted that the individual Ψ_i and coefficients c_i are unknown. Once the Φ becomes orthonormal, the normality of Φ imposes a constraint on the coefficients.

$$\begin{aligned}\int \Phi^2 dr = 1 &= \int \sum_i c_i \Psi_i \sum_j c_j \Psi_j dr \\ &= \sum_{ij} c_i c_j \int \Psi_i \Psi_j dr \\ &= \sum_{ij} c_i c_j \delta_{ij} \\ &= \sum_i c_i^2 . \end{aligned} \tag{2.10}$$

$$\therefore \sum_i |c_i|^2 = 1. \tag{2.11}$$

Considering the energy evaluated with the wavefunction Φ, as shown in equation

$$\begin{aligned}\int \Phi \hat{H} \Phi dr &= \int \left(\sum_i c_i \Psi_i \right) \hat{H} \left(\sum_j c_j \Psi_j \right) dr \\ &= \sum_{ij} c_i c_j \int \Psi_i \hat{H} \Psi_j dr \\ &= \sum_{ij} c_i c_j E_j \delta_{ij} \\ &= \sum_i c_i^2 E_i . \end{aligned} \tag{2.12}$$

The expectation energy, E_i, associated with the generic wavefunction Φ is determined from all of the coefficients c_i. Then, the trial energy E_i will be compared with the ground state energy E_0,

$$\int \Phi \hat{H} \Phi dr - E_0 \int \Phi^2 dr = \sum_i c_i^2 (E_i - E_0). \tag{2.13}$$

Assuming the coefficients to be real numbers, each term must be zero or positive value. Therefore, (E_i-E_0) must be greater than or equal to zero.

$$\int \Phi \hat{H} \Phi dr - E_0 \int \Phi^2 dr \geq 0 \tag{2.14}$$

or

$$\frac{\int \Phi \hat{H} \Phi dr}{\int \Phi^2 dr} \geq E_0. \tag{2.15}$$

By means of variation principle, the trial wavefunction with lower energy is a better trial wavefunction. On the other hand, the best trial wavefunction is the function that gives the lowest expectation energy.

2.1.4 Molecular orbital (MO) theory

Molecular orbital (MO) are formed by combining atomic orbitals (AOs) of the constituent atoms, called *Linear Combination of Atomic Orbitals to*

Molecular Orbitals (LCAO-MO) method. This is one of the most important and widely used ideas in quantum chemistry. The LCAO-MO can be expressed as

$$\psi_i = \sum_{\mu=1}^{n} c_{\nu i}\phi_\nu , \tag{2.16}$$

where ψ_i refers to the *i-th* molecular orbital. The $c_{\upsilon i}$ are set of coefficients weighting the contributions of the atomic orbital to the molecular orbitals, which can be calculated by using variation principle. The ϕ_υ defines the *υ-th* atomic orbital and *n* is the number of atomic basis functions.

2.1.4.1 Basis sets

According to equation (2.16), a set of *n* atomic basis function ϕ_υ is called basis set. John C. Slater was the first one who turned to orbital computation using basis sets, knows as Slater Type Orbitals (STOs) (Slater, 1930). The Schrödinger equation for one-electron ions, *i.e*. hydrogen or other ions, give atomic orbitals which are product of radial function that depend on the distance of the electron from the nucleus and a spherical harmonic. Slater proposed that one could use functions that consisted only of the spherical harmonics and the exponential term. Slater-type orbitals represent the real situation for the electron density in the valence region and beyond, but are not suitable for the description at distance close to the nucleus. The STOs were used as basis functions due to their similarity to atomic orbitals of the hydrogen atom. The general from of basis function can be expressed as

$$Basis\ \ function,\ \ BF = N \times e^{(-\alpha r)}, \tag{2.17}$$

where N is the normalization constant, α is the orbital exponent and r is the radius in angstroms. STOs are described by the function depending on spherical coordinates:

$$\phi_1(\alpha, n, l, m, r, \theta, \phi) = N r^{n-1} e^{-\alpha r} Y_{l,m}(\theta, \phi). \tag{2.18}$$

The r, θ and ϕ are spherical coordinates, and $Y_{l,m}$ is the angular momentum part. The n, l, and m are quantum numbers: principal, angular momentum and magnetic, respectively. Simplifying the equation for hydrogen-like systems, the STO equation takes the form of

$$STO = \left[\frac{\alpha^3}{\pi}\right]^{0.5} e^{(-\alpha r)}, \tag{2.19}$$

where α is the Slater orbital exponent.

In spite of its accuracy, the STOs are time-consuming for solving integral of the wave equation. In the 1950s, Frank Boys has introduced Gaussian Type Orbitals (GTOs) (Boy, 1950) which is a modification to the wavefunction, called gaussian type functions. Such functions contain the exponential $e^{-\beta r2}$, rather than the $e^{-\alpha r}$ of the STOs. Such functions are relatively fast and easy to evaluate, but of course, they are less accurate than the STOs. These functions neither represent the electron density of the real situation nor the STOs. However, this

problem can be solved by using more GTOs. Thus, the shape of STO function can be estimated from a linear combination of GTO functions with different set of exponents and coefficients. The expansions of any number of GTOs are possible, but generally not more than six functions because of computational reasons. For example, GTO (3G) can be written as

$$GTO(3G) = c_1 e^{-\beta_1 r^2} + c_2 e^{-\beta_2 r^2} + c_3 e^{-\beta_3 r^2}, \tag{2.20}$$

where three values of c and β are fixed. The values of c and β can be evaluated by fitting the above equation to a STO using a least-squares method. The other method to evaluate c and β is varying them in atomic calculation to minimize the energy. Sometimes, the GTOs are called *Gaussian primitives* or *Cartesian Gaussian*. For example, a Cartesian Gaussian centered on atom a can be represented as

$$G_{i,j,k} = N x_a^i y_a^j z_a^k e^{-\alpha r_a^2}, \tag{2.21}$$

where i, j, and k are non-negative integers, α is a positive orbital exponent, x_a, y_a, and z_a are Cartesian coordinates with the origin at a, and N is the Cartesian Gaussian normalization constant.

The differences between STOs and GTOs can be shown in Figure 2.1. Note that the r-factor of the exponential in GTO is squared.

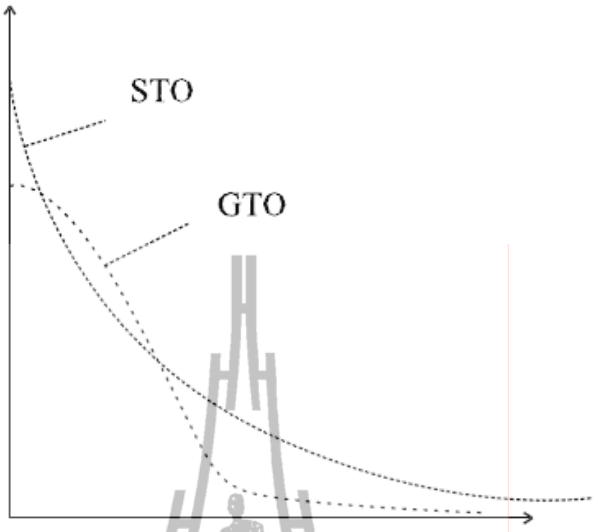

Figure 2.1 Comparison of STO ($e^{-\alpha r}$) and GTO ($e^{-\alpha r^2}$).

2.1.4.2 Classification of basis sets

Nowadays, a number of standard basis sets are widely used in the quantum mechanical calculations. The minimal basis sets, also known as a single-zeta (SZ) basis set, select one basis function for every atomic orbital required to describe the free atom. The most common minimal basis set is STO-nG; STO-2G, STO-3G, STO-4G, STO-6G and STO-3G* (a polarized version of STO-3G), proposed by John Pople and his group. It involves a linear combination of "*n*" GTOs fitted to each STO. Thus, when a basis function contains more than one primitive Gaussian, it can be considered as "contracted". Since the valence shell electrons are most important for interaction between atoms, the split-valence (SV) basis sets are introduced which represent valence orbital by more than one basis function. The basis sets with multiple basis functions corresponding to each valence atomic orbital are called valence double (DZ), triple (TZ), quadruple-zeta (QZ), and so on, basis sets.

The notation for split-valence basis sets is typically written as *X*-*YZ*g, where *X* represents the number of primitive Gaussians comprising each core atomic orbital, *Y* and *Z* indicate that the valence orbitals are composed of two basis functions each. In this case, the presence of two numbers after hyphens implies that this basis set is a split-valence double-zeta basis set. The smallest split-valence basis set is denoted as 3-21G, *i.e.*, it uses a three-primitive expansion for the 1s orbital and then splits the valence orbitals into a two basis function, the inner function being a contraction of two Gaussians and the outer function used s single Gaussian primitive.

Another type of basis sets is polarized and diffuse basis sets. The polarization functions are important for reproducing chemical bonding, *i.e.*, when bonds are formed in molecules, the atomic orbitals are distorted (polarized) from their original shapes to form optimal bonding. The notations of polarized functions are *p*- , *d*- or *f*-type, which describe the distortion of *s*, *p* or *d* orbitals, respectively. For example, double-zeta plus polarization (DZP) basis sets in Pople nomenclature can be written as 6-31G(*d*) (or 6-31G*) which adds *d*-type functions to basis set of all heavy atoms, and 6-31G(*d*,*p*) (or 6-31G**) which adds *d*-type functions to heavy atoms and *p*-type functions to H atom. The diffuse functions have small exponents, they are necessary for accurate polarizabilities or binding energies of van der Waals complexes (bound by dispersion), especially for lone pairs, anion exited states, as well as weak interacting systems. The notation for diffuse functions is +, such as in Pople nomenclature, the 6-31+G means that the diffuse function is added for heavy atoms, and the 6-31++G means that the diffuse functions are add for both heavy and H atom. In practice, these functions can directly be added into the basis sets to obtain more accurate data. Another type of basis sets is the correlation-consistent basis sets,

developed by Dunning and coworkers. These basis sets include shell of polarization (correlating) functions (*d*, *f*, *g*, etc.) that can yield convergence of the electronic energy to the complete basis set limit. Examples of the correlation-consistent basis sets are cc-pVDZ, cc-pVTZ, cc-pVQZ, cc-pV5Z, aug-cc-pVDZ, etc. Nowadays, these basis sets have become widely used for correlated or post-Hartree Fock calculations.

2.1.5 The Hartree-Fock (HF) method

By solving the Schrödinger equation, some approximations are required. According to the variation method, the form of wavefunction is guessed, called the trial wavefunction. For *N*-electron system, a trial wavefunction can be written as

$$\Psi = \chi_1(1)\chi(2)\cdots\chi_N(N), \tag{2.22}$$

where $\chi_i(i)$ is the spin orbitals of the *i-th* electron, and then the trial wavefunction can be expressed in the form of Slater determinant to ensure the antisymmetry upon the interchange of electron coordinates,

$$\Psi = \frac{1}{\sqrt{N!}}\begin{vmatrix} \chi_1(1) & \chi_2(1) & \cdots & \chi_N(1) \\ \chi_1(2) & \chi_2(2) & \cdots & \chi_N(2) \\ \vdots & \vdots & \ddots & \vdots \\ \chi_1(N) & \chi_2(N) & \cdots & \chi_N(N) \end{vmatrix}. \tag{2.23}$$

The spin orbital (χ_i) is the product of a spatial function or molecular orbital, ψ_i, and a spin function, α or β called as spin up and spin down, respectively. The electronic spin is quantized by ±1/2; +1/2 spin defines α-electron and -1/2 spin defines β-spin. The spin orbital can be written as

$$\chi_i = \psi_i(x_i, y_i, z_i)\alpha(\sigma_i), \tag{2.24}$$

or

$$\chi_i = \psi_i(x_i, y_i, z_i)\beta(\sigma_i). \tag{2.25}$$

The set of spin orbital must have orthonormal properties which defined by

$$\int \chi_i^* \chi_j d\tau = \delta_{ij} \begin{cases} 0 & i \neq j \\ 1 & i = j. \end{cases} \tag{2.26}$$

According to the variation method, the best sets of spin orbital correspond to the one that give the lowest expectation value of energy. Consequently, the appropriate sets of spin orbital can be solved from the HF equation,

$$\hat{F}_i(1)\chi_i(1) = \varepsilon_i \chi_i(1). \tag{2.27}$$

In this respect, the solution of HF equation are set of eigen value, $\{\varepsilon_i\}$, and eigen function, $\{\chi_i(1)\}$, which corresponds to the lowest energy. By means of the HF method, the Hamiltonian operator considers that each electron individually move in the average field of all other electrons in the molecule. This is the basis of the self-consistent field (SCF) procedure. For closed-shell systems (all electrons spin-paired, two per occupied orbital), the formalism is well known as restricted Hartree-Fock (RHF). The Hamiltonian operator for one-electron is called Fock operator, $\hat{F}$, which can be defined for each electron j as

$$\hat{F}(1) = \hat{H}^{core}(1) + \sum_{j=1}^{N/2}(2\hat{J}_j(1) - \hat{K}_j(1)), \tag{2.28}$$

where $\hat{H}^{core}(1)$ is the core Hamiltonian operator,

$$\hat{H}^{core}(1) = -\frac{1}{2}\nabla_1^2 - \sum_{A=1}^{N/2}\frac{Z_A}{r_{1A}}, \tag{2.29}$$

where $\hat{J}_j$ is Coulomb operator representing the classical repulsion between two electron distributions (*i.e.*, interaction potential of electron j with all of the other electrons), which can be defined as

$$\hat{J}_j(1)\chi_i(1) = \left[\int d\tau_2 \chi_j(2)\frac{1}{r_{12}}\chi_j(2)\right]\chi_i(1), \tag{2.30}$$

and $\hat{K}_j$ is exchange operator representing the exchange function according to the fact that the two electrons exchange their positions corresponds to Pauli's principle. The exchange of electrons in two-spin orbitals can be defined as

$$\hat{K}_j(1)\chi_i(1) = \left[\int d\tau_2 \chi_j(2)\frac{1}{r_{12}}\chi_i(2)\right]\chi_j(1). \tag{2.31}$$

The total energy of the system can be obtained from the summation of energy of each electron,

$$\sum_i^{n/2}\varepsilon_i = \sum_i^{n/2}\left\langle \chi_i(1)\middle|\hat{F}(1)\middle|\chi_i(1)\right\rangle. \tag{2.32}$$

In general, the HF wavefunction is not complicated when apply for atoms. However, it is more complicated for molecules since there is more than one center. As a consequence, the Roothaan-Hall equation has been proposed to write the one-electron molecular wavefunction in terms of atomic wavefunction or basis functions based on the concept of the LCAOs, as shown in equation (2.16). Then, the HF equation can be written as

$$\hat{F}_i(1)\sum_{\nu=1}^{N} c_{\nu i}\phi_\nu = \varepsilon_i \sum_{\nu=1}^{N} c_{\nu i}\phi_\nu. \tag{2.33}$$

The above equation can be solved easily by converting it into a matrix problem, *i.e.*, multiply on the left hand side by an integration term,

$$\sum_{\nu=1}^{N} c_{\nu i} \int \phi_{\mu}(1) \hat{F}_i \phi_{\nu}(1) d\nu_1 = \varepsilon_i \sum_{\nu=1}^{N} c_{\nu i} \int \phi_{\mu}(1) \phi_{\nu}(1) d\nu_1, \tag{2.34}$$

and then

$$\sum_{\nu=1}^{N} \hat{F}_{\mu\nu} c_{\nu i} = \varepsilon_i \sum_{\nu=1}^{N} S_{\mu\nu} c_{\nu i}, \tag{2.35}$$

or

$$\sum_{\nu=1}^{N} (\hat{F}_{\mu\nu} - \varepsilon_i S_{\mu\nu}) c_{\nu i} = 0, \qquad \mu = 1,2,3,\ldots,N. \tag{2.36}$$

The above equation is called Roothaan-Hall equation, where $S_{\mu\upsilon}$ is overlap matrix,

$$S_{\mu\nu} = \int d\nu_1 \phi_{\mu}(1) \phi_{\nu}(1). \tag{2.37}$$

The expression for each element $\hat{F}_{\mu\nu}$ of Fock matrix elements for a closed-shell system of N electrons becomes

$$\hat{F}_{\mu\nu} = H_{\mu\nu}^{core} + \sum_{\lambda=1}^{N}\sum_{\sigma=1}^{N} P_{\lambda\sigma}\left[\langle\mu\nu|\lambda\sigma\rangle - \frac{1}{2}\langle\mu\lambda|\nu\sigma\rangle\right], \tag{2.38}$$

where $H_{\mu\nu}^{core}$ is a one electron integral that can be written as

$$H_{\mu\nu}^{core} = \int d\nu_1 \phi_\mu(1) H^{core}(1) \phi_\nu(1), \tag{2.39}$$

in which

$$H^{core}(1) = -\frac{1}{2}\nabla^2 - \sum_{A=1}^{M}\frac{Z_A}{|r_1 - R_A|}. \tag{2.40}$$

Here, Z_A is the atomic number of atom A. $P_{\lambda\sigma}$ is density matrix,

$$P_{\sigma\lambda} = 2\sum_{i}^{N/2} c_{\lambda i} c_{\sigma i}. \tag{2.41}$$

According to equation (2.38), $\langle\mu\nu|\lambda\sigma\rangle$ refers to coulomb integral (two electron repulsion integral) in terms of basis functions and $\langle\mu\lambda|\nu\sigma\rangle$ represents exchange integral. Then, the total energy of a molecule can be expressed as

$$E_{molecule} = E_{elec} + E_{nuc}, \tag{2.42}$$

where E_{elec} and E_{nuc} are electronic energies of the system and nuclear repulsion, respectively, given by

$$E_{elec} = \frac{1}{2}\sum_{\mu=1}^{N}\sum_{\nu=1}^{N} P_{\mu\nu}\left(F_{\mu\nu} + H_{\mu\nu}^{core}\right), \tag{2.43}$$

and

$$E_{nuc} = \sum_{A=1}^{N}\sum_{B=1}^{N}\frac{Z_A Z_B}{R_{AB}}. \tag{2.44}$$

2.1.6 Electron correlation

The electron correlation is the electron-electron energy missing in the HF calculation. According to variational principle, the energy computed will always be higher than the exact energy (ground state energy). The difference between these two energies is called correlation energy, and can be expressed as

$$E_{corr} = E_{exact} - E_{HF}. \tag{2.45}$$

Since the HF energy is always above the exact energy, the correlation energy is always negative,

$$E_{corr} < 0. \tag{2.46}$$

It is so named to reflect the movement of electrons in HF method, since each electron moves in the static electric field of other electron and cannot see other electrons in the system.

Consequently, the improvement of MO calculations is achieved by including this correlation energy. Such calculations can be classified as wavefunction-based methods (Configuration interaction (CI) (Bauschlicher, Langhoff, and Taylor, 1990), Many-body perturbation theory (MBPT) (Møller and Plesset, 1934), Couple cluster (CC) (Bartlett, 1989)) and electron density based methods such as density functional theory (DFT) (Jones and Gunnarrson, 1989). In this work, MP2 (second-order Møller-Plesset perturbation) (Head-Gordon, Pople, and Frisch, 1988; Møller and Plesset, 1934) and B3LYP (Becke, three-parameter, Lee-Yang-Parr) (Becke, 1993; Lee, Yang, and Parr, 1988; Stephens, Devlin, Chabalowski, and Frisch, 1994) levels of accuracy will be employed for studying the effects of electron correlation on the structure and dynamics of the hydrated H_3O^+.

2.1.6.1 Density functional theory

The DFT method allows to compute all properties of systems by the electron density, $\rho(r)$, which is the function of three variables: $\rho(r) = f(x,y,z)$. The DFT method was continuously developed. The major developments are as follows: Thomas-Fermi model was introduced in 1920, Hohenberg-Kohn proved the existent DFT (Hohenberg and Kohn, 1964), the Kohn-Sham (KS) scheme was proposed (Kohn and Sham, 1965), the DFT method was applied in molecular dynamic simulations (Car-Parrinello, 1985), Becke and LYP functional was developed (Becke,

1986; Becke, 1988; Lee, Yang, and Parr, 1988) and in 1998 Walter Kohn received the Nobel prize for developing a complete DFT.

The DFT of Hohenberg, Kohn and Sham is based on the fact that the sum of the exchange and correlation energies of an electron can be calculated exactly only its density. By means of the Kohn-Sham method, the ground state electronic energy, E, can be written as

$$E = E_T + E_V + E_J + E_{xc}, \tag{2.47}$$

where E_T, E_V, E_J, and E_{xc} refer to kinetic, potential (electron-nuclear interaction energy), Coulomb and the exchange/correlation energy, respectively. All components depend on the total electron density, $\rho(r)$, except (E_T).

$$\rho(r) = 2\sum_{i}^{orbitals} \left|\psi_i(r)\right|^2 . \tag{2.48}$$

Here, ψ_i is called Kohn-Sham orbitals and the summation is carried out over pairs of electrons. Each energy components within the finite basis set can be written as

$$E_T = \sum_{\mu}^{basis\ functions} \sum_{\nu} \int \phi_\mu(r)\left[-\frac{1}{2}\nabla^2\right]\phi_\nu(r)dr, \tag{2.49}$$

$$E_\nu = \sum_{\mu}^{basis\ functions} \sum_{\nu} P_{\mu\nu} \sum_{A}^{nuclei} \int \phi_\mu(r)\left|\frac{Z_A}{r - R_A}\right|\phi_\nu(r)dr, \tag{2.50}$$

$$E_J = \sum_{\mu}^{basis\ functions} \sum_{\nu} \sum_{\lambda} \sum_{\sigma} P_{\mu\nu} P_{\lambda\sigma} (\mu\nu|\lambda\sigma), \tag{2.51}$$

$$E_{xc} = \int f(\rho(r), \nabla\rho(r), ...) dr, \tag{2.52}$$

where Z is the nuclear charge, r-R represents the distance between the electron and nucleus. f refers to exchange/correlation functional, which depends on the electron density and the gradient of the density.

There are three types of exchange/correlation functions that are presently in use: (i) functions based on the local spin density approximation, which is referred to local density model, (ii) functions based on the generalized gradient approximation, and (iii) functions that employs the exact HF exchange. The last two functions are referred to as non-local models.

In general, the DFT method divides the problem into two parts. The first part involves everything as employed in the HF method, except the exchange/correlation function. This is known as pure density functional method, including the local density model and non-local models. For example, BP, BLYP and EDF1 model, which require only the HF coulomb term (equation (2.30)). The special algorithms based on multipole expansions have been developed, called as hybrid density functional models, such as the widely used B3LYP model (which makes use of the HF exchange terms). The second part of the DFT method involves the exchange/correlation function in the calculation.

2.1.6.2 Many-body perturbation theory (MBPT)

The MBPT computes the electron correlation by treating it as a perturbation to the HF wavefunction. The basic idea of perturbation theory is to expand the energy and wavefunctions of the system in power of the small potential $\hat{V}$,

$$\hat{H} = \hat{H}_o + \lambda \hat{V}. \tag{2.53}$$

Here, $\hat{H}$ is exact Hamiltonian, $\hat{H}_0$ refers to HF Hamiltonian in ground-state, and λ is a perturbation parameter and $\hat{V}$ is the perturbation operator. The perturbed wavefunction and energy can be written in terms of Taylor expansion in powers of the perturbation parameter as,

$$E = E^{(0)} + \lambda E^{(1)} + \lambda^2 E^{(2)} + ..., \tag{2.54}$$

$$\Psi = \Psi_0 + \lambda \Psi^{(1)} + \lambda^2 \Psi^{(2)} + ... \tag{2.55}$$

The suffix 0, 1, 2,… represent zero, first and second-order corrections, respectively, and so on.

The correction energy using second-order perturbation theory (MBPT(2)) is known as second-order Møller-Plesset perturbation theory (MP2). The correction energy of MP method can be written as

$$E_{corr} = E_0^{(2)} + E_0^{(3)} + E_0^{(4)} + ... \tag{2.56}$$

The correction through $E^{(2)}$, called MP2 correction, which considers the first term of the above equation as

$$E_0^{(2)} = \sum_{b=a+1}^{\infty} \sum_{a=n+1}^{\infty} \sum_{i=J+1}^{n} \sum_{j=1}^{n-1} \frac{\left| \left\langle ab \left| \frac{1}{r_{12}} \right| ij \right\rangle - \left\langle ab \left| \frac{1}{r_{12}} \right| ji \right\rangle \right|^2}{\left(\varepsilon_i + \varepsilon_j - \varepsilon_a - \varepsilon_b \right)}. \qquad (2.57)$$

The MP2 is size consistent, it is not variational, and so the computed energy may be less than the true energy. The MP2 is perhaps the simplest model based on electron promotion which developed over HF theory. In general, the MP2 level of theory is more reliable than DFT. In practices, however, it's quite time-consuming.

2.2 Computational method

2.2.1 Molecular dynamics (MD) simulation

The MD method was firstly proposed by Alder and Wainwright (Alder and Wainwright, 1957; Alder and Wainwright, 1959) to study the interactions of hard spheres. In 1964, the major development was done by Rahman, who carried out the first simulation using realistic potential for liquid argon (Rahman, 1964). The first MD simulation of a realistic system was done for liquid water in 1974 (Stillinger and Rahman, 1974). Nowadays, the MD method becomes a very powerful tool and is widely used for the study of numerous complex matter systems.

The schematic details of MD simulation are summarized in Figure 2.2. The simulation starts with reading in the starting configurations, velocities,

accelerations and forces. The initial configuration has two simple forms, one using the random configurations and the other starting from a lattice. The essential condition of the simulation is that there are no explicitly time-dependent or velocity dependent forces that shall act on the system. In practice, the trajectories cannot be directly obtained from Newton's equation of motion. In this respect, the positions, velocities and accelerations of atom can be obtained from time integration algorithms of two successive time steps (small time interval). The energy of the system can be calculated using either molecular mechanics (MM) or QM method. Forces on each atom in the system can be derived from the energy with respect to change in the atom's position. These new forces will be used to obtain new configurations and the steps will be repeated until the system reaches equilibrium. Then, the coordinates, velocities, accelerations, forces and so on are collected for further structural and dynamical property calculations. In general, only positions and velocities are usually stored since most of the important and interesting properties can be obtained from these two quantities.

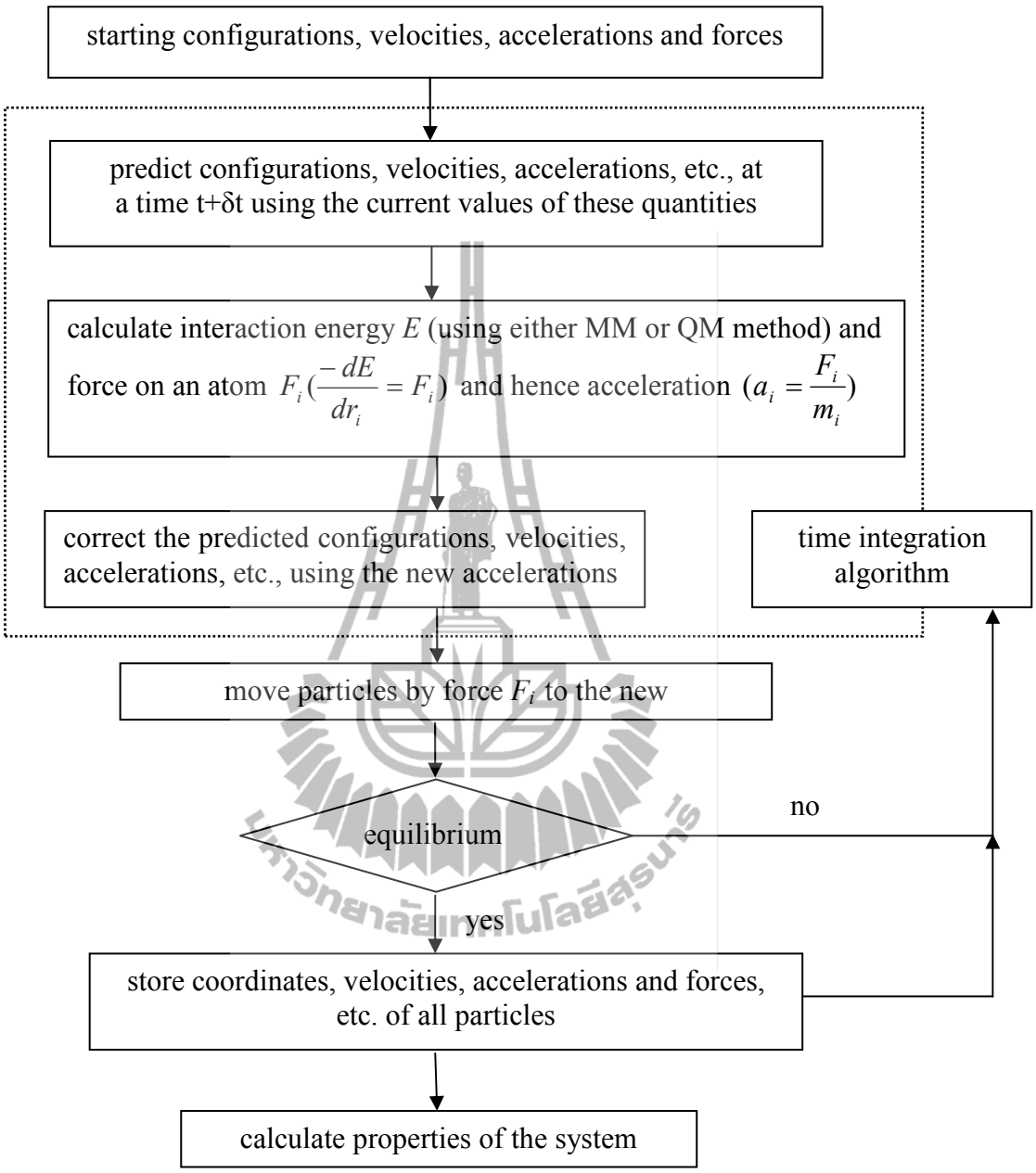

Figure 2.2 The schematic of MD simulation.

2.2.2 Statistical mechanics

The results obtained from the MD simulation provide information at the microscopic level, including atomic positions and velocities. The conversion of

microscopic information to macroscopic observables can be achieved by using statistical mechanics. The mechanical or microscopic state of a system is defined by the atomic position, *q*, and momenta, *p*, which can also be considered as coordinates in a multidimensional space, called phase space. A single point in phase space, denoted by *G*, describes the state of the system. The collection of points in phase space is known as an ensemble.

An experiment is usually made on a macroscopic sample, which contains an extremely large number of atoms or molecules sampling a huge number of conformations. In statistical mechanics, averages corresponding to experimental observables are defined in terms of ensemble averages. An ensemble average is average taken over a number of replicas of the system considered simultaneously, which can be expressed as

$$\langle A \rangle_{ensemble} = \iint dp^N dr^N A(p^N, r^N) \rho(p^N, r^N), \tag{2.58}$$

where $A(P^N,r^N)$ is the observable of interest and it is expressed as a function of the momenta, *p*, and the position, *r*, of the system. The integration is over all possible variables of *r* and *p*. The probability density of the ensemble is given by

$$\rho(p^N, r^N) = \frac{1}{Q} \exp\left[-\hat{H}(p^N, r^N)/k_B T\right], \tag{2.59}$$

where $\hat{H}$ is the Hamiltonian, *T* is the temperature, k_B is Boltzmann's constant and *Q* is the partition function,

$$Q = \iint dp^N dr^N) \exp\left[-\hat{H}(p^N, r^N)/k_B T\right] \tag{2.60}$$

This integral is extremely difficult to calculate since it must calculate all possible states of the system. By means of statistical mechanics, the experimental observables are defined in terms of time averages of property A that can be measured throughout infinite time, which can be expressed as

$$\langle A \rangle_{time} = \lim_{\tau \to \infty} \int_{t=0}^{\tau} A\left(p^N(t), r^N(t)\right) dt \approx \frac{1}{M} \sum_{t=1}^{M} A(p^N, r^N), \tag{2.61}$$

where τ is the simulation time, M is the number of time steps in the simulation and $A(P^N,r^N)$ is the instantaneous value of A.

The relationship between time averages and ensemble averages can be achieved using the Ergodic hypothesis, which states that the time averages equals the ensemble average, *i.e.*, the estimation of time average can be obtained over an enormous number of replicas of the system considered simultaneously,

$$\langle A \rangle_{time} = \langle A \rangle_{ensemble}. \tag{2.62}$$

2.2.3 Intermolecular potentials

The intermolecular interactions of the system can be described by intermolecular potential. The system's interactions can be expressed as

$$V_{total} = \sum V(i,j) + \sum V(i,j,k) + ... + \sum V(i,j,k,...,N). \quad (2.63)$$

The total interactions can be obtained from summation of two-body, three-body up to *N*-body interactions, respectively, as shown in the above equation. However, most of earlier simulations had neglected the higher order interactions (three, four,…, *N*-body), *i.e.*, they are assumed to converge rather slowly and the terms tend to have alternating signs (Kistenmacher, Popkie, and Clementi, 1974). Therefore, the system's interactions are mostly relied on the summation of all two-body interactions,

$$V_{pair} = \sum_{i<j}^{N} V_{ij}\left(\left|r_i - r_j\right|\right), \quad (2.4)$$

where r_i and r_j are the position of species i and j, respectively. This is known as pairwise additive approximations.

2.2.4 Integration algorithms

The MD method solves Newton's equation of motion for atom by taking small steps in time and using approximate numerical methods to predict all its future positions and velocity. A collection of positions is known as a trajectory. The approximate numerical method employed by one time step is known as an integration algorithm. All the integration algorithms assume that the position, velocities and accelerations can be expressed by a Taylor series expansion,

$$r(t+\delta t) = r(t) + v(t)\delta t + \frac{1}{2}a(t)\delta t^2 + \cdots, \tag{2.65}$$

$$v(t+\delta t) = v(t) + a(t)\delta t + \frac{1}{2}b(t)\delta t^2 + \cdots, \tag{2.66}$$

$$a(t+\delta t) = a(t) + b(t)\delta t + \cdots, \tag{2.67}$$

where r is the position, v is the velocity (the first derivative with respect to time) and a is the acceleration (the second derivative with respect to time).

Many integration algorithms have been developed for integrating the equations of motion. Two popular integration algorithms are Verlet algorithm (Verlet, 1967) and the predictor-corrector algorithms (Gear, 1971). The Verlet algorithm can be derived from

$$r(t+\delta t) = r(t) + v(t)\delta t + \frac{1}{2}a(t)\delta t^2, \tag{2.68}$$

$$r(t-\delta t) = r(t) - v(t)\delta t + \frac{1}{2}a(t)\delta t^2. \tag{2.69}$$

The summation of these two equations yields

$$r(t+\delta t) = 2r(t) - r(t-\delta t) + a(t)\delta t^2. \tag{2.70}$$

The Verlet algorithm uses positions and accelerations at time t and the position from time t-δt to calculate new positions at time t+δt. This algorithm can be carried out without explicit velocities, and thus this algorithm is straightforward and requires

modest storage. However, the disadvantage of this algorithm is regarded as moderate precision.

Another type of Verlet algorithm is Leap-frog algorithm (Hockney, 1970). By this algorithm, the velocities are firstly calculated at time $t+1/2\delta t$, which will further be employed to calculate the position at time $t+\delta t$. The idea of this type is that the velocities leap over the positions, and then the positions leap over the velocities. The algorithm can be expressed as

$$r(t+\delta t) = r(t) + v\left(t+\frac{1}{2}\delta t\right)\delta t, \tag{2.71}$$

$$v\left(t+\frac{1}{2}\delta t\right) = v\left(t-\frac{1}{2}\delta t\right) + a(t)\delta t. \tag{2.72}$$

The advantage of this algorithm is that the velocities are explicitly calculated, but the disadvantage is that they are not calculated at the same time as the positions. The velocities at time t can be written as

$$v(t) = \frac{1}{2}\left[v\left(t-\frac{1}{2}\delta t\right) + v\left(t+\frac{1}{2}\delta t\right)\right]. \tag{2.73}$$

For better precision, the velocity Verlet algorithm was employed. This algorithm yields positions, velocities and accelerations at time t.

$$r(t+\delta t) = r(t) + v(t)\delta t + \frac{1}{2}a(t)\delta t^2, \tag{2.74}$$

$$v(t+\delta t) = v(t) + \frac{1}{2}[a(t) + a(t+\delta t)]\delta t. \tag{2.75}$$

Another algorithm closely related to the Verlet algorithm is Beeman's algorithm (Beeman, 1976), expressed as

$$r(t+\delta t) = r(t) + v(t)\delta t + \frac{2}{3}a(t)\delta t^2 - \frac{1}{6}a(t-\delta t)\delta t^2, \tag{2.76}$$

$$v(t+\delta t) = v(t) + v(t)\delta t + \frac{1}{3}a(t)\delta t + \frac{5}{6}a(t)\delta t - \frac{1}{6}a(t-\delta t)\delta t. \tag{2.77}$$

The advantage of this algorithm is that it provides more accuracy for the velocities and better energy conservation. However, the performance of this algorithm is more complicate, and thus this make the calculation become more expensive.

For the predictor-corrector algorithm, this algorithm composes of three basic steps. In the first step, the new positions, velocities, accelerations and high-order terms are predicted by means of the Taylor series expansion:

$$r^p(t+\delta t) = r(t) + v(t)\delta t + \frac{1}{2}a(t)\delta t^2 + \frac{1}{6}b(t)\delta t^3 + \frac{1}{24}c(t)\delta t^4 + \cdots, \tag{2.78}$$

$$v^p(t+\delta t) = v(t) + a(t)\delta t + \frac{1}{2}b(t)\delta t^2 + \frac{1}{6}c(t)\delta t^3 + \cdots, \tag{2.79}$$

$$a^p(t+\delta t) = a(t) + b(t)\delta t + \frac{1}{2}c(t)\delta t^2 + \cdots, \tag{2.80}$$

$$b^p(t+\delta t) = b(t) + c(t)\delta t + \cdots. \tag{2.81}$$

Here, the superscript *p* represents as predicted values, *r* and *v* stand for the complete set of positions and velocities, respectively, and *a* represents the accelerations and *b* denotes all the third time derivatives of *r*. The next step is to calculate the force at time $t+\delta t$ from the new position r^p to give the correct accelerations, $a^c(t+\delta t)$. The difference between the correct acceleration and predicted acceleration constitutes an error signal.

$$\Delta a(t+\delta t) = a^c(t+\delta t) - a^p(t+\delta t). \tag{2.82}$$

The last step is the corrector, in which the error signal is used to correct position and their derivatives.

$$r^c(t+\delta t) = r^p(t+\delta t) + c_0 \Delta a(t+\delta t), \tag{2.83}$$

$$v^c(t+\delta t) = v^p(t+\delta t) + c_1 \Delta a(t+\delta t), \tag{2.84}$$

$$a^c(t+\delta t) = a^p(t+\delta t) + c_2 \Delta a(t+\delta t), \tag{2.85}$$

$$b^c(t+\delta t) = b^p(t+\delta t) + c_3 \Delta a(t+\delta t). \tag{2.86}$$

2.2.5 Periodic boundary condition

The periodic boundary is an important technique in the MD simulation. This technique is employed for removing effect of the surface, which influence in finite sample of matter.

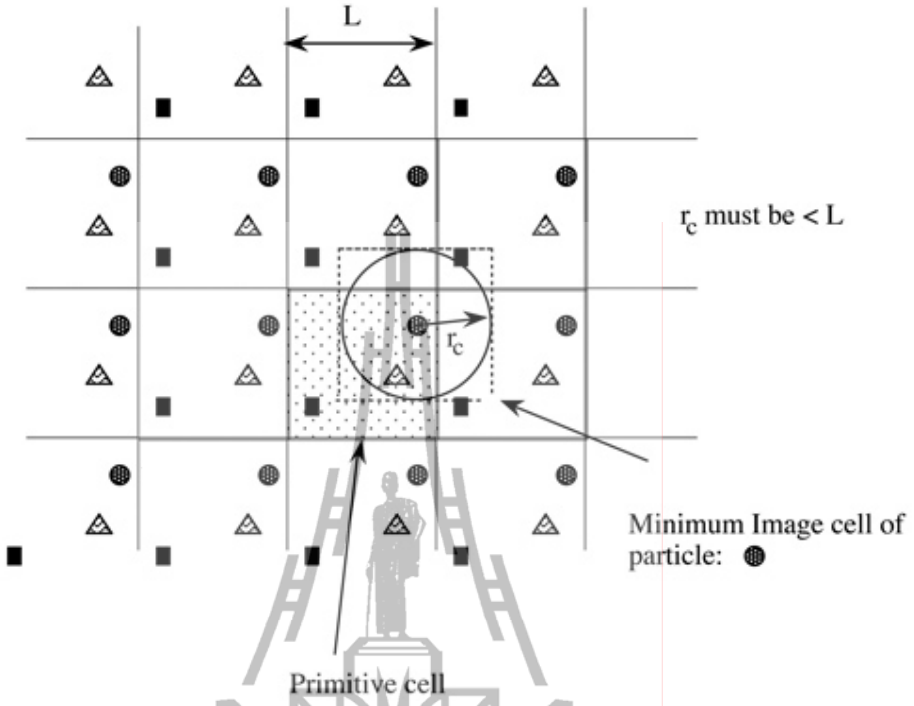

Figure 2.3 Periodic boundary condition in two dimensions.

Figure 2.3 illustrates the concept of periodic boundary conditions. The shaded box represents the system we are simulating, called primitive cell. The surrounding boxes are exact copies of the primitive cell in every detail, *i.e.*, every particle together with the velocities are equivalent. The procedure is that whenever an atom leaves the primitive cell, it is replaced by another one with the same velocity entering from the opposite cell face. Thereby the number of atom in cell is conserved.

The periodic boundary condition can solve the problem of surface effect. However, according to this technique, each particle in primitive cell can interact not only with other particles in the same cell, but also with their images in the neighboring cell. To solve this problem, the minimum image criterion is then

employed, in which particles in the primitive cell are allowed to interact only with the particles or particle images closest to them, as shown in Figure 2.3.

2.2.6 Cut-off and potential at cut-off

With regard to Figure 2.3, r_c is the cut-off radius, which is commonly applied along with the minimum image criterion when calculating the energy and force between two atoms, *i.e.*, in order to reduce the number of non-bonded interactions that will be calculated in each MD step. In general, the non-bonded interactions are of the most time-consuming part of the energy and force calculations in classical MD simulation. For example, for N atom system, the number of non-bonded interactions are $N*(N-1)/2$. In general, the cut-off limit should be no more than half of the box length ($\leq L/2$). On the other hand, only non-bonded interactions for $r \leq r_c$ are taken into account for calculating energy or force, while the interactions for $r > r_c$ are ignored.

According to cut-off, the most straightforward way is the simple truncation at $r = r_c$. This leads to a discontinuity in potential energy and force at the cut-off distance. In practice, the MD simulation cannot deal with such situation because of poor energy conservation. To solve this problem, a shifted potential is employed in order to modify the potential at the cut-off radius,

$$V(r) = \begin{cases} \phi_{LJ}(r) - \phi_{LJ}(r_c) & if \quad r \leq r_c \\ 0 & if \quad r > r_c \end{cases}, \tag{2.87}$$

where $\phi_{LJ}(r_c)$ is equal to the value of the potential at the cut-off distance. Another way is to switch off the potential between a chosen distance r and r_c, which may not affect the equilibrium structure due to applied switching function over a narrow range, which can be expressed as

$$V^{SF}(r) = \begin{cases} \phi_{LJ}(r) - \phi_{LJ}(r_c) - \left(\frac{d\phi_{LJ}(r)}{dr}\right)_{r=r_c}(r - r_c) & r \le r_c \\ 0 & r > r_c. \end{cases} \tag{2.88}$$

2.2.7 Neighbor lists

Although the cut-off is used, this may not actually reduce the time for calculating the non-bonded interactions because the distance between every pair of atoms still have to be calculated in each simulation step. In practice, since most of atoms move within a time step of less than 0.2 Å, the local neighbors of a given atom remain the same for many time steps.

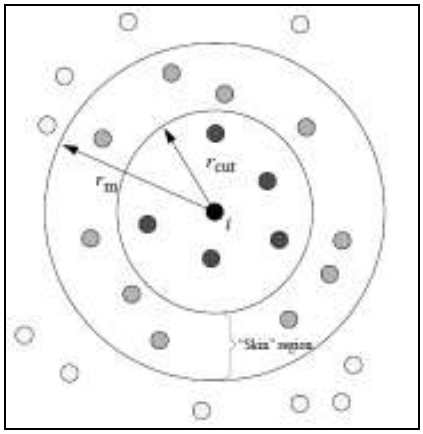

Figure 2.4 Verlet neighbor list.

To avoid wasteful recalculation for every single time, the Verlet neighbor list (see Figure 2.4) is employed, which creates lists of all atoms within a certain distance of every atom. In this respect, every atom only interacts in its neighbor list. That is, it stores all atoms within the cut-off distance (r_{cut}) and all atoms that locate slightly further away from the cut-off distance (r_m).

2.2.8 Long-range interactions

Since the charge-charge interactions in a range greater than half of box length still has significance, the neglect of long-range interactions of cut-off may introduce serious errors in the simulation. There are two common methods used for the treatment of long-range forces. One is Ewald summation (Ewald, 1921; Heyes, 1981), computing the interaction energy of ionic crystals by including the interaction of the particle with all the other of periodic systems. The potential energy of the Ewald summation can be expressed as

$$V^{ZZ} = \frac{1}{2}\sum_{n}{}' \left(\sum_{i=1}^{N}\sum_{j=1}^{N} Z_i Z_j \left| r_{ij} + n \right|^{-1} \right), \qquad (2.89)$$

where Z_i and Z_j are charges. The sum over n is the sum over all simple cubic lattice point. The prime indicates that we omit $t = j$ for $n = 0$.

However, the Ewald summation is quite an expensive task. An alternative is to apply a reaction field method (Foulkes and Haydock, 1989). In the reaction field method, it is assumed that any given molecule is surrounded by a spherical cavity (R) of finite radius. By this scheme, the electrostatic interactions in

the sphere cavity are calculated explicitly, while outside the cavity the system is treated as a dielectric continuum, which dielectric responds to instantaneous dipole inside the sphere. This contributes to the energy as

$$U_{rf} = \frac{1}{2}\sum_{i=1}\mu_i \cdot \frac{2\left(\varepsilon'_s - 1\right)}{2\varepsilon'_s + 1}\frac{1}{r_c^3}\sum_{j\in R_i}\mu_j . \tag{2.90}$$

2.3 Research methodology

2.3.1 Conventional *ab initio* QM/MM MD simulation

By means of the conventional QM/MM technique (Intharathep, Tongraar, and Sagarik, 2006; Kerdcharoen, Liedl, and Rode, 1996; Rode, Schwenk, Hofer, and Randolf, 2005; Rode, Schwenk, and Tongraar, 2004), the system is divided into two parts, namely QM and MM regions. The QM region, *i.e.*, a sphere which includes the H_3O^+ ion and its surrounding water molecules, is treated by quantum mechanics, while the MM region, the rest of the system, is described by classical pair potentials.

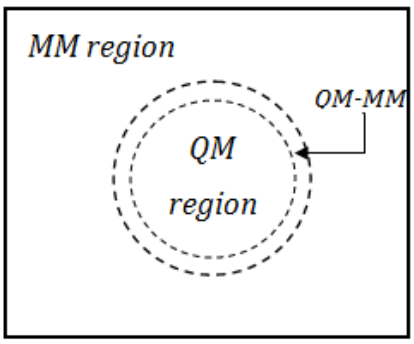

Figure 2.5 QM/MM scheme.

According to Figure 2.5, the total energy (E_{tot}) of the system can be obtained from the summation of three component parts, namely the interactions within the QM, in the MM and between the QM and MM regions;

$$E_{tot} = \left\langle \Psi_{QM} \middle| \hat{H} \middle| \Psi_{QM} \right\rangle + E_{MM} + E_{QM-MM}, \tag{2.91}$$

where $\left\langle \Psi_{QM} \middle| \hat{H} \middle| \Psi_{QM} \right\rangle$ refers to the interactions within the QM region, E_{MM} is the interactions within the MM region and $E_{QM\text{-}MM}$ is the interactions between the QM and MM regions.

By the conventional QM/MM technique, a thin switching layer located between the QM and MM regions is introduced to smooth the transition due to the solvent exchange, as show in Figure 2.6.

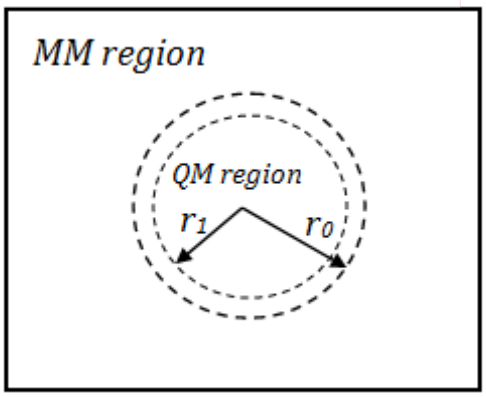

Figure 2.6 System's partition.

During the QM/MM simulation, exchanges of water molecules between the QM and MM regions can occur frequently. With regard to this point, the force acting on each particle in the system is switched according to which region the water molecule was entering or leaving the QM region and was defined as

$$F_i = S_m(r)F_{QM} + (1 - S_m(r))F_{MM}, \tag{2.92}$$

where F_i refers to force on each particle in the system, F_{QM} and F_{MM} are quantum mechanical and molecular mechanical forces, respectively. $S_m(r)$ is a smoothing function,

$$S_m(r) = 1 \qquad for\, r \le r_1, \tag{2.93}$$

$$S_m(r) = \frac{\left(r_0^2 - r^2\right)\left(r_0^2 + 2r^2 - 3r_1^2\right)}{\left(r_0^2 - r_1^2\right)^3} \qquad r_1 < r < r_0, \tag{2.94}$$

$$S_m(r) = 0 \qquad for\, r > r_0, \tag{2.95}$$

where r_1 and r_0 are the distances characterizing the start and the end of the QM region, applied within an interval of 0.2 Å to ensure a continuous change of forces at the transition between QM and MM regions.

2.3.2 QM/MM MD based on ONIOM-XS method

The conventional QM/MM technique is an efficient tool for studying several systems. However, some unsolved problems still exist for such QM/MM

scheme. First, only the exchanging particles crossings between QM and MM regions are treated by the smoothing function, but ignore the whole particles in the QM region. This is not reliable since immediate addition or deletion of a particle in the QM region due to the solvent exchange also affects the forces acting on the remaining particles in the QM region. Thus, the conventional QM/MM simulation may provide numerical instability of forces whenever the solvent exchange process occurs in the system. Second, the conventional QM/MM scheme cannot clearly define the appropriate energy expression when the solvent exchange process occurs during the simulation.

To solve these problems, a more sophisticated QM/MM MD technique based on ONIOM-XS method has been proposed (Kerdcharoen and Morokuma, 2002; Kerdcharoen and Morokuma, 2003). The ONIOM (Own N-layered Integrated molecular Orbital and molecular Mechanics) method was originally proposed by Morokuma *et al* (Svensson, Humbel, Froese, Matsubara, Sieber, and Morokuma, 1996) and the extension of the ONIOM method for studying condensed-phase systems was carried out by Kerdcharoen and co-worker, called ONIOM-XS (XS = eXtension to Solvation)

By the ONIOM-XS method, the system can handle not only the QM + MM combination in the simulation box (*i.e.*, similar to the conventional QM/MM method) but also the QM + QM combination or multilayer combination, such as QM + QM + QM or QM + QM + MM. In addition, this technique allows forces on all QM particles to be smoothed during particle exchange, and thus, clearly defines the system's energy expression.

With regard to the ONIOM-XS MD simulation, the system is divided into two subsystems (QM + MM). The H_3O^+ ion and some water molecules were treated by quantum mechanics in the "high-level" QM sphere floating inside a cube of "low-level" MM subsystem. A thin switching shell located between the QM and MM subsystems is introduced to smooth the transition due to the solvent exchange, as shown in Figure 2.7

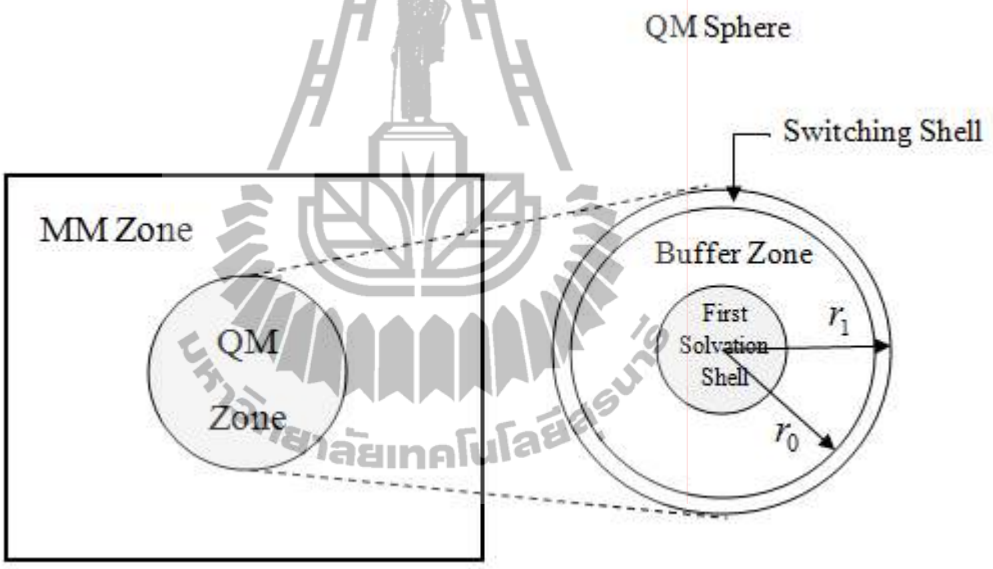

Figure 2.7 Schematic diagram of the QM/MM MD technique based on ONIOM-XS method.

Given n_1, l and n_2 as number of particles in the QM, in the switching shell and in the MM zone, respectively, and N as the total number of particles (= n_1 + l + n_2), the potential energy of the system can be written in two ways based on the

ONIOM extrapolation scheme (Kerdcharoen and Morokuma, 2003). If the switching layer is included into the QM zone, the energy expression is defined as

$$E^{ONIOM}(n_1+l;N) = E^{QM}(n_1+l) - E^{MM}(n_1+l) + E^{MM}(N). \qquad (2.96)$$

On the other hand, if the switching layer is considered as part of the MM subsystem, the energy expression is described by

$$E^{ONIOM}(n_1;N) = E^{QM}(n_1) - E^{MM}(n_1) + E^{MM}(N). \qquad (2.97)$$

The potential energy of the entire system is then the combination between the energy in equations (2.96) and (2.97);

$$E^{ONIOM\text{-}XS}(\{r_1\}) = (1-\bar{s}(\{r_1\}))\cdot E^{ONIOM}(n_1+l;N) + \bar{s}(\{r_1\})\cdot E^{ONIOM}(n_1+N), \qquad (2.98)$$

where $\bar{s}(\{r_l\})$ is an average over a set of switching functions for individual exchanging particle in the switching layer $s_i(x_i)$,

$$\bar{s}(\{r_1\}) = \frac{1}{l}\sum_{i=1}^{l} s_i(x_i). \qquad (2.99)$$

To describe how equation (2.96) – (2.99) work; suppose that one particle is leaving the QM sphere and entering into the switching layer, the immediate disappearance of

a particle affects the QM energy, calculated by equation (2.97). In order to reduce the energy shock, the exchanging particle is still including in the QM calculation as shown in equation (2.96). The exchanging particle contributes to the total energy as shown in equation (2.98) but it will be gradually decreased depending on the distance it move away from the QM sphere until becomes to zero at the boundary between the switching layer and the MM zone. If there are multiple exchanging particles, an average over the switching functions is used, as shown in equation (2.99). The switching function can be written in a polynomial form as

$$S_i(x_i) = 6\left(x_i - \frac{1}{2}\right)^5 - 5\left(x_i - \frac{1}{2}\right)^3 + \frac{15}{18}\left(x_i - \frac{1}{2}\right) + \frac{1}{2}, \qquad (2.100)$$

where $x_i = ((r_i - r_0)/(r_1 - r_0))$, and r_0 and r_1 are the radius of inner and outer surfaces of the switching shell, respectively, and r_i is the distance between the center of mass of the exchanging particle and the center of QM sphere. The switching function has an S-shape and converges to 0 and 1 at r_0 and r_1, respectively. The gradient of the energy can be written as

$$\begin{aligned}\nabla_R E^{ONIOM-XS}(\{r_l\}) = &\left(1 - \bar{s}(\{r_l\})\right)\cdot \nabla_R E^{ONIOM}(n_l + l; N) + \bar{s}(\{r_l\}) \\ &\cdot \nabla_R E^{ONIOM}(n_1; N) + \frac{1}{(r_1 - r_0)} \nabla \bar{s}(\{r_l\}) \\ &\cdot \left(E^{ONIOM}(n_1; N) - E^{ONIOM}(n_1 + l; N)\right).\end{aligned} \qquad (2.101)$$

CHAPTER III

RESEARCH PROCEDURES

3.1 Estimation of electron correlation effects

On the basis of the QM/MM technique, the quality of the simulation results depends crucially on the selection of QM method, as well as the basis set and size of QM region. In this respect, the use of correlated methods, although it is extremely time-consuming, can significantly improve the quality of the simulation results. To estimate the effects of electron correlation, geometry optimizations of the H_3O^+-$(H_2O)_3$ complex were carried out using the *ab initio* calculations at different levels of accuracy, namely HF, B3LYP and higher correlated levels using D95(d,p) basis set (Dunning, and Hay, 1976; Hay, and Wadt, 1985) with BSSE correction (Intharathep, Tongraar, and Sagarik, 2006). The D95(d,p) basis set was chosen, since it was employed in this thesis. This basis set was considered to be large enough with respect to the available computer facility. The structures and binding energies of the optimized H_3O^+-$(H_2O)_3$ complex are summarized in Table 3.1. In comparison with the results of the highly correlated methods, such as MP2, MP4, CCD and CID, it is clear that the neglect of electron correlation at the HF level results in a recognizable weakening of the binding energies. In contrast, the B3LYP calculations, although they provide reasonable geometries, predict too strong ion-water interactions. The reason could be ascribed to the overestimation of the correlation energy (Rode, 2004). With regard to the data in Table 3.1, it is obvious that the inclusion of electron correlation

effects, if possible, could more or less improve the quality of the QM/MM results. In this work, therefore, two QM/MM MD simulations, namely B3LYP/MM and MP2/MM, will be performed in order to investigate the effects of electron correlation on the structure and dynamics of the hydrated H_3O^+ ion.

Table 3.1 Structures and binding energies of optimized H_3O^+-$(H_2O)_3$ complex, calculated at HF, B3LYP, MP2 and higher correlated methods using D95(d,p) basis set (Intharathep, Tongraar, and Sagarik, 2006).

Method	ΔE(kcal mol^{-1})	∠HOH (°)	O-H (Å)	O-O (Å)
HF	-76.917	112.90	1.03	2.56
B3LYP	-90.365	114.19	1.02	2.54
MP2	-82.696	113.08	1.01	2.55
MP4	-79.580	113.29	1.00	2.56
CCD	-79.403	113.25	1.00	2.56
CID	-80.737	114.26	0.99	2.56

O-H and ∠HOH denote the geometry of H_3O^+ and O-O refers to the distance between the oxygen atom of H_3O^+ and of water.

3.2 Selection of QM size

To define the size of QM region, the preliminary HF/MM, B3LYP/MM and MP2/MM simulations, in which only the ion was treated quantum mechanically using HF, B3LYP and MP2 methods, respectively, have been performed for 30,000 time steps, and the corresponding O_{ox}-O_w RDFs are plotted in Figure 3.1. Here, the size of QM region could be defined with respect to the first minimum of the O_{ox}-O_w RDFs.

As can be seen in Figure 3.1, the first minimum of the O_{ox}-O_w RDFs obtained from all simulation types are located at around 3.0 Å, where the integrations up to the first minima yield about 3-4 water molecules. This implied that a QM size with diameter of 6.0 Å seems to be sufficient to include the whole first hydration shell of H_3O^+. However, since it has been suggested that the PT mechanism is motivated by fluctuations in the second shell of HB network around H_3O^+, a larger QM size seems to be necessary for this particular system. In this regard, it should be noted that the increase of QM size can significantly increase the number of water molecules, and thus the amount of CPU time. Figure 3.2 shows the requirement of CPU time for HF, B3LYP and MP2 force calculations with respect to the size of $H_3O^+(H_2O)_n$ complexes. In comparison to the HF calculations, it is obvious that the calculations based on both B3LYP and MP2 methods are rather time-consuming. For the first part of this work, therefore, the B3LYP/MM and MP2/MM simulations will be performed using a moderate QM size with diameter of 7.6 Å. This QM region includes the complete first hydration shell of H_3O^+ (*i.e.*, the ion plus 3-4 water molecules) and some (3-4) next nearest-neighbor water molecules.

For the second part of this work, since the HF method is employed, the conventional HF/MM and ONIOM-XS MD simulations will be performed using a relatively larger QM size with diameter of 8.4 Å. This QM region contains the ion and about 8-12 nearest-neighbor water molecules.

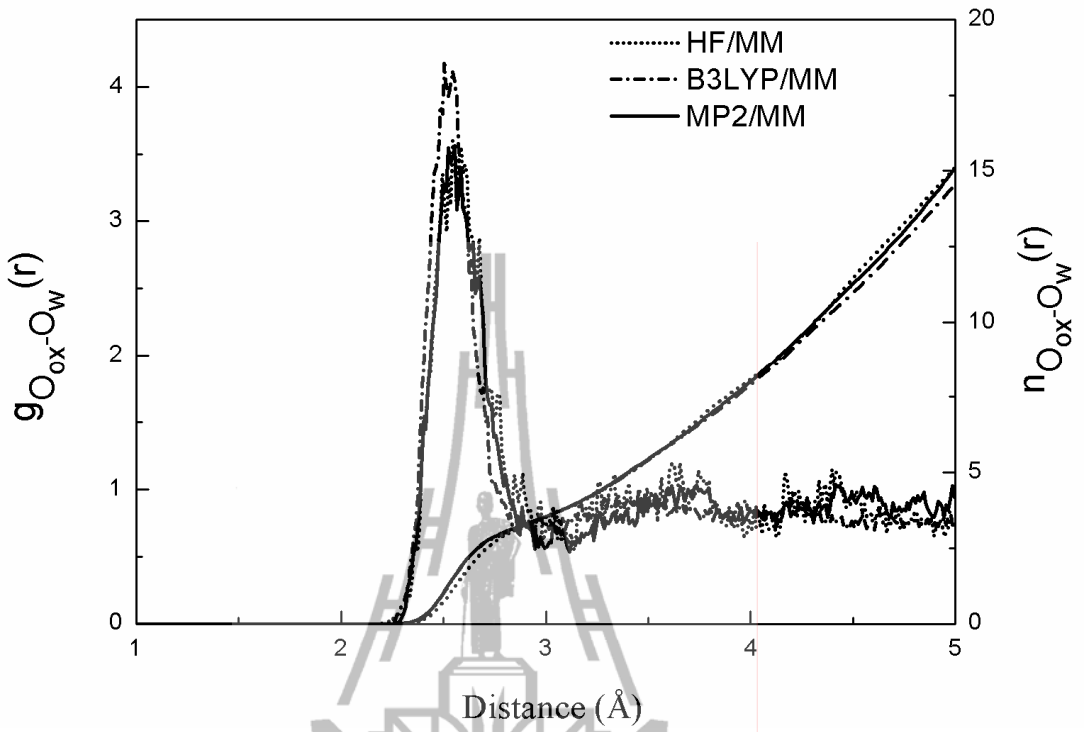

Figure 3.1 O_{ox}-O_w radial distribution functions and their corresponding integration numbers, as obtained from the preliminary HF/MM, B3LYP/MM and MP2/MM simulations using DZP(d,p) basis set.

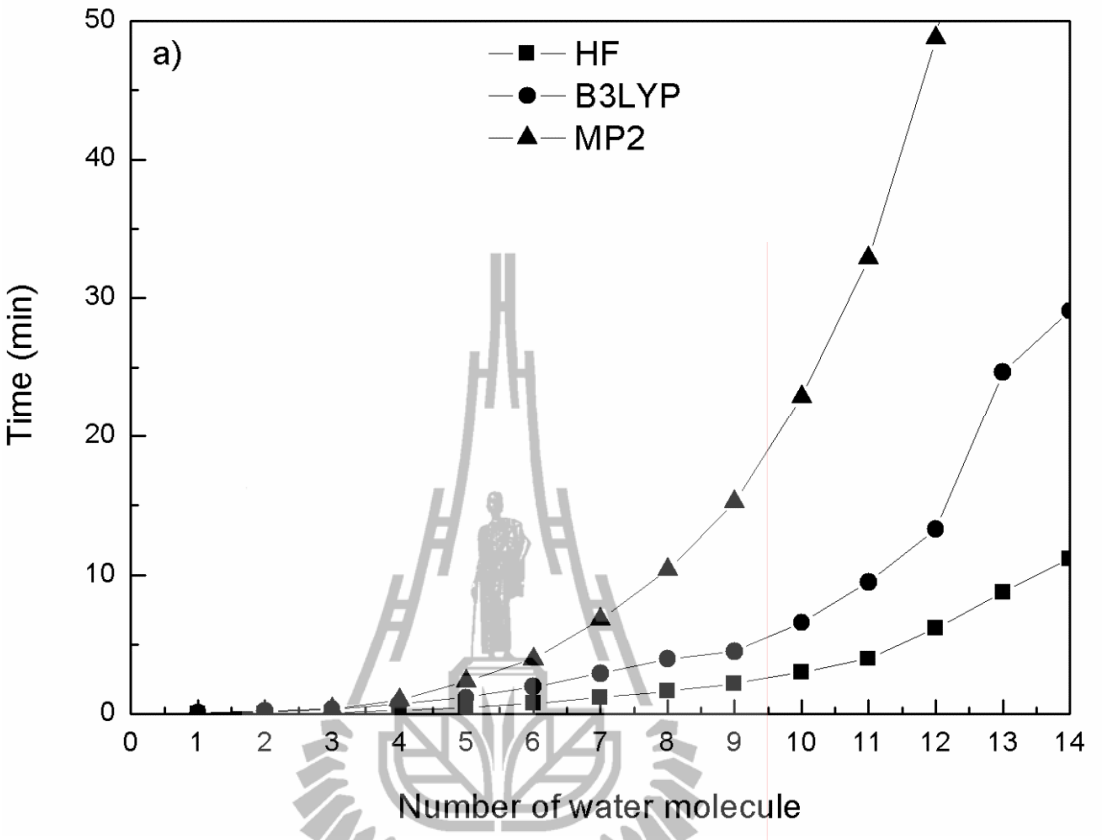

Figure 3.2 The requirement of CPU time for HF, B3LYP and MP2 force calculations with respect to the size of $H_3O^+(H_2O)_n$ complexes. All calculations were performed on the computational chemistry research laboratory cluster (CPU 4×2.60 GHz, memory (RAM) 2.94 GB) with Gaussian 03 packages of program.

3.3 Simulation details

For the first part of this work, the B3LYP/MM and MP2/MM MD simulations were separately performed in a canonical ensemble at 298 K with periodic boundary conditions. The starting configuration was the one obtained from the previous HF/MM work (Intharathep, Tongraar, and Sagarik, 2006). The system's temperature was kept constant using the Berendsen algorithm (Berendsen, Postma, van Gunsteren,

DiNola, and Haak, 1984). A periodic box, with a box length of 18.17 Å, contains one H_3O^+ and 199 water molecules, corresponding to the experimental density of pure water. For the QM size, a QM diameter of 7.6 Å was chosen, *i.e.*, the same QM size as employed in the previous HF/MM MD study (Intharathep, Tongraar and Sagarik, 2006). The reaction-field method (Adams, Adams, and Hills, 1979) was employed for the treatment of long-range interactions. The Newtonian equations of motions were treated by a general predictor-corrector algorithm. The time step size was set to 0.2 fs, which allows for the explicit movement of the hydrogen atoms of water molecules. The B3LYP/MM and MP2/MM MD simulations were started with the system's re-equilibration for 20,000 time steps, followed by another 108,000 (B3LYP/MM) and 79,000 (MP2/MM) time steps to collect system's configurations at every 10^{th} steps.

In the second part, the conventional HF/MM and ONIOM-XS MD simulations were carried out using the same simulation protocol as employed in the first part. By the use of larger QM size with diameter of 8.4 Å, all interactions within the QM region were treated at HF level of accuracy. Both conventional HF/MM and ONIOM-XS MD simulations were started with the system's re-equilibration for 20,000 time steps, followed by another 100,000 time steps to collect system's configurations at every 10^{th} steps.

3.4 Determination of system's properties

3.4.1 Structural properties

Structure of the hydrated H_3O^+ will be analyzed with respect to pair-pair radial distribution functions (RDFs), a measure to determine the correlation between particles within a system. It is a measure of, on average, the probability of

finding a particle at a distance of r away from a given reference particle, *i.e.*, determining how many particles are located within a distance of r and $r+\Delta r$ away from a particle. The radial distribution function can be expressed as

$$g_{\alpha\beta} = N_{\alpha\beta}(r)/\left(4\pi r^2 \Delta r \rho_\beta\right), \tag{3.1}$$

where $N_{\alpha\beta}(r)$ is the average number of β sites located in the shell (r, $r+\Delta r$) centered on site α, and $\rho_\beta = \frac{N_\beta}{v}$ is the average number density of β sites in the system.

In addition, the structural properties of the hydrated H_3O^+ will be interpreted in terms of angular distribution functions (ADFs) and the orientation of water molecules surrounding the ions.

3.4.2 Dynamic properties

In this work, the dynamical properties of the hydrated H_3O^+ will be interpreted with respect to the mean residence times (MRTs). MRTs are the average amount of time that a particle spends in a particular system. During the QM/MM MD simulations, trajectories of each species in the system were monitored. In this work, the rate of water exchange processes at the ions was determined through the MRT of water molecules, which calculated using a "direct" method (Hofer, Tran, Schwenk, and Rode, 2004). Based on the direct method, the whole trajectories were inspected either the leaving or entering a coordination shell of ligands. The direct method can be expressed as

$$MRT(\tau) = \frac{CN \times t_{sim}}{N_{ex}}, \tag{3.2}$$

where CN is the average number of ligand in the shell, t_{sim} is the duration of the simulation and N_{ex} equals the number of events. In this work, the parameters t^* were set to 0.0 and 0.5 ps, which correspond to the lifetime of hydrogen bond and a suitable exchange of ligands in the immediate neighborhood of given molecule, respectively.

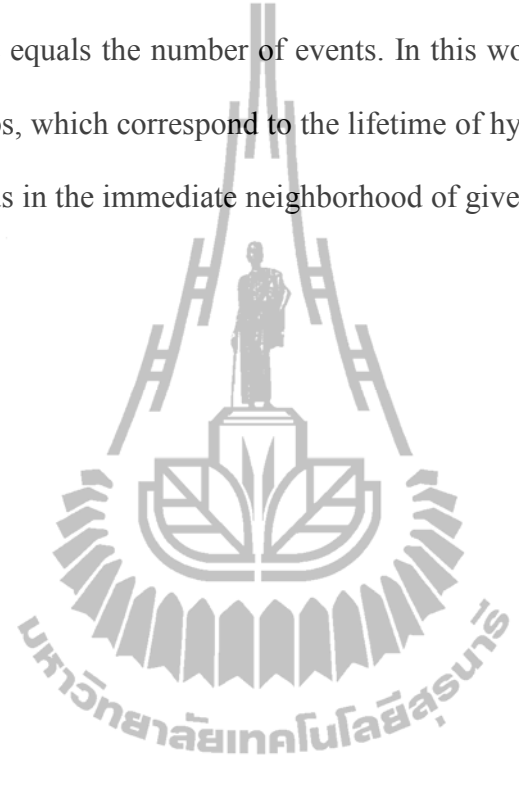

CHAPTER IV

RESULTS AND DISCUSSION

According to the research objectives in Chapter I, the results of this study will be divided into two parts, namely 1) the study of electron correlation effects on the structure and dynamics of the hydrated H_3O^+ ion and 2) the assessment of the conventional QM/MM scheme for the study of such system and the comparing to the results obtained by the more accurate QM/MM technique based on ONIOM-XS method. In this context, it should be noted that the results obtained by the QM/MM simulations can provide detailed information with respect to the structure and dynamics of the hydrated H_3O^+ complex at the state "before" and/or "after" the actual PT process, rather than to visualize pathway of the PT mechanism.

4.1 Correlation effects on the structure and dynamics of the H_3O^+ hydrate: B3LYP/MM and MP2/MM MD simulations

4.1.1 Structural properties

Structural properties of the hydrated H_3O^+ obtained by the B3LYP/MM and MP2/MM MD simulations are characterized through a set of O_{ox}-O_w, O_{ox}-H_w, H_{ox}-O_w and H_{ox}-H_w RDFs and their corresponding integration numbers, as shown in Figure 4.1. In this context, the subscripts "ox" and "w" refer to H_3O^+ and water, respectively. As can be seen in Figure 4.1, the hydration shell structure of H_3O^+ derived by means of B3LYP/MM and MP2/MM simulations is rather identical, and is

significantly different from the previous HF/MM work. In terms of O_{ox}-O_w RDFs (Figure 4.1a), both B3LYP/MM and MP2/MM simulations show slightly sharper first O_{ox}-O_w peaks with maxima at shorter distances of 2.57 and 2.54 Å, respectively, when compared to the HF/MM's O_{ox}-O_w peak with a maximum at 2.60 Å. Integrations of the O_{ox}-O_w peaks up to their first minimum yield average coordination numbers of 3.4 and 3.3, respectively. These observed coordination numbers are in good accord with the recent experimental data (Botti, Bruni, Imberti, Ricci, and Soper, 2005), which demonstrate the prevalence of a distorted $H_9O_4^+$ structure (*i.e.*, as a consequence of a fourth water molecule that can be found occasionally within the first hydration shell of H_3O^+). With regard to the previous HF/MM study (Intharathep, Tongraar, and Sagarik, 2006), although it revealed a slightly more flexible hydration shell structure of H_3O^+, the observed coordination number of 3.4 is consistent with the present B3LYP/MM and MP2/MM simulations. According to Figure 4.1a, the first O_{ox}-O_w peaks are not well separated from the bulk region, indicating that exchange of water molecules between the first hydration shell and the bulk can take place frequently during the simulations. In Figure 4.1b, both B3LYP/MM and MP2/MM simulations reveal the first O_{ox}-H_w peaks with a maximum of about 0.2 Å shorter than that of the HF/MM's O_{ox}-H_w peak. In spite of the observed shortening of the O_{ox}---H_w distances, the feature of the first O_{ox}-H_w peaks from both B3LYP/MM and MP2/MM simulations clearly suggests less possibility of finding O_{ox}---H_w hydrogen bond interactions on top of the H_3O^+ ion. This implicates that the H_3O^+ ion is not strongly shared in a local tetrahedral network of water.

The characteristics of hydrogen bonds between the H_3O^+ ion and its nearest-neighbor water molecules can be interpreted from the H_{ox}-O_w and H_{ox}-H_w

RDFs, as shown in Figure 4.1c and d, respectively. As compared to the previous HF/MM work (Intharathep, Tongraar, and Sagarik, 2006), both B3LYP/MM and MP2/MM simulations reveal significantly sharper first H_{ox}-O_w and H_{ox}-H_w peaks with a maximum exhibited at the shorter H_{ox}---O_w and H_{ox}---H_w distances, which are consistent with the resulting O_{ox}-O_w and O_{ox}-H_w RDFs. In this respect, the observed differences between the present B3LYP/MM and MP2/MM simulations and the previous HF/MM results could be attributed to the inclusion of the electron correlation effects at the B3LYP and MP2 levels of accuracy, which is reflected in strengthening of the H_3O^+-water hydrogen bond interactions. According to the B3LYP/MM results, however, it should be realized that the DFT methods usually do account for an unknown (uncontrollable) amount of electron correlation, *i.e.*, as a consequence of the semiempirical character of the exchange-correlation functional (Becke, 1993). On the other hand, the MP2/MM results would be the most suitable benchmark in discussing the effects of electron correlation. Recently, a MP2/MM simulation of pure water has also reported the influence of electron correlation in tightening the structure of the water's first coordination shell (Xenides, Randolf, and Rode, 2005). This clearly indicates the important treatment of electron correlation in describing both the H_3O^+-water and water-water interactions. In Figure 4.1c, the integrations up to the first minimum of the H_{ox}-O_w RDFs yield one (*i.e.*, 0.98 and 1.01 for the B3LYP/MM and MP2/MM simulations, respectively) well-defined hydrogen bond between each hydrogen atom of H_3O^+ and its nearest-neighbour water molecules.

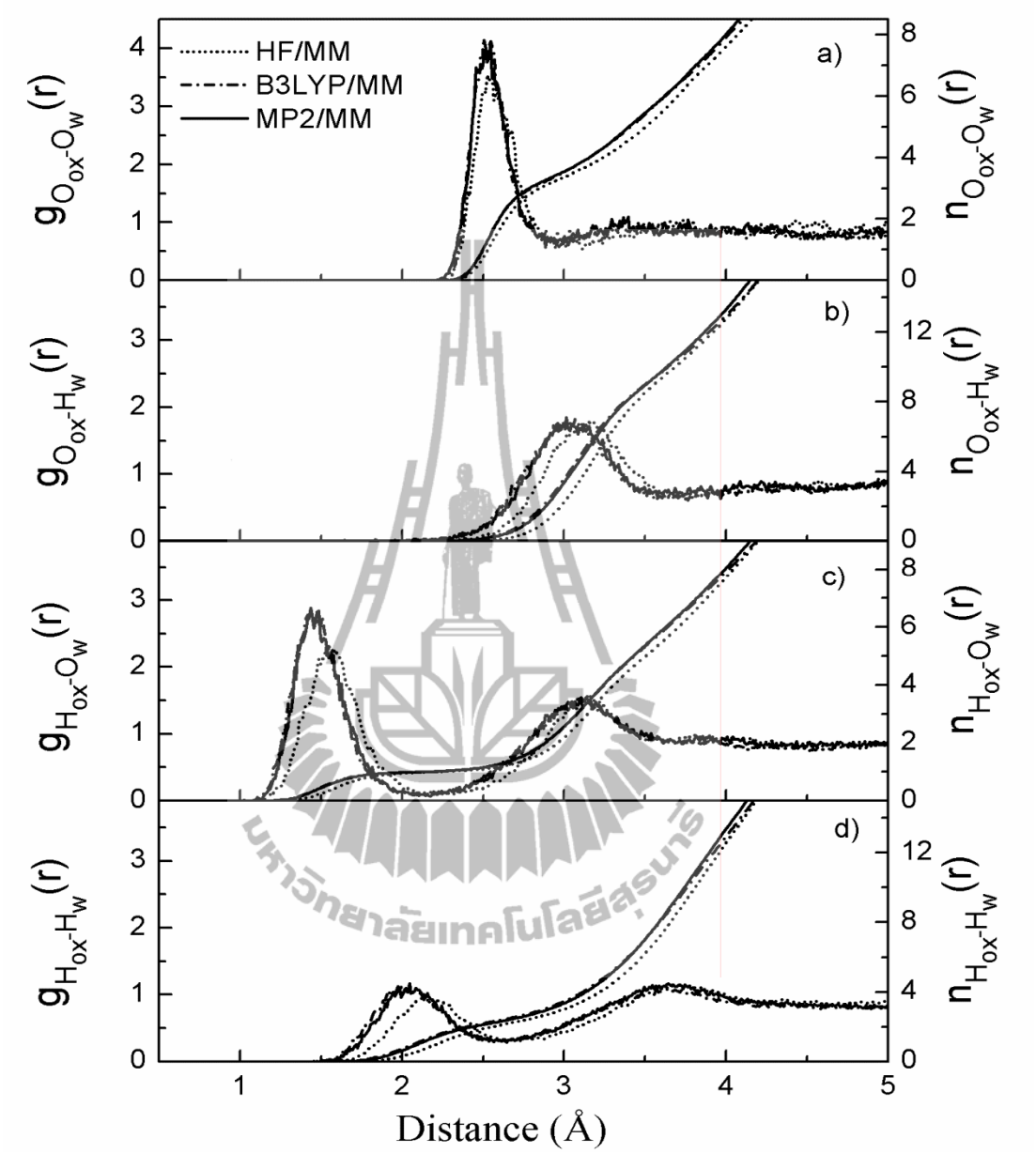

Figure 4.1 a) O_{ox}-O_w, b) O_{ox}-H_w, c) H_{ox}-O_w and d) H_{ox}-H_w radial distribution functions and their corresponding integration numbers, as obtained from HF/MM (Intharathep, Tongraar, and Sagarik, 2006), B3LYP/MM and MP2/MM MD simulations.

Figure 4.2 shows the probability distributions of the number of surrounding water molecules, calculated up to first minimum of the O_{ox}-O_w RDFs. With regard to all QM/MM simulation types, it is obvious that the first hydration shell of H_3O^+ prefers a coordination number of 3, which corresponds to the three nearest-neighbor water molecules strongly H-bonded to each of H_3O^+ hydrogen atoms. Nevertheless, a contribution of the coordination number of 4 is remarkable. In this respect, it could be demonstrated that besides the first three nearest-neighbor water molecules that strongly H-bonded to the H_3O^+, other nearest-neighbor waters, in particular the forth water molecule, can play a role in the formation and orientation of the hydrated H_3O^+ complex.

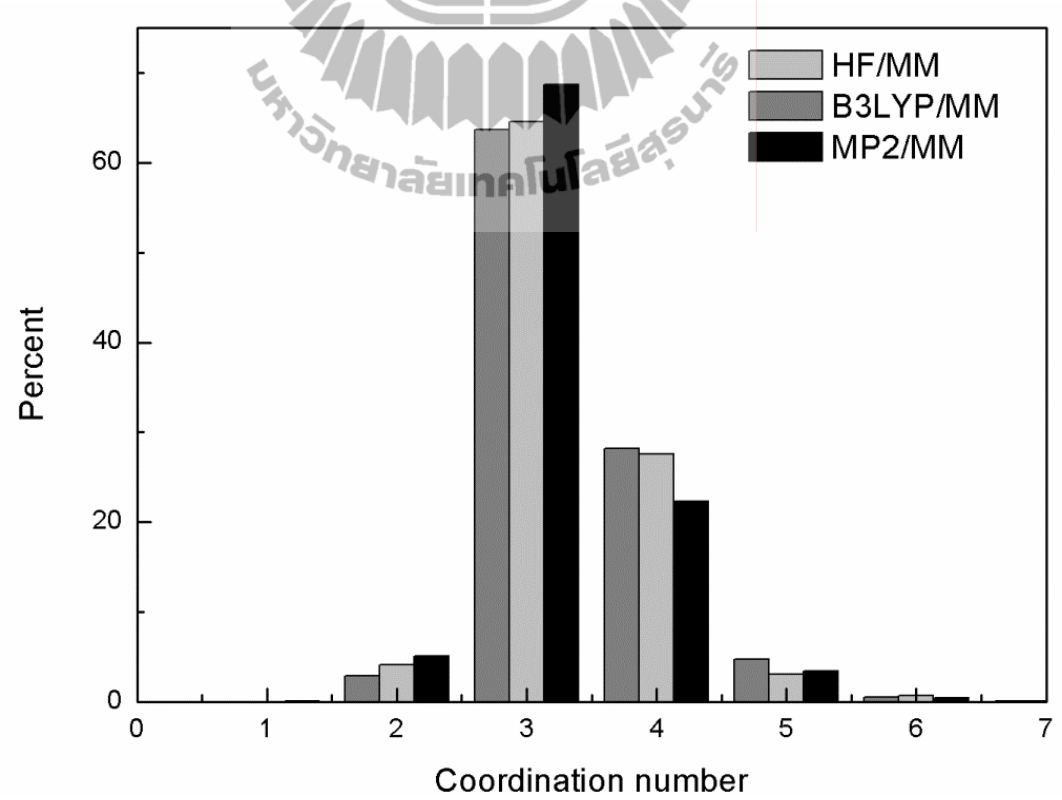

Figure 4.2 Distributions of CN, calculated up to first minimum of the O_{ox}-O_w RDF.

To provide more detailed analysis on the H_3O^+-water hydrogen bonds, the probability distributions of the O_{ox}-H_{ox}---O_w angle (γ) and of angle θ (defined as an angle between the intramolecular O-H vector and the water dipole vector), calculated up to the first minimum of the H_{ox}-O_w RDFs, are plotted in Figure 4.3a and b, respectively. According to the distributions of the O_{ox}-H_{ox}---O_w angle (Figure 4.3a), the results obtained by the B3LYP/MM and MP2/MM simulations, as well as by the HF/MM model (Intharathep, Tongraar, and Sagarik, 2006), apparently show that the first shell water molecules form almost linear hydrogen bonds with each of the oxonium hydrogens. However, a further difference between the present B3LYP/MM and MP2/MM simulations and the previous HF/MM study is observed in the distributions of the θ angle. As can be seen in Figure 4.3b, the B3LYP/MM and MP2/MM simulations, although predicting a clear dipole-oriented arrangement of nearest-neighbor water molecules toward the H_3O^+ ion similar to that found in the HF/MM study, indicate less influence of the ion on the orientations of its nearest-neighbor water molecules. This suggests that, besides the relatively strong H_{ox}---O_w hydrogen bonds, water molecules in the first hydration shell of H_3O^+ could be somewhat oriented with respect to the influence of other nearest-neighbor waters, either those inside the first hydration shell or those in the bulk region.

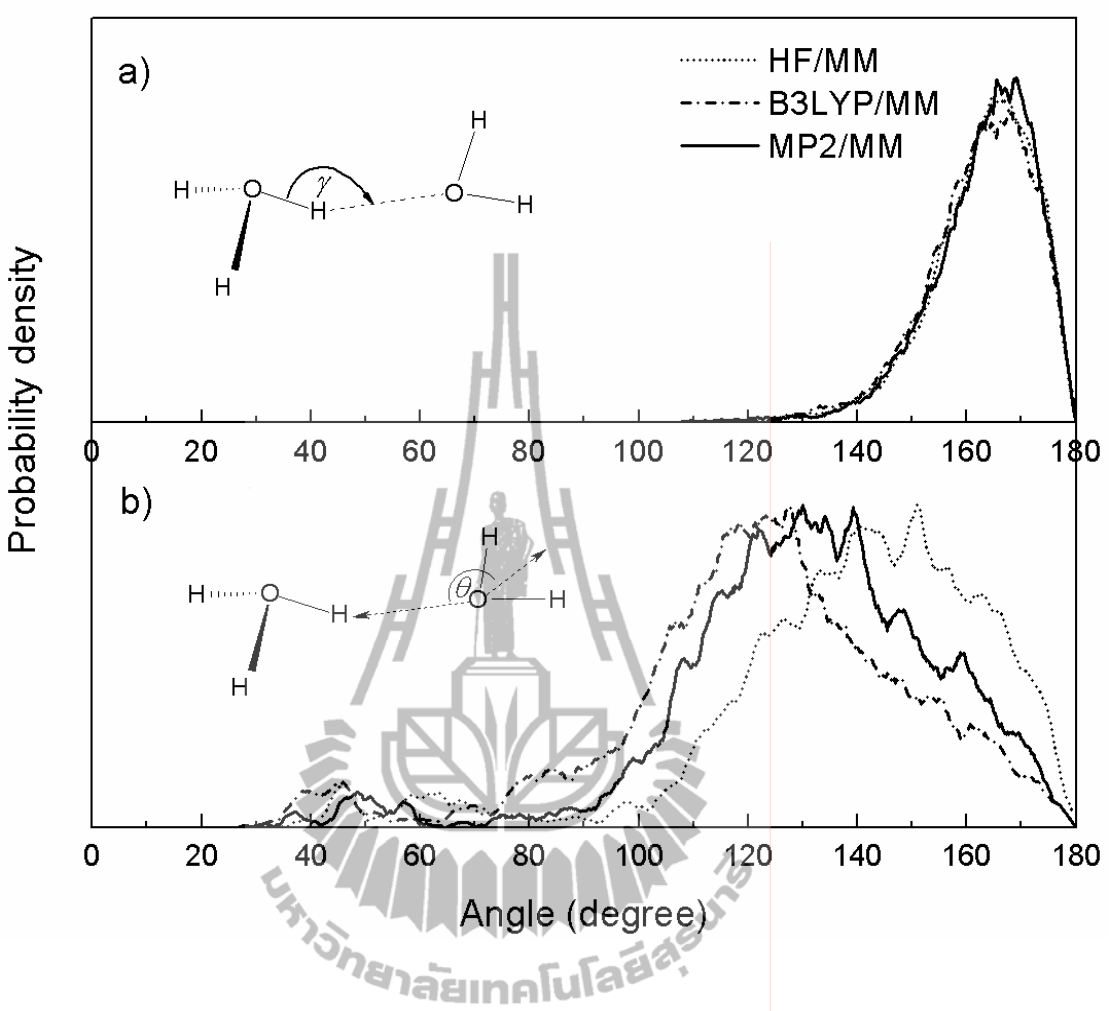

Figure 4.3 Distributions of a) O_{ox}-H_{ox}---O_w angle (γ) and b) angle θ (defined as an angle between the intramolecular O-H vector and the water dipole vector), calculated up to first minimum of the H_{ox}-O_w RDFs.

The distributions of water orientations around the H_3O^+ ion can be described by the angle β between the dipole vector of H_3O^+ ion and the O_{ox}-O_w distance vector, as can be seen in Figure 4.4. The results obtained by the B3LYP/MM and MP2/MM simulations as well as by the HF/MM simulation are similar, indicating that no water molecule bound in the lone pair direction of the H_3O^+ ion.

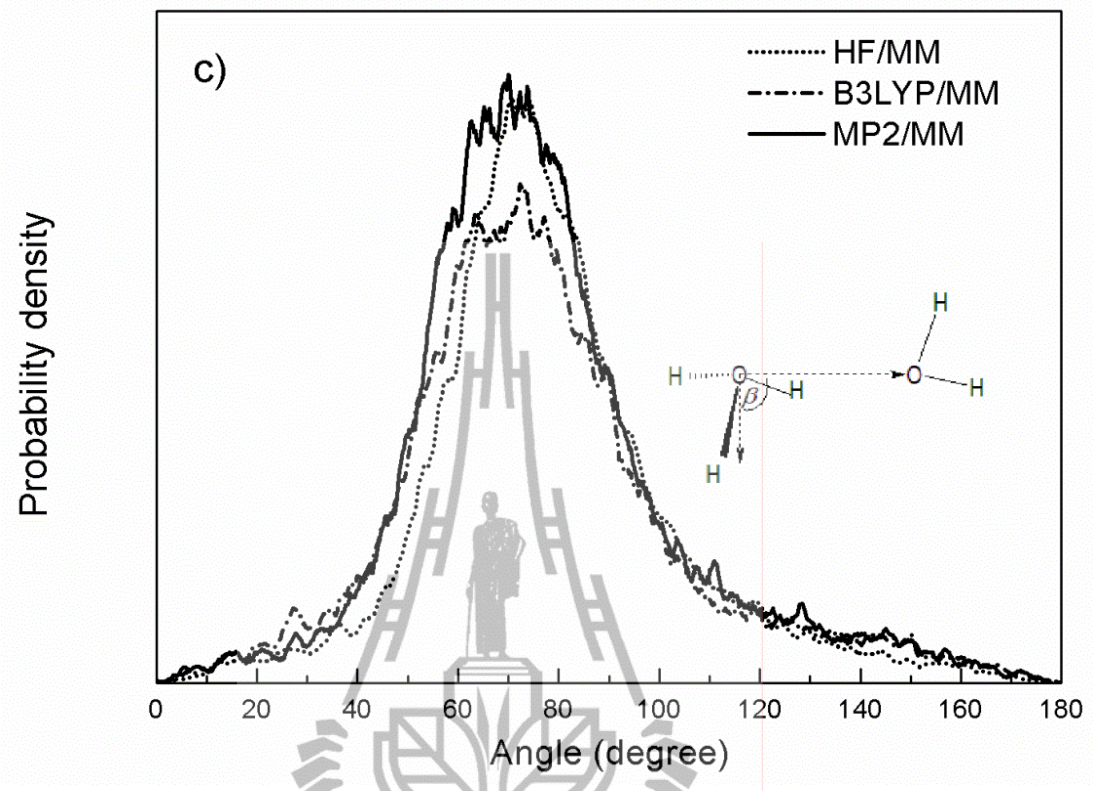

Figure 4.4 Distributions of the angle β between the dipole vector of H_3O^+ ion and the O_{ox}-O_w distance vector, calculated up to first minimum of the O_{ox}-O_w RDFs.

The intramolecular geometry of the H_3O^+ ion and of its surrounding water molecules can be described by the distributions of their O-H bond lengths and H-O-H bond angles, as depicted in Figure 4.5a and b, respectively. As compared to the previous HF/MM results, the inclusion of electron correlation through the B3LYP/MM and MP2/MM models leads to significant elongation of O-H bond lengths as well as to slight broader H-O-H angles of the H_3O^+ ion and the first shell water molecules. Overall, the distributions of the bond length and bond angle of H_3O^+ are broader than those of the first shell water molecules, as a consequence of the partial formation of $H_5O_2^+$ in which the intramolecular O_{ox}-H_{ox} bond is fully extended

with respect to the arrangement of strong O_{ox}-H_{ox}---O_w hydrogen bond interactions. This implies that the inclusion of electron correlation effects with respect to the B3LYP/MM and MP2/MM models may result in a more frequent $H_5O_2^+$ formation. To clarify this point, the probability distributions of the *longest* intramolecular O_{ox}-H_{ox} bond distance (*i.e.*, obtained by choosing the longest O_{ox}-H_{ox} bond in each analyzed configuration) are plotted in Figure 4.6, together with the *shortest* intermolecular H_{ox}---O_w distance. In the gas phase, it has been demonstrated that the $H_5O_2^+$ complex is considered to be 'formed' when the O_{ox}---O_w distance (*e.g.*, the summation of O_{ox}-H_{ox} and H_{ox}---O_w distances in the symmetrical H_2O---H^+---OH_2 formation) in the original $H_9O_4^+$ complex is smaller than 2.4 Å (Agmon, 1995). In the condensed phase, however, the equilibrium O_{ox}---O_w distance could be slightly larger. As can be seen in Figure 4.6, the distributions of the *longest* intramolecular O_{ox}-H_{ox} bond length of H_3O^+ as obtained by both B3LYP/MM and MP2/MM simulations are shifted towards the corresponding O_{ox}---O_w distance of the symmetrical $H_5O_2^+$ ion, compared to the HF/MM results. In combination with the distributions of the *shortest* intermolecular H_{ox}---O_w distance with a maximum around 1.4 Å and a range down to about 1.1 Å, this corresponds to a higher possibility of finding the $H_5O_2^+$ complex in aqueous solution. With regard to the present B3LYP/MM and MP2/MM simulations, since the use of the restricted QM region allows the proton to oscillate only between the H_3O^+ ion and its surrounding water molecules, it should be noted that no actual PT has occurred during the simulations. Instead, the simulation results can provide data with respect to the structure and dynamics of the hydrated H_3O^+ complex at the state "before" and "after" the actual PT process, rather than visualize the pathway of the PT mechanism.

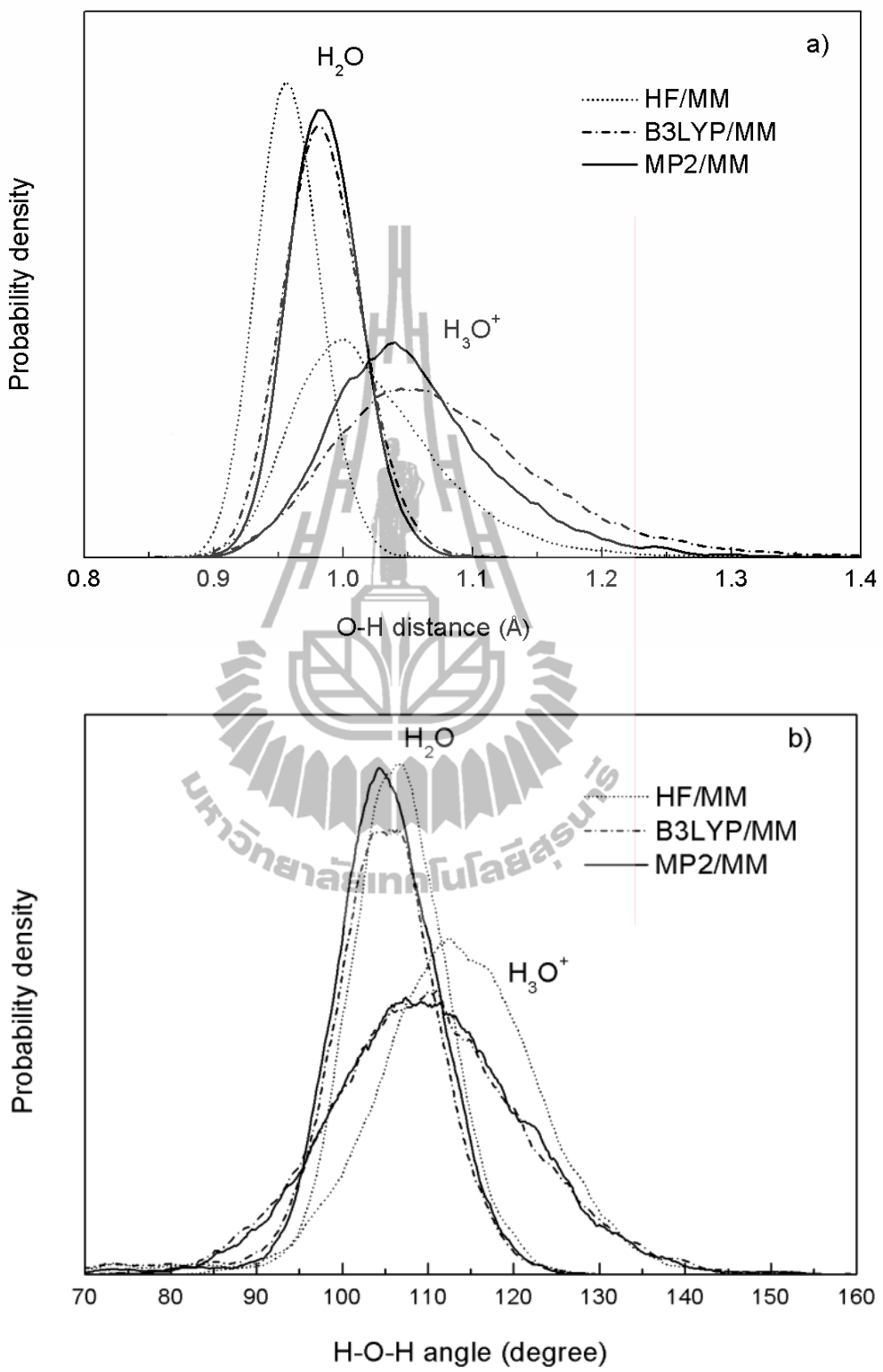

Figure 4.5 Distributions of a) O-H bond lengths and b) H-O-H angles of H_3O^+ and first-shell water molecules.

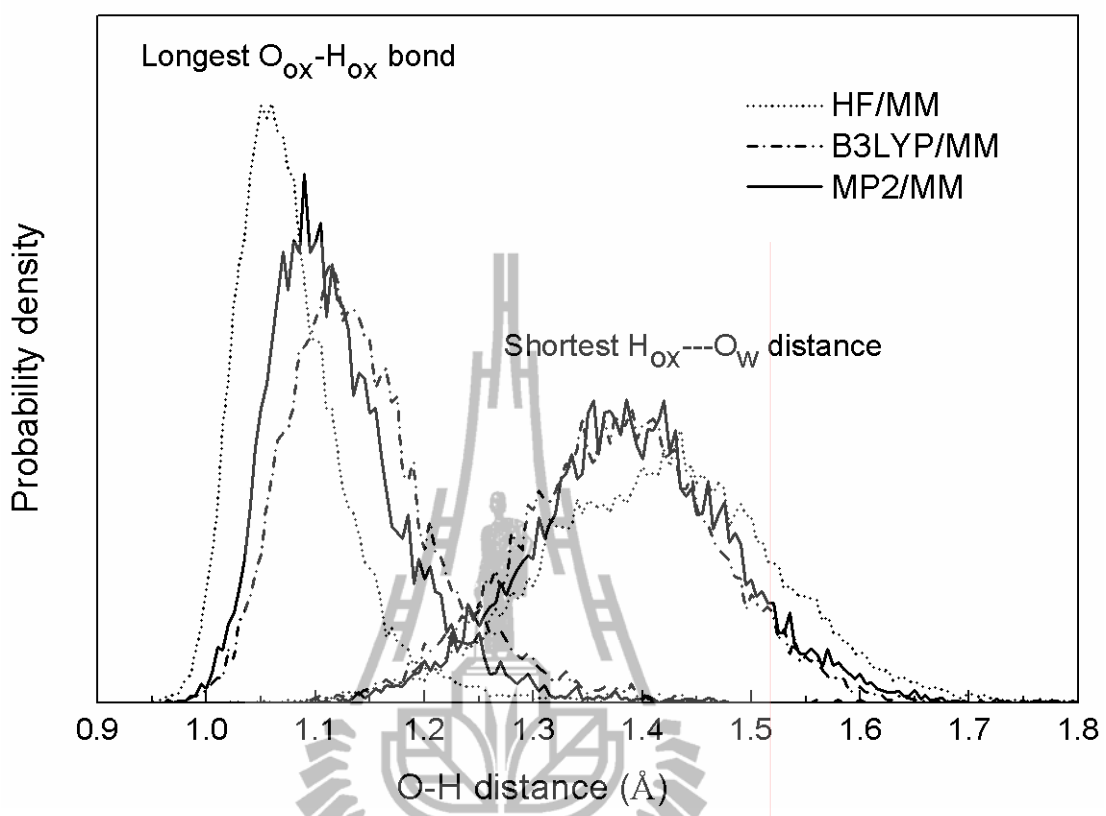

Figure 4.6 Distributions of the *longest* intramolecular O_{ox}-H_{ox} bond length and of the *shortest* intermolecular H_{ox}---O_w distance, as obtained from the HF/MM (Intharathep, Tongraar, and Sagarik, 2006), B3LYP/MM and MP2/MM MD simulations.

4.1.2 Dynamic properties

The process of water exchange at each of the oxonium hydrogens can be visualized by the plots of the H_{ox}---O_w distances against the simulation time, as shown in Figures 4.7 and 4.8 for the MP2/MM and B3LYP/MM simulations, respectively. In addition, the distributions of the intramolecular O_{ox}-H_{ox} bonds are also plotted in order to provide information on the frequency of the $H_5O_2^+$ formation. In aqueous solution, it is well-established that the $H_9O_4^+$ and $H_5O_2^+$ complexes are the most important species, and that the PT process is an extremely fast dynamics process

(*e.g.*, the interconversion period between the $H_9O_4^+$ and $H_5O_2^+$ structures is found to be less than 100 fs (Woutersen and Bakker, 2006)), with the $H_5O_2^+$ form being the most important transition state complex. On the basis of both B3LYP/MM and MP2/MM simulations, the formation of the $H_9O_4^+$ complex is apparently found to be the most prevalent species in aqueous solution, followed by smaller proportions of $H_5O_2^+$ and $H_7O_3^+$ (*i.e.*, a complex in which two of the O_{ox}---O_w distances of the original $H_9O_4^+$ are ≤ 2.5 Å). In fact, the formation of the $H_5O_2^+$ and $H_7O_3^+$ complexes could be regarded as the fluctuation of the $H_9O_4^+$ structure, *i.e.*, a small shift of the hydrogen atoms of H_3O^+ along their O_{ox}-H_{ox} bonds transiently converts the symmetrical $H_9O_4^+$ complex into either $H_7O_3^+$ or $H_5O_2^+$ complexes, and *vice versa*.

According to Figures 4.7 and 4.8, several water exchange processes were observed during the MP2/MM and B3LYP/MM simulations. The rate of water exchange processes at each of the oxonium hydrogens was evaluated through the mean residence times (MRTs) of the water molecules. In this work, the MRT data were calculated using the "direct" method (Hofer and Tran, 2004), as the product of the average number of water molecules in the first shell with the duration of the MD simulation, divided by the observed number of exchange events lasting for a given time interval t^*. In general, it has been demonstrated that a t^* value of 0.0 ps is suitable for the estimation of hydrogen bond lifetimes, and a value of 0.5 ps is considered as a good measure for water exchange processes (Hofer and Tran, 2004). The calculated MRT data with respect to t^* values of 0.0 and 0.5 ps are summarized in Table 4.1, together with the corresponding data obtained from the previous HF/MM study (Schmitt and Voth, 1998) and the MRT data for pure water derived by the similar QM/MM scheme (Adams, D. J., Adams, E. H., and Hills, 1979; Brooks *et al*., 1983).

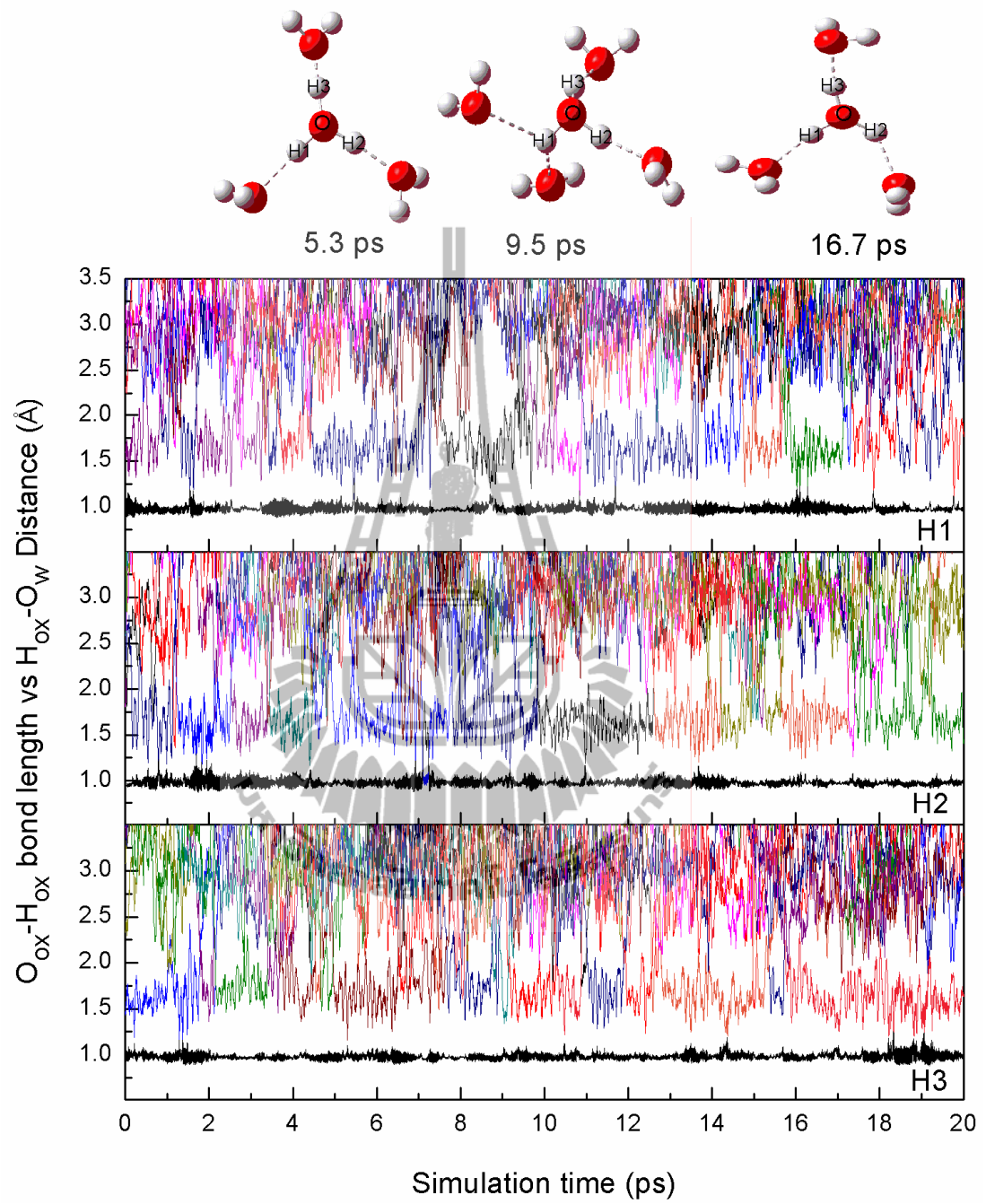

Figure 4.7 Time dependence of intramolecular O_{ox}-H_{ox} bond lengths (black line) and H_{ox}---O_w distances, as obtained from the MP2/MM MD simulation.

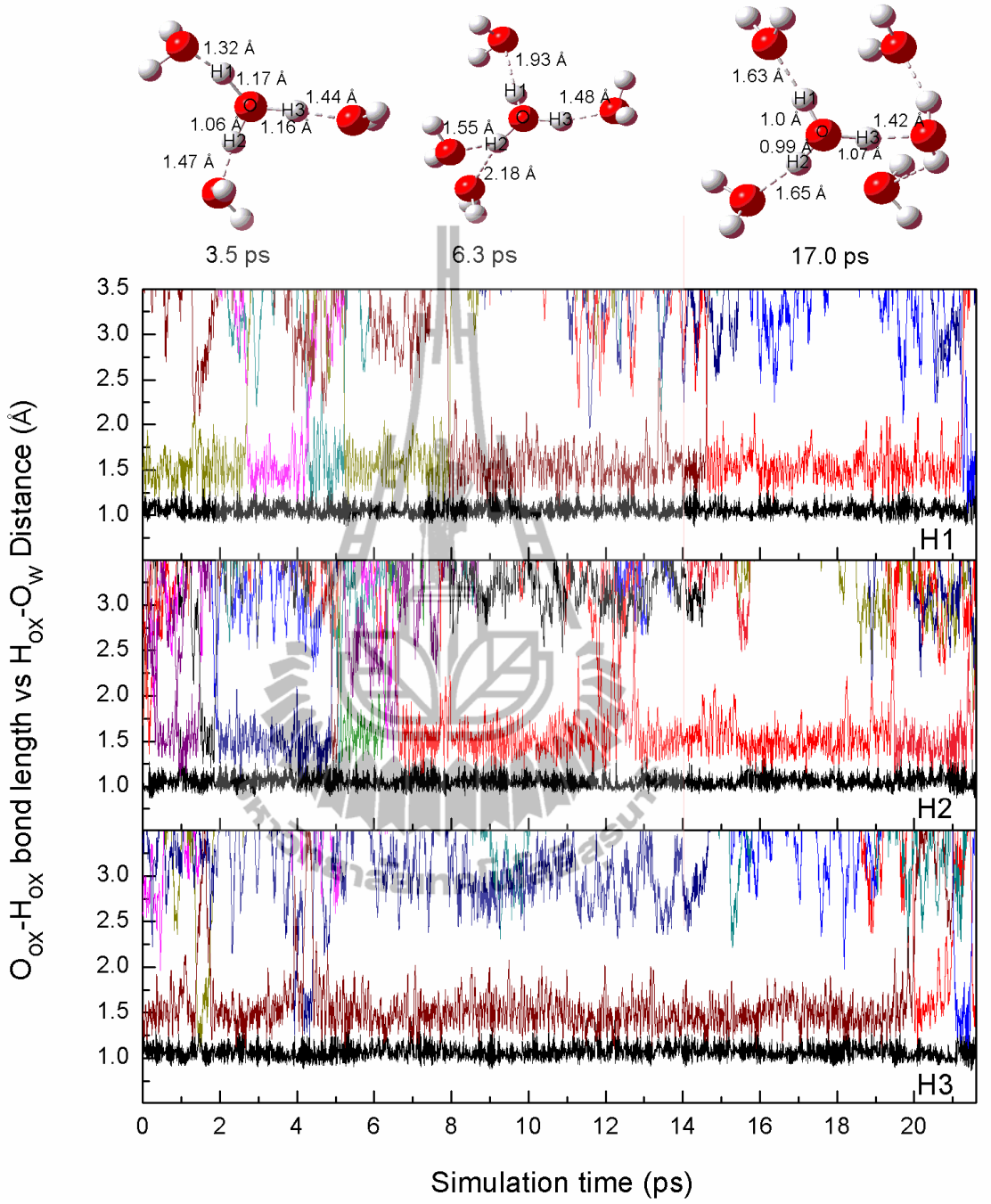

Figure 4.8 Time dependence of intramolecular O_{ox}-H_{ox} bond lengths (black line) and H_{ox}---O_w distances, as obtained from the B3LYP/MM MD simulation.

By means of the MP2/MM simulation, the MRT values at each of the oxonium hydrogens for both t^* = 0.0 and 0.5 ps are of the same order of magnitude as for pure water (Xenides, Randolf, and Rode, 2005). This clearly indicates fast dynamics of water molecules surrounding the H_3O^+ ion. According to the MP2/MM data in Table 4.1, the slightly observed different MRT values at each of the oxonium hydrogens could be attributed partly to the limitation of the MP2/MM simulation time, as well as to the imbalance of their H_3O^+-water hydrogen bond strengths, *i.e.*, as a consequence of the temporary formation of $H_5O_2^+$ (or $H_7O_3^+$) complexes. As one can see in Table 4.1, the corresponding MRT data obtained from the previous HF/MM study show good agreement with the present MP2/MM results. This supplies information that the neglect of electron correlation effects at the HF level of accuracy appears to have small influence on the dynamics properties of the H_3O^+ hydrate.

In the course of the B3LYP/MM simulation, however, it is found that one nearest-neighbor water molecule spends more than 15 ps long lasting with one hydrogen atom of H_3O^+ (*e.g.*, H3 in Figure 4.8). Consequently, this leads to an extremely slow exchange process of water molecules, *i.e.*, the MRT value on this site is about 3.5 times higher than that of the other hydrogen atoms of H_3O^+. According to the plots of the time dependence of the O_{ox}-H_{ox} bond lengths and H_{ox}---O_w distances in Figure 4.8, in particular for the trajectories between 4 and 20 ps, the average O_{ox}---O_w distance with respect to the O_{ox}-$H3_{ox}$---O_w bond is found to be relatively shorter than the O_{ox}---O_w distances along the O_{ox}-$H1_{ox}$---O_w and O_{ox}-$H2_{ox}$---O_w bonds. In addition, there are many situations in which the intramolecular O_{ox}-$H3_{ox}$ and the intermolecular $H3_{ox}$---O_w distances are equal. This suggests that the symmetric $H_5O_2^+$ structure could be formed frequently in aqueous solution, *i.e.*, the strongest O_{ox}-$H3_{ox}$--

-O_w bond in the $H_9O_4^+$ complex can transiently convert back and forth into the $H_5O_2^+$ formation. Under this circumstance, it could be demonstrated that the B3LYP/MM simulation predicts the $H_5O_2^+$ complex which is relatively too stable to represent a transition state complex in the PT process. The artificially slow water exchange processes predicted by the B3LYP method have also been found in the B3LYP/MM simulation of pure water (Xenides, Randolf, and Rode, 2005). Recently, it has been demonstrated that the performance of the CP-MD scheme with simple DFT functionals, such as BLYP and PBE, could not provide reasonable properties of the solvent water itself, *i.e.*, predicting a glassy state rather than a liquid at room temperature and up to 400 K (Yoo, Zeng, and Xantheas, 2009). In this context, since the interconversion between $H_9O_4^+$ and $H_5O_2^+$ complexes is coupled to the hydrogen bonds dynamics of water molecules in the second hydration or in the bulk, the B3LYP/MM results clearly indicate the deficiency of the B3LYP method in describing the mechanism of PT in water.

Table 4.1 Mean residence times of water molecules in the bulk and in the first hydration shell of H_3O^+ hydrogens, as obtained from the HF/MM (Intharathep, Tongraar, and Sagarik, 2006), B3LYP/MM and MP2/MM MD simulations.

QM/MM Model	CN	t_{sim}	$t^* = 0$ ps		$t^* = 0.5$ ps	
			$N_{ex}^{0.0}$	$\tau^{0.0}$	$N_{ex}^{0.5}$	$\tau^{0.5}$
MP2/MM						
H1	1.01	15.8	63	0.25	11	1.45
H2	1.01	15.8	50	0.32	6	2.65
H3	1.01	15.8	54	0.30	8	2.00
Pure H_2O*	4.60	5.0	-	0.28	-	2.45
B3LYP/MM						
H1	0.98	21.6	71	0.30	10	2.12
H2	0.97	21.6	123	0.17	11	1.91
H3	0.98	21.6	46	0.46	3	7.08
Pure H_2O*	4.20	30.0	-	1.07	-	7.84
HF/MM						
H1**	1.0	20.0	65	0.31	8	2.50
H2**	1.0	20.0	113	0.18	11	1.82
H3**	1.0	20.0	47	0.42	8	2.50
Pure H_2O*	4.20	40.0	-	0.33	-	1.51
Pure H_2O***	4.60	12.0	292	0.20	31	1.80

*(Xenides, Randolf, and Rode, 2005)

**(Intharathep, Tongraar, and Sagarik, 2006)

***(Tongraar and Rode, 2004)

CN = average coordination number of the first hydration shell of water and of each of hydrogen atoms of H_3O^+.

t^* = minimum duration of the ligand's displacement from its original coordination shell.

t_{sim} = simulation time in ps

$N_{ex}^{t^*}$ = number of exchange events

τ = Mean residence time

4.2 A comparative study of conventional QM/MM and ONIOM-XS MD simulations

The second part of this work focuses on the reliability and accuracy of the conventional QM/MM MD approach for the treatment of such system. Here, the results obtained by the conventional QM/MM MD simulation will be compared and discussed with respect to the corresponding data obtained by the more sophisticated QM/MM MD simulation based on ONIOM-XS method. Due to the limitation of the CPU time, the HF method is employed for the description of all interactions inside the QM region. Apart from the results and discussion in section 4.1, the results obtained by the present ONIOM-XS MD simulation will not be interpreted in terms of the correct description of the H_3O^+ hydrate, but instead, will be compared and discussed with respect to the reliability of the conventional QM/MM scheme. To improve the quality of the simulation results, a larger QM size with diameter of 8.4 Å is employed in this section.

4.2.1 Structural properties

The O_{ox}-O_w, O_{ox}-H_w, H_{ox}-O_w and H_{ox}-H_w RDFs, together with their corresponding integration numbers, as obtained by the conventional HF/MM and ONIOM-XS MD simulations, are plotted in Figure 4.9. For the conventional HF/MM simulation, the use of larger QM size with diameter of 8.4 Å produces structural details of the hydrated H_3O^+ similar to the previous HF/MM study using smaller QM size with diameter of 7.6 Å (*e.g.*, compared to the HF/MM results shown in Figure 4.1). This implies that, on the basis of the HF method, the QM size with diameter of 7.6 Å is considerably large enough to provide the structural data of the H_3O^+ hydrate. However, the results obtained by the conventional HF/MM simulation are apparently different from those obtained by the ONIOM-XS simulation. As can be seen in Figure 4.9a and b, the ONIOM-XS simulation reveals relatively wider first O_{ox}-O_w and O_{ox}-H_w peaks, in which the integration up to first O_{ox}-O_w minimum yields higher average coordination number of 7.5, *i.e.*, compared to the corresponding value of 3.6 derived from the conventional HF/MM simulation.

The characteristics of the H_3O^+-water hydrogen bonds can be visualized through the H_{ox}-O_w and H_{ox}-H_w RDFs, as depicted in Figure 4.9c and d, respectively. With regard to both conventional HF/MM and ONIOM-XS simulations, the integrations up to first minimum of the H_{ox}-O_w RDFs yield about one water molecule that directly hydrogen bonded to each of H_3O^+ hydrogens. As compared to the conventional HF/MM results, the observed large number of first-shell waters in the ONIOM-XS simulation clearly indicates a higher possibility of the nearest-neighbor waters, besides the first three waters that strongly hydrogen bonded to each of H_3O^+ hydrogens, to be involved in the formation of H_3O^+-water complex. Figure

4.10 shows distributions of the average number of water molecules at each of H_3O^+ hydrogens, calculated up to first minimum of the H_{ox}-O_w RDFs. Obviously, both conventional HF/MM and ONIOM-XS simulations clearly reveal single well-defined hydrogen bond between each hydrogen atom of H_3O^+ and its nearest-neighbor water molecules, *i.e.*, showing the prevalence of the $H_9O_4^+$ species. However, as compared to the conventional HF/MM results, the H_{ox}-O_w and H_{ox}-H_w RDFs obtained by the ONIOM-XS simulation are relatively broad and less pronounced, which is an indicative of the weakening of H_3O^+-water hydrogen bond interactions. In addition, the first H_{ox}-O_w peak is not well separated from the second one, (*i.e.*, compared to the corresponding H_{ox}-O_w peak of the conventional HF/MM simulation), implying a higher possibility of water exchange processes at each hydrogen atom of H_3O^+.

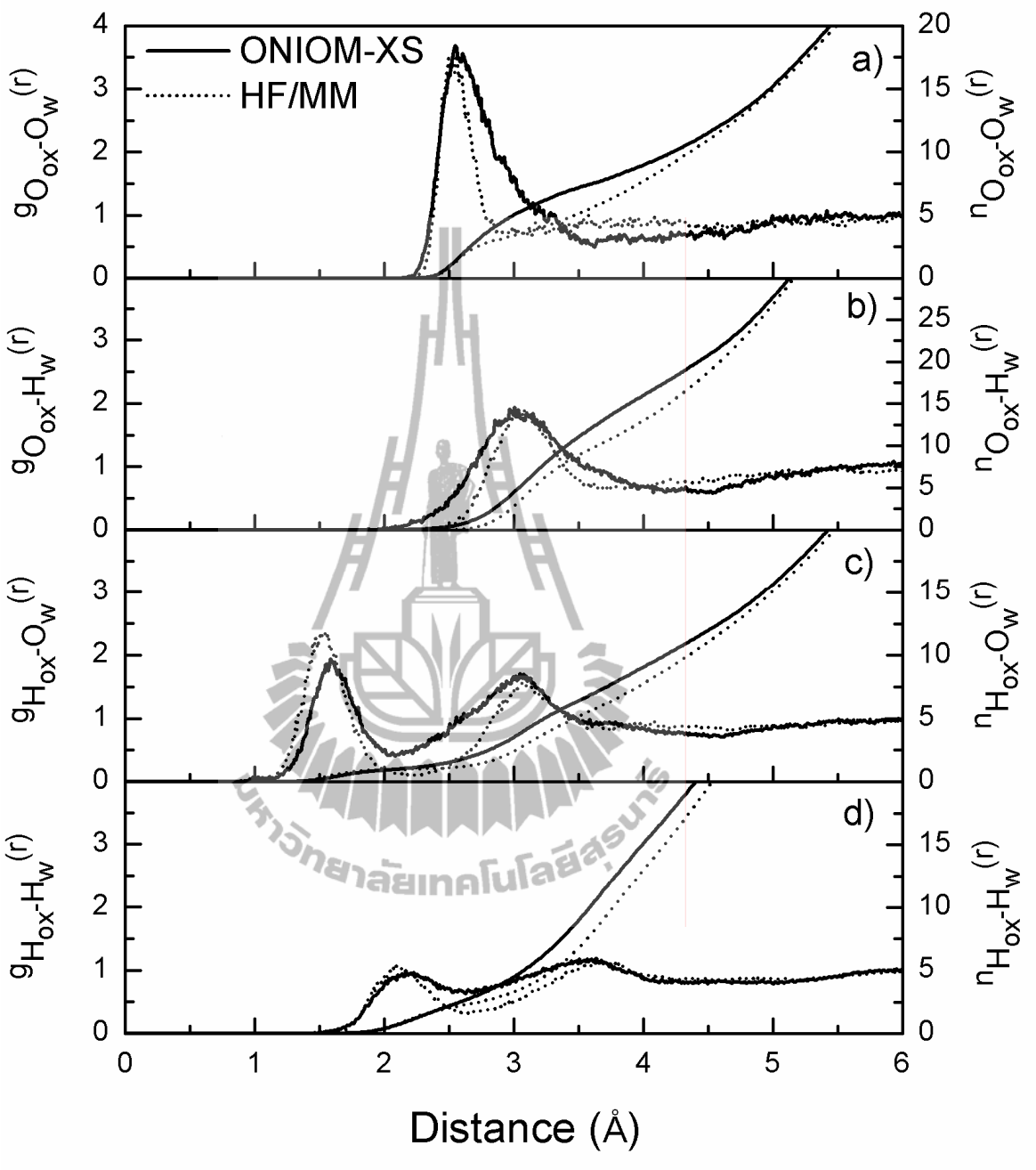

Figure 4.9 a) O_{ox}-O_w, b) O_{ox}-H_w, c) H_{ox}-O_w and d) H_{ox}-H_w radial distribution functions and their corresponding integration numbers, as obtained by the conventional HF/MM and ONIOM-XS MD simulations.

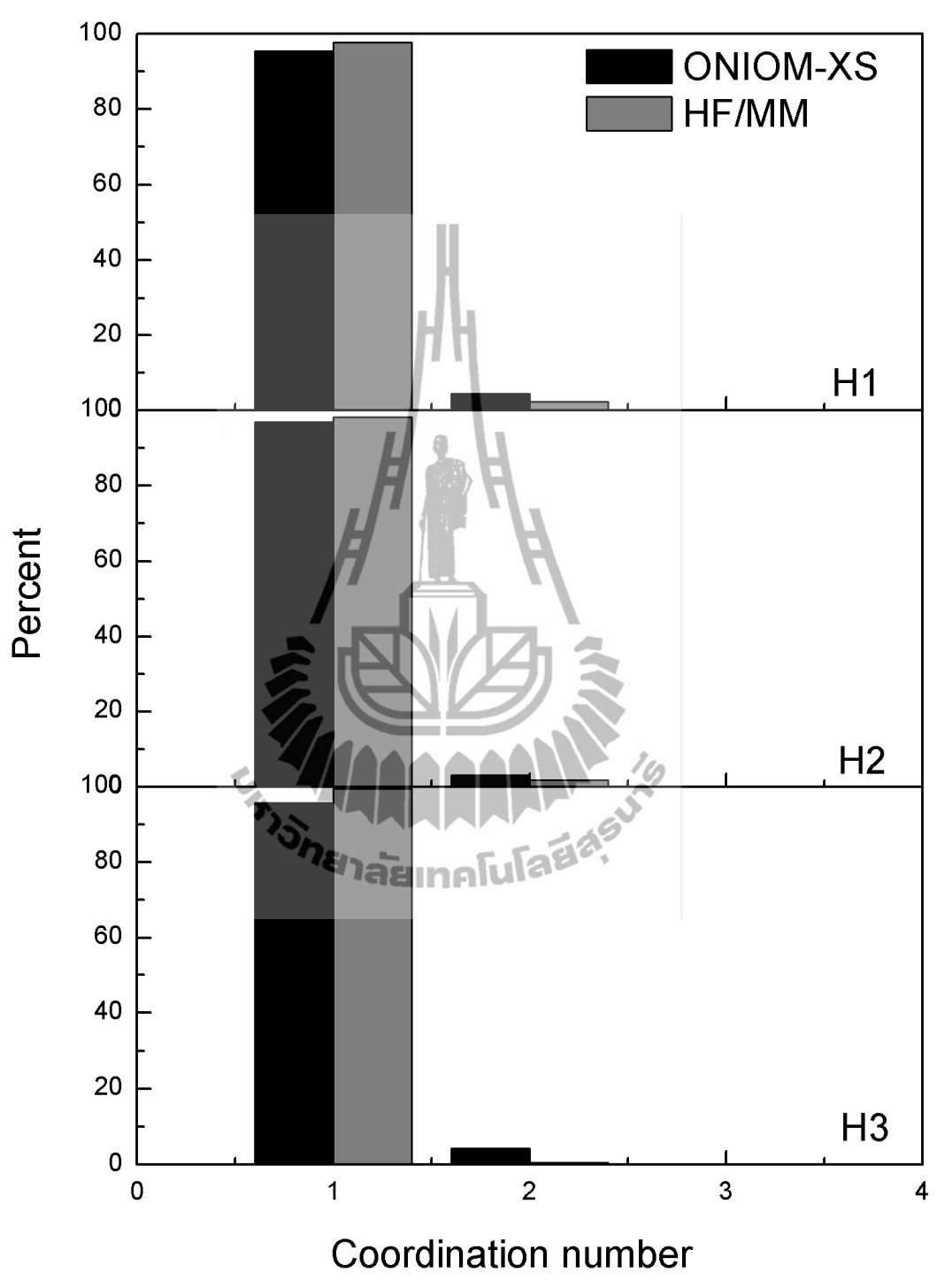

Figure 4.10 Distributions of coordination number at each of H_3O^+ hydrogens, calculated up to first minimum of the H_{ox}-O_w RDFs.

The distributions of water orientations around the ion are displayed in terms of the distributions of the angle β between the O_{ox}-O_w distance vector and the dipole vector of the H_3O^+ ion, as shown in Figure 4.11. Obviously, the feature of the peak as obtained by the conventional HF/MM simulation clearly indicate less possibility of finding O_{ox}-H_w hydrogen bond interactions on top of the H_3O^+ ion. In contrast to the conventional HF/MM results, the ONIOM-XS simulation shows significantly higher possibility of such arrangement. In this respect, other nearest-neighbor water molecules, *i.e.*, those besides the first three waters that directly hydrogen bonded to each of H_3O^+ hydrogen atoms, are more frequently bound in the lone pair direction of the H_3O^+ ion. On the other hand, the ONIOM-XS results provide information that the H_3O^+ ion is strongly shared in a local tetrahedral network of water.

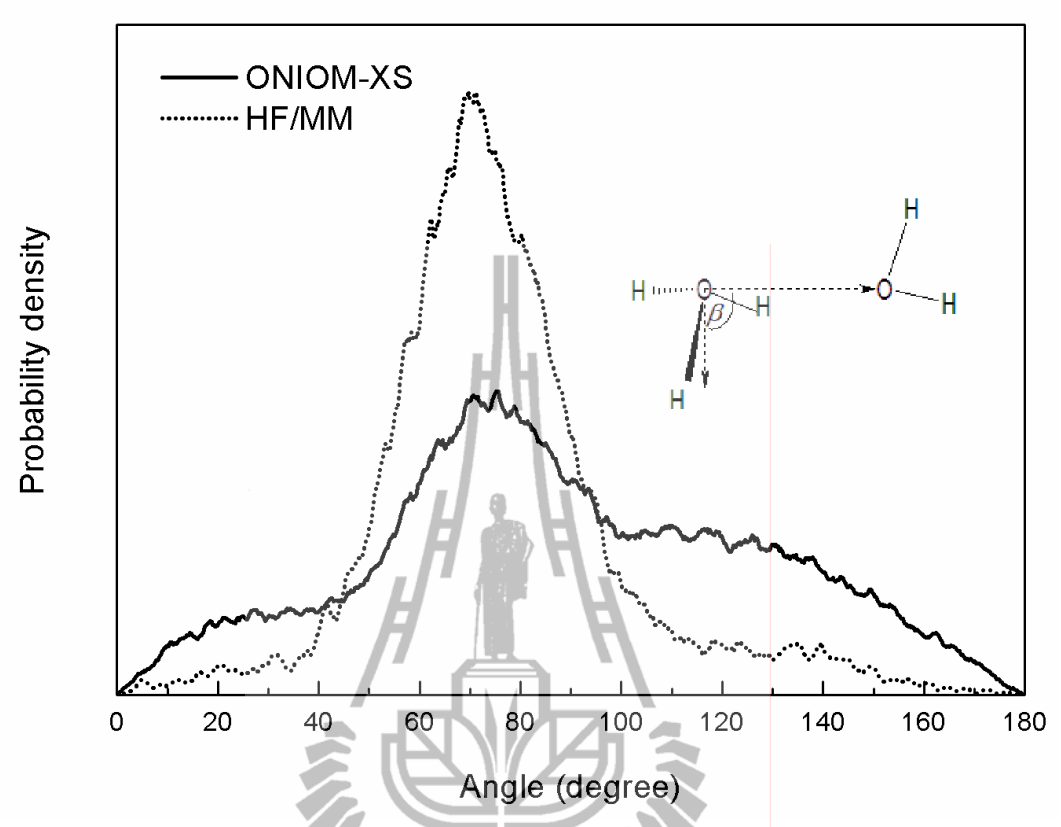

Figure 4.11 Distributions of angle β, calculated up to first minimum of the O_{ox}-O_w RDFs.

More detailed information on the H_3O^+-water hydrogen bonds can be visualized from the distributions of the O_{ox}-H_{ox}---O_w angle (γ) and of angle θ, as depicted in Figure 4.12. Overall, both conventional HF/MM and ONIOM-XS simulations reveal that first-shell water molecules form almost linear hydrogen bonds with each of H_3O^+ hydrogens. In comparison to the conventional HF/MM results, however, the ONIOM-XS simulation predicts slightly higher flexibility of the O_{ox}-H_{ox}---O_w angle, *i.e.*, as a consequence of the observed weakening of the H_3O^+-water hydrogen bond interactions (*e.g.*, see Figure 4.9c).

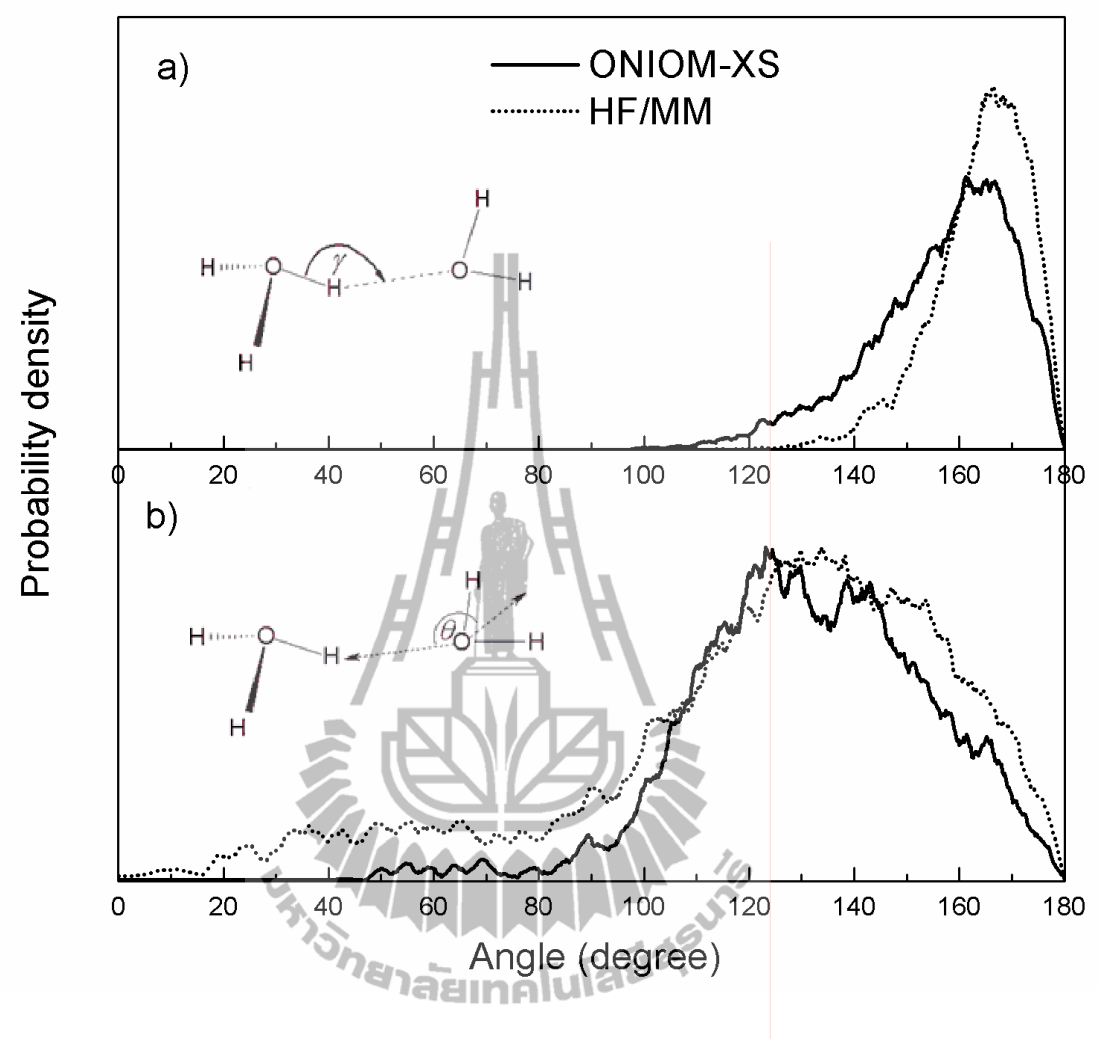

Figure 4.12 Distributions of a) O_{ox}-H_{ox}---O_w angle (γ) and b) angle θ, calculated up to first minimum of the H_{ox}-O_w RDFs.

The intramolecular geometries of the H_3O^+ ion and of the surrounding water molecules (*i.e.*, in terms of the distributions of O-H bond lengths and H-O-H bond angles), as obtained by the conventional HF/MM and ONIOM-XS simulations, are shown in Figure 4.13. In the ONIOM-XS simulation, the observed shortening of the O-H bond lengths of H_3O^+, *i.e.*, compared to the conventional HF/MM results, corresponds to the observed weakening of the H_3O^+-water hydrogen bonds.

Figure 4.14 shows the probability distributions of the *longest* intramolecular O_{ox}-H_{ox} bond length and the *shortest* intermolecular H_{ox}---O_w distance, *i.e.*, as chosen from each of the analyzed configurations. With regard to Figure 4.14, the distribution of the *longest* intramolecular O_{ox}-H_{ox} bond length of H_3O^+ as obtained by the ONIOM-XS simulation is shifted outwards the corresponding O_{ox}---O_w distance of the symmetrical $H_5O_2^+$ ion, *i.e.*, compared to the conventional HF/MM results (see the discussion in section 4.1). In conjunction with the distribution of the *shortest* intermolecular H_{ox}---O_w distance with a maximum of around 0.1 Å longer than that of the conventional HF/MM simulation, this corresponds to a less possibility of finding the $H_5O_2^+$ complex in aqueous solution. The observed differences between the conventional HF/MM and ONIOM-XS simulations clearly indicate the deficiency of the conventional QM/MM scheme for the treatment of such system. In this respect, since the effects of electron correlation have been shown to play an important role in the description of the H_3O^+ hydrate, the ONIOM-XS simulation in conjunction with the use of correlated methods, such as MP2, would be highly recommended in order to obtain a more accurate description of this ion in aqueous solution.

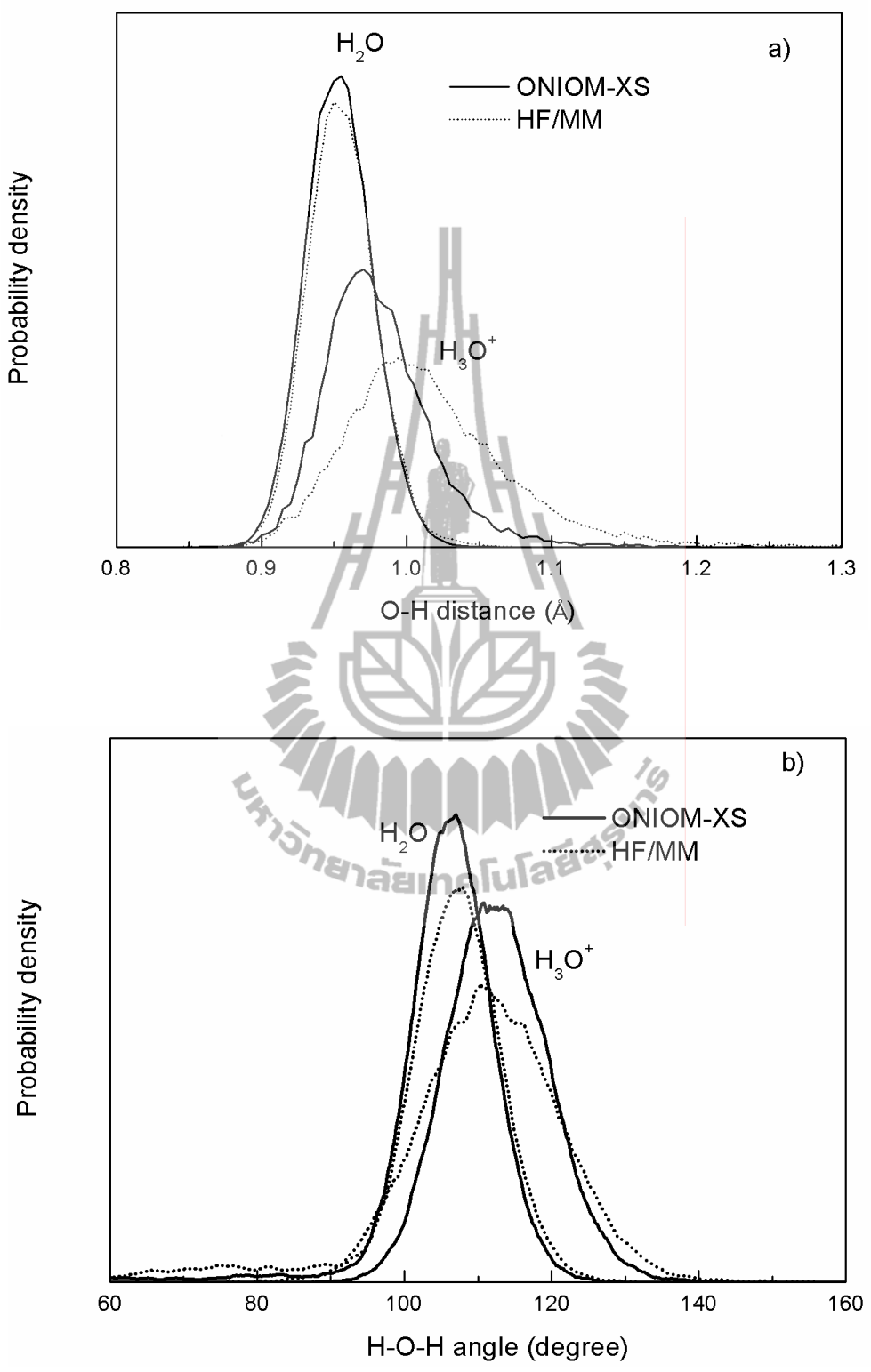

Figure 4.13 Distributions of a) O-H bond lengths and b) H-O-H angles of H_3O^+ and the nearest-neighbor water molecules that directly H-bonded to the ion.

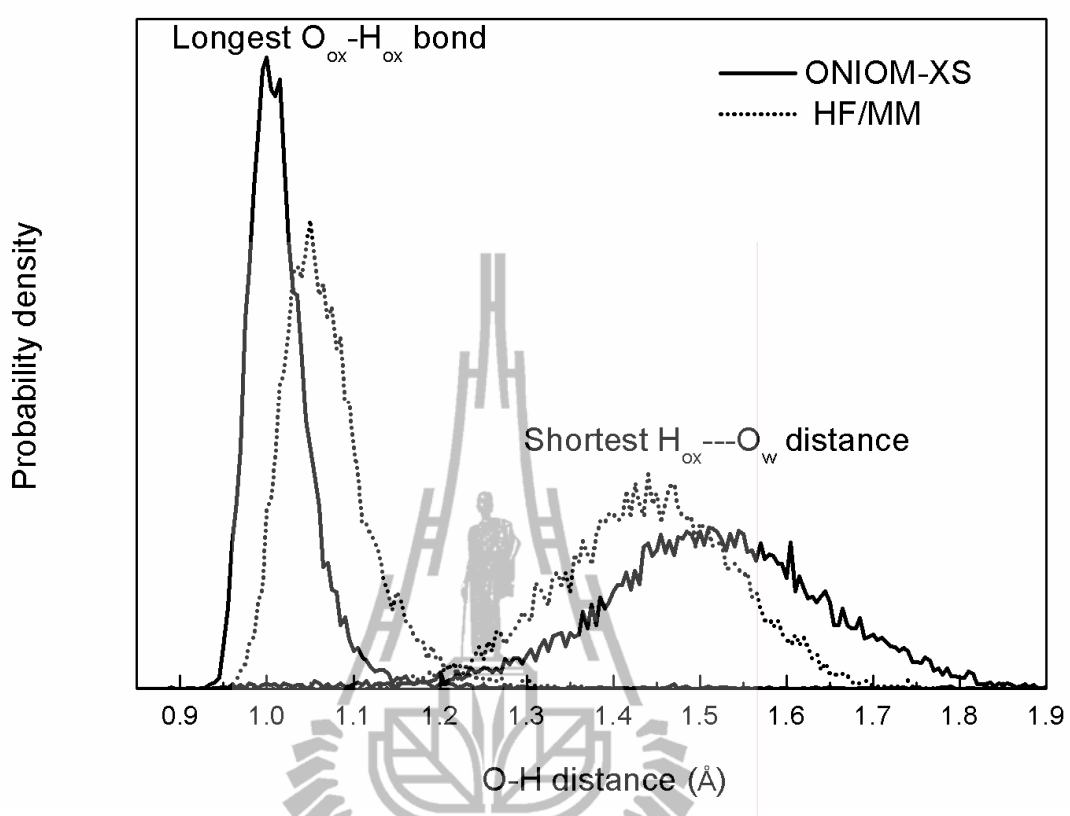

Figure 4.14 Distributions of the *longest* intramolecular O_{ox}-H_{ox} bond length and of the *shortest* intermolecular H_{ox}---O_w distance, as obtained by the conventional HF/MM and ONIOM-XS MD simulations.

4.2.2 Dynamic properties

The exchange processes of water molecules near each of the H_3O^+ hydrogen atoms can be visualized through the plots of time dependence of intramolecular O_{ox}-H_{ox} bond lengths and H_{ox}---O_w distances, as shown in Figures 4.15 and 4.16 for the ONIOM-XS and the conventional HF/MM simulations, respectively. In the course of ONIOM-XS simulation (Figure 4.15), several water exchange processes are more frequently observed at each of H_3O^+ hydrogens, *i.e.*, compared to the conventional HF/MM simulation (Figure 4.16). This corresponds to the observed

large number of nearest-neighbor water molecules, as well as the observed weakening of the H_3O^+-water hydrogen bonds. The calculated MRT data with respect to t^* values of 0.0 and 0.5 ps are summarized in Table 4.2. According to the ONIOM-XS simulation, the MRT values at each of the H_3O^+ hydrogens for both t^* = 0.0 and 0.5 ps are slightly less than those observed in the conventional HF/MM simulation. Regarding to the data in Table 4.2, another significant difference between the conventional HF/MM and ONIOM-XS simulations is observed in the number of exchange events. As compared to the conventional HF/MM results, the MRT data obtained by the ONIOM-XS simulation clearly indicate fast dynamics of water molecules surrounding the H_3O^+ ion. Overall, these observed differences clearly confirm the deficiency of the conventional QM/MM scheme in predicting the properties of this hydrated ion.

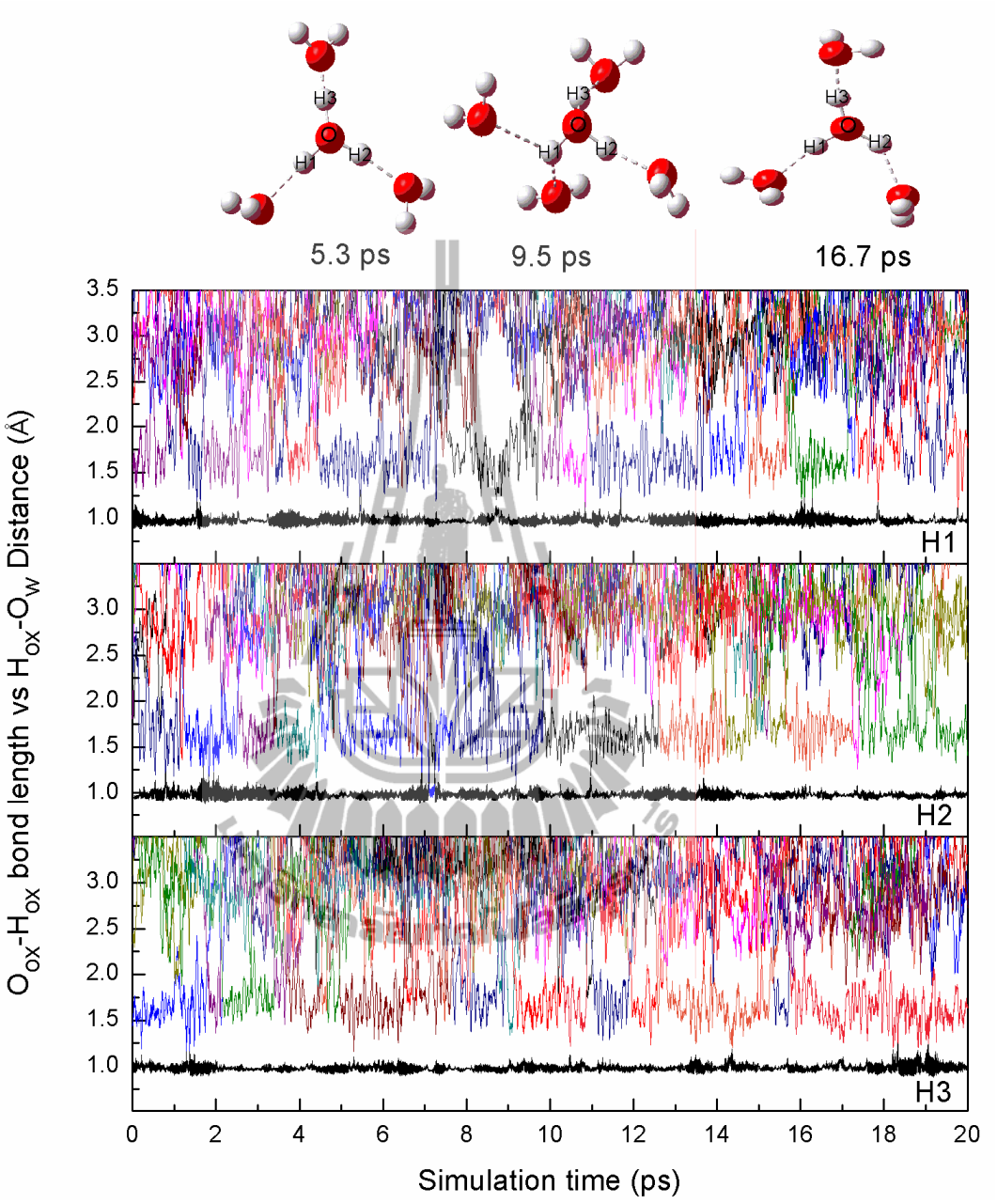

Figure 4.15 Time dependence of intramolecular O_{ox}-H_{ox} bond lengths (black line) and H_{ox}---O_w distances, as obtained by the ONIOM-XS MD simulation.

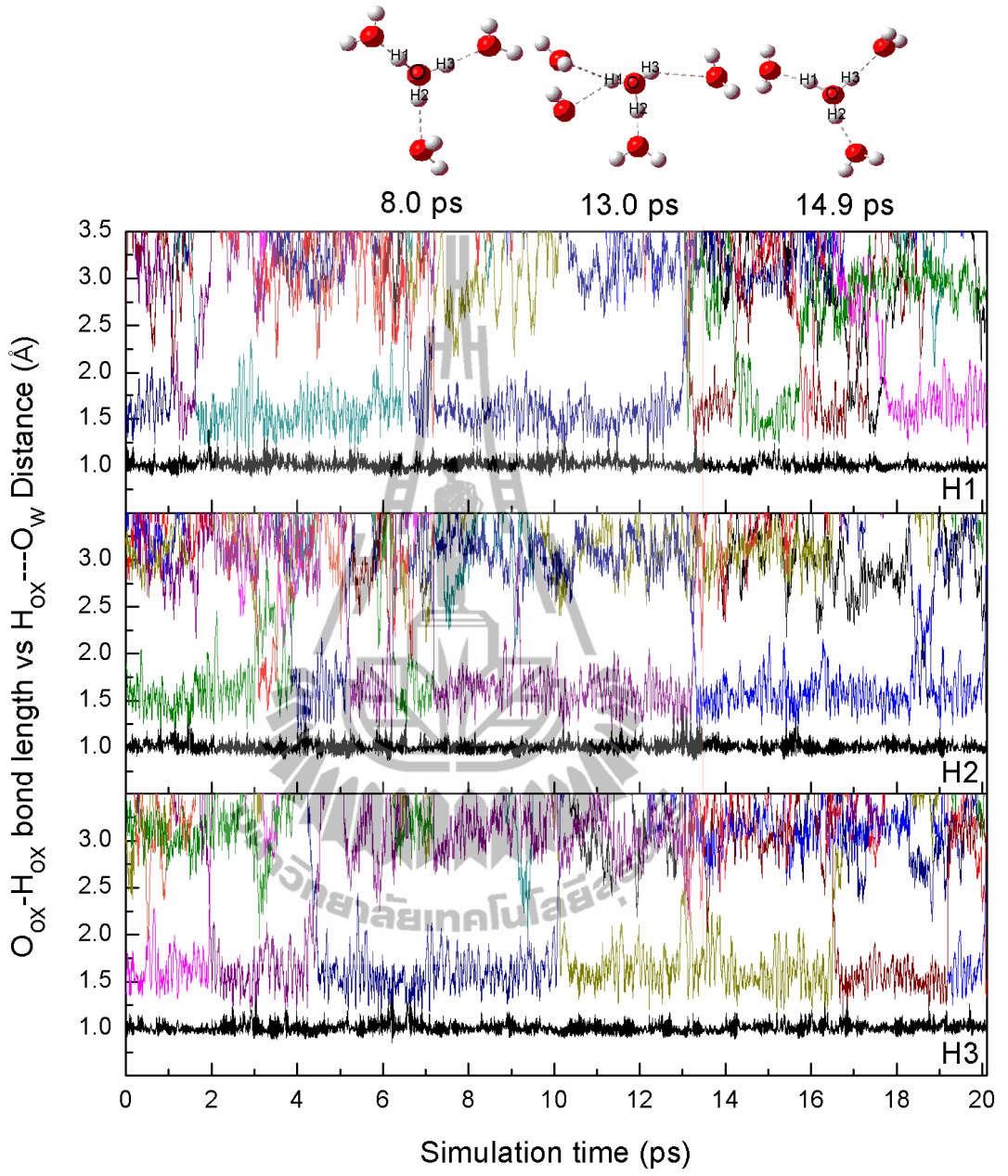

Figure 4.16 Time dependence of intramolecular O_{ox}-H_{ox} bond lengths (black line) and H_{ox}---O_w distances, as obtained by the conventional HF/MM MD simulation.

Table 4.2 Mean residence times of water molecules in the bulk and in the first hydration shell of H_3O^+ hydrogens, as obtained from the conventional HF/MM and ONIOM-XS MD simulations.

QM/MM Model	CN	t_{sim}	t^* = 0 ps		t^* = 0.5 ps	
			$N_{ex}^{0.0}$	$\tau^{0.0}$	$N_{ex}^{0.5}$	$\tau^{0.5}$
ONIOM-XS						
H1	0.96	20.0	289	0.07	16	1.22
H2	0.98	20.0	192	0.10	18	1.06
H3	0.99	20.0	210	0.09	16	1.26
HF/MM						
H1	1.01	20.0	100	0.20	12	1.69
H2	1.01	20.0	93	0.22	10	2.03
H3	0.99	20.0	50	0.40	10	1.99
Pure H_2O^*	4.20	40.0	-	0.33	-	1.51
Pure H_2O^{**}	4.60	12.0	292	0.20	31	1.80

*(Xenides, Randolf, and Rode, 2005)

**(Tongraar and Rode, 2004)

CN = average coordination number of the first hydration shell of water and of each of hydrogen atoms of H_3O^+.

t^* = minimum duration of the ligand's displacement from its original coordination shell.

t_{sim} = simulation time in ps

$N_{ex}^{t^*}$ = number of exchange events

τ = Mean residence time

CHAPTER V

CONCLUSION

In this work, a series of QM/MM MD simulations was performed in order to investigate the structural and dynamics properties of H_3O^+ in aqueous solution. Firstly, the effects of electron correlation on the structure and dynamics of the hydrated H_3O^+ ion were studied by performing the B3LYP/MM and MP2/MM MD simulations, and the results are compared to those obtained by the HF/MM scheme. Then, the validity of the QM/MM technique for the treatment of such system was evaluated by performing a more sophisticated QM/MM MD technique based on ONIOM-XS method. In this respect, the reliability of the conventional QM/MM scheme was discussed with respect to the different results obtained in the ONIOM-XS MD simulation.

In the first part, as compared to HF/MM data previously published by other, the inclusion of electron correlation effects with respect to the B3YLP/MM and MP2/MM simulations results in stronger H_3O^+-water hydrogen bond interactions as well as in a slightly greater compactness of the H_3O^+ hydrate. By means of the B3LYP/MM simulation, however, the overestimation of the H_3O^+-water hydrogen bond strength is recognizable, which leads to an artificial slow dynamics nature of some first shell waters, and thus to a too long-living $H_5O_2^+$ complex. With regard to the reported tendency of the DFT methods to predict too rigid ion solvation complexes, as well as wrong dynamics of the liquid water, it is worth noting that the

DFT methods should be used with special caution, especially for the description of such hydrogen-bond systems.

In the second part, a more sophisticated QM/MM MD based on ONIOM-XS method (abbreviated as ONIOM-XS MD) was performed, and the results are compared to those obtained by the conventional QM/MM scheme. In this work, since the performance of the ONIOM-XS MD simulation is rather time-consuming, the HF method was selected for describing all interactions within the QM region. As compared to the conventional HF/MM results, the ONIOM-XS simulation provides remarkable different data, both in the structure and dynamics of the H_3O^+ hydrate. For example, the ONIOM-XS simulation predicts relatively weak H_3O^+-water hydrogen bonds, *i.e.*, compared to the conventional HF/MM results, which reflects in the observed lower MRT values of water molecules at each of H_3O^+ hydrogens. In addition, the ONIOM-XS results clearly indicate that several water molecules (up to 7-8 waters) can be involved in the formation of H_3O^+ hydration. Consequently, these nearest-neighbor water molecules can also be expected to play an important role in the formation of H_3O^+-water species in aqueous solution. These observed differences clearly indicate the deficiency of the conventional QM/MM scheme for the treatment of such system. However, since the effects of electron correlation have been shown to play an important role in the structure and dynamics of the H_3O^+ hydrate, the ONIOM-XS simulation in conjunction with the use of correlated methods, such as MP2, would be highly recommended in order to obtain a more accurate description of this hydrated ion in aqueous solution.

APPENDICES

APPENDIX A

PRESENTATION

1. Thanawat Somtua and Anan Tongraar. (January 21-23, 2010). Effects of electron correlation on the structural properties of the hydrated H_3O^+: B3LYP/MM and MP2/MM MD simulations. **Pure and Applied Chemistry International Conference (PACCON 2010)**. Sunee Grand Hotel and Convention Center, Ubon Ratchathani, Thailand.

APPENDIX B

PUBLICATION

PCCP

Dynamic Article Links

Cite this: *Phys. Chem. Chem. Phys.*, 2011, **13**, 16190–16196

www.rsc.org/pccp

PAPER

Correlation effects on the structure and dynamics of the H_3O^+ hydrate: B3LYP/MM and MP2/MM MD simulations

Thanawat Somtua and Anan Tongraar*

Received 19th March 2011, Accepted 15th July 2011
DOI: 10.1039/c1cp20823c

Two combined quantum mechanics/molecular mechanics (QM/MM) molecular dynamics (MD) simulations, namely B3LYP/MM and MP2/MM, have been performed to investigate the possible influence of electron correlation on the structure and dynamics of the H_3O^+ hydrate. In comparison to the previously published HF/MM results, both B3LYP/MM and MP2/MM simulations clearly reveal stronger H_3O^+–water hydrogen bond interactions, which are reflected in a slightly greater compactness of the H_3O^+ hydrate. However, the B3LYP/MM simulation, although providing structural details very close to the MP2/MM data, shows an artificially slow dynamic nature of some first shell water molecules as a consequence of the formation of a long-lived H_3O^+–H_2O hydrogen bonding structure.

1. Introduction

Due to the anomalously high mobility of protons in aqueous solution, *i.e.*, about 5–8 times greater than other cations, many experiments[1–4] and theoretical investigations[5–30] have been carried out in order to analyze and describe such fast proton mobility. In experiments, the characteristics of the hydrated proton have not yet been identified unambiguously since it is rather difficult to prepare protonated water clusters. Alternatively, computer simulations by means of Monte Carlo (MC) and molecular dynamics (MD) have become a powerful tool to elucidate such details, in particular at the molecular level. In this respect, a hydronium ion (H_3O^+), *i.e.*, the cation that forms from water in the presence of hydrogen ions, has been widely used as a model system for studying proton migration in liquid water.[5–30] In fact, according to the IUPAC nomenclature of organic and inorganic chemistry, the appropriate nomenclature of H_3O^+ is *oxonium* (systematic: *oxidanium*).

In general, the mobility of protons in water has been regarded as a combination of rapid protons jumping between different water molecules, known as the Grotthuss mechanism,[31] and the diffusion of the entire protonated water complexes through the hydrogen bond network, *i.e.*, in a way similar to other simple ions. According to most recent studies,[3,4,24–30,32,33] it has been postulated that Eigen ($H_9O_4^+$) and Zundel ($H_5O_2^+$) complexes are the primarily important species in the aqueous proton transfer (PT) mechanism. The $H_9O_4^+$ is formed when the three hydrogen atoms in H_3O^+ are equivalently hydrated, forming three analogous hydrogen bonds with the three nearest-neighbor water molecules, while the $H_5O_2^+$ is formed when one hydrogen atom of the H_3O^+ ion is symmetrically shared with its hydrogen bonding water molecule. Comparing between the H_3O^+ and $H_5O_2^+$ complexes, it has been shown that H_3O^+ is more stable (longer living) than $H_5O_2^+$, and that the mechanism of PT in water involves single PT events, *i.e.*, the more stable H_3O^+ is converted into the less stable $H_5O_2^+$ and *vice versa*.[19] Of particular interest, it has been explored that this interconversion is coupled to hydrogen bond dynamics of water molecules in the second solvation shell of H_3O^+, and that the rate-limiting step of the aqueous PT mechanism was hydrogen bond cleavage, rather than water cluster growth or proton motion.

In terms of quantum-mechanics-based simulations, a well-known Car–Parrinello (CP) MD technique has been employed for studying the excess proton in water, providing reasonable chemical rearrangement of the Grotthuss mechanism.[9,10,12,19] By means of the CP-MD technique, however, some methodical drawbacks come from the use of a relatively small system size, as well as from the use of simple generalized gradient approximation (GGA) density functionals. With respect to some earlier CP-MD studies,[9,20] the stability of the $H_5O_2^+$ complex is rather overestimated, which reflects the coexistence of the $H_9O_4^+$ and $H_5O_2^+$ formation. Recently, the use of simple density functionals in the CP-MD scheme was also found to give poor structural and dynamical data even for the underlying liquid water.[34–36] Consequently, this leads to serious issues on the accuracy and reliability of the density functional theory (DFT) in describing such hydrogen bond systems, since it is known that the hydrogen bonds in water are constantly breaking and forming and that these hydrogen bond dynamics are coupled to the process of proton mobility in water.

Recently, the structure and dynamics of the H_3O^+ hydrate have been investigated on the basis of the combined quantum mechanics/molecular mechanics (QM/MM) MD technique.[30] With respect to the QM/MM MD scheme, the H_3O^+ ion and

School of Chemistry, Institute of Science, Suranaree University of Technology, Nakhon Ratchasima 30000, Thailand. E-mail: anan_tongraar@yahoo.com; Fax: +66-44-224185

its surrounding water molecules were treated at the HF level of accuracy, while the rest of the system was described by classical pair potentials, *i.e.*, called HF/MM MD. The HF/MM results showed that the $H_9O_4^+$ complex, the most prevalent species found in aqueous solution, can frequently convert back and forth into the $H_5O_2^+$ structure. In addition, it has been demonstrated that the next-nearest neighbor water molecules can occasionally participate in the arrangement of the hydrogen bond network during the fluctuative formation of the $H_5O_2^+$ ion, and thus contribute to the Grotthuss transport of the proton. By means of the HF/MM simulation, however, the effects of electron correlation were not taken into consideration, as a consequence of the rather high computational expense. In ref. 30, the geometry optimizations of the H_3O^+–$(H_2O)_3$ complex with respect to the HF calculations resulted in an observed weakening of the binding energies, when compared to the corresponding data obtained by the correlated methods. With regard to this point, the effects of electron correlation could be expected to affect the behavior of the H_3O^+ that was solvated in aqueous solution.

In the present study, therefore, two combined QM/MM MD simulations, namely B3LYP/MM and MP2/MM, will be carried out in order to evaluate the possible influence of electron correlation on the structure and dynamics of the hydrated H_3O^+ ion.

2. Method

By the QM/MM MD technique,[30,37–39] the system is divided into two parts, namely the QM and MM regions, in which the total interaction energy of the system is defined as

$$E_{\text{total}} = \langle \Psi_{\text{QM}} | \hat{H} | \Psi_{\text{QM}} \rangle + E_{\text{MM}} + E_{\text{QM-MM}}, \quad (1)$$

where $\langle \Psi_{\text{QM}} | \hat{H} | \Psi_{\text{QM}} \rangle$ refers to the interactions within the QM region, while E_{MM} and $E_{\text{QM-MM}}$ represent the interactions within the MM and between the QM and MM regions, respectively. The QM region, the most interesting part which contains the ion and its surrounding water molecules, is treated quantum mechanically, while the rest of the system is described by classical pair potentials. By this scheme, the total force of the system is described by the following formula:

$$F_{\text{tot}} = F_{\text{MM}}^{\text{sys}} + (F_{\text{QM}}^{\text{QM}} - F_{\text{MM}}^{\text{QM}}), \quad (2)$$

where $F_{\text{MM}}^{\text{sys}}$, $F_{\text{QM}}^{\text{QM}}$, and $F_{\text{MM}}^{\text{QM}}$ are the MM force of the total system, the QM force in the QM region, and the MM force in the QM region, respectively. Here, the $F_{\text{MM}}^{\text{QM}}$ term accounts for the coupling between the QM and MM regions.

In this work, the B3LYP/MM and MP2/MM MD simulations were performed with the same simulation protocol as reported in the previous HF/MM MD study.[30] A significant modification is that all interactions inside the QM region, the most interesting part which contains the H_3O^+ ion and its surrounding water molecules, were treated at B3LYP and MP2 levels of accuracy, respectively, using the D95(d,p) basis set.[40] For the QM size, a QM diameter of 7.6 Å was chosen, which includes the whole first hydration shell of H_3O^+ and some (about 3–4) next nearest-neighbor water molecules. With regard to the QM/MM scheme, the use of bigger QM size can be expected to provide more reliable results. However, it was too time-consuming for the present study, especially for the case of MP2/MM simulation. All quantum mechanics calculations were carried out using Gaussian03 series of program.[41] The B3LYP method, although inferior for most hydrated cations,[38,39] is also employed in this work in order to verify the limitation of this approach in comparison to the MP2/MM results. In fact, according to the original article[42] which notified that exchange–correlation functional employed in the density-functional theory (DFT) contains semiempirical character, this method could probably be considered as a semiempirical approach. For the description of all interactions within the MM and between the QM and MM regions, a flexible model, which describes intermolecular[43] and intramolecular[44] interactions, was employed for water and the pair potential functions for describing H_3O^+–H_2O interactions were obtained from the previous HF/MM work.[30]

Since exchange of water molecules between the QM and MM regions can take place frequently during the B3LYP/MM and MP2/MM simulations, the forces acting on each particle in the system were switched according to which region the water molecule was entering or leaving and is defined as

$$F_i = S_m(r)F_{\text{QM}} + (1 - S_m(r))F_{\text{MM}}, \quad (3)$$

where F_{QM} and F_{MM} are quantum mechanical and molecular mechanical forces, respectively. $S_m(r)$ is a smoothing function[45] described by

$$\begin{aligned} S_m(r) &= 1, && \text{for } r \le r_1, \\ S_m(r) &= \frac{(r_0^2 - r^2)^2 (r_0^2 + 2r^2 - 3r_1^2)}{(r_0^2 - r_1^2)^3}, && \text{for } r_1 < r \le r_0, \\ S_m(r) &= 0, && \text{for } r > r_0, \end{aligned} \quad (4)$$

where r_1 and r_0 are distances characterizing the start and the end of the QM region, applied within an interval of 0.2 Å (*i.e.*, between the $O_{ox}\cdots O_w$ distances of 3.6–3.8 Å).

The B3LYP/MM and MP2/MM MD simulations were separately performed in a canonical ensemble at 298 K under periodic boundary conditions. The starting configuration was the one obtained from the previous HF/MM work.[30] The system's temperature was kept constant using the Berendsen algorithm.[46] A periodic box, with a box length of 18.17 Å, contains one H_3O^+ and 199 water molecules, corresponding to the experimental density of pure water. The reaction-field method[47] was employed for the treatment of long-range interactions. The Newtonian equations of motions were treated by a general predictor–corrector algorithm. The time step size was set to 0.2 fs, which allows for the explicit movement of the hydrogen atoms of water molecules. The B3LYP/MM and MP2/MM MD simulations were started with the system's re-equilibration for 20 000 time steps, followed by another 108 000 (B3LYP/MM) and 79 000 (MP2/MM) time steps to collect the system's configurations at every 10th step.

3. Results and discussion

Structural properties of the hydrated H_3O^+ ion obtained by the B3LYP/MM and MP2/MM MD simulations are characterized through a set of radial distribution functions (RDFs) and the corresponding integration numbers, as depicted in Fig. 1. In this context, the subscripts "ox" and

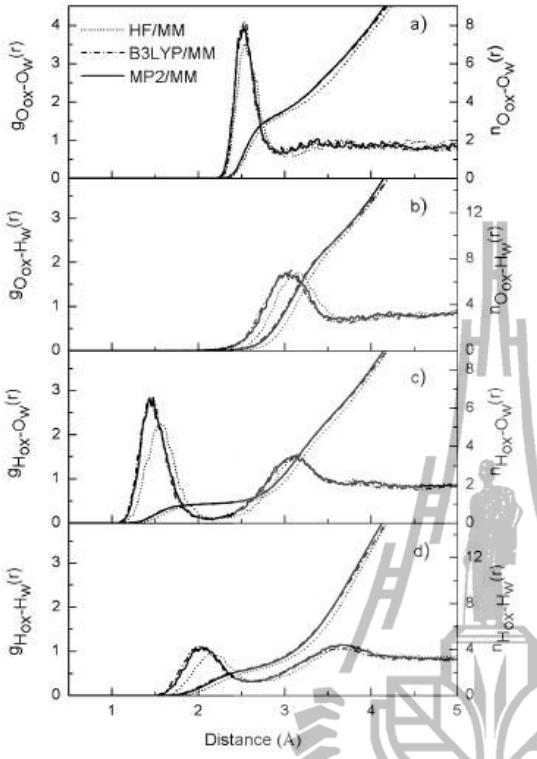

Fig. 1 (a) O_{ox}–O_w, (b) O_{ox}–H_w, (c) H_{ox}–O_w and (d) H_{ox}–H_w radial distribution functions and their corresponding integration numbers, as obtained from HF/MM,[30] B3LYP/MM and MP2/MM MD simulations.

"w" refer to H_3O^+ and water, respectively. To reliably describe the effects of electron correlation on the hydration shell structure of H_3O^+, the corresponding data obtained from the previous HF/MM study[30] are also given for comparison. As can be seen in Fig. 1, the hydration shell structure of H_3O^+ derived by means of B3LYP/MM and MP2/MM simulations is rather identical, and is significantly different from the previous HF/MM work. In terms of O_{ox}–O_w RDFs (Fig. 1a), both B3LYP/MM and MP2/MM simulations show slightly sharper first O_{ox}–O_w peaks with maxima at shorter distances of 2.57 and 2.54 Å, respectively, when compared to the HF/MM's O_{ox}–O_w peak with a maximum at 2.60 Å. Integrations of the O_{ox}–O_w peaks up to their first minimum yield average coordination numbers of 3.4 and 3.3, respectively. These observed coordination numbers are in good accord with the recent experimental data,[4] which demonstrate the prevalence of a distorted $H_9O_4^+$ structure (*i.e.*, as a consequence of a fourth water molecule that can be found occasionally within the first hydration shell of H_3O^+). Regarding the previous HF/MM study,[30] although it revealed a slightly more flexible hydration shell structure of H_3O^+, the observed coordination number of 3.4 is consistent with the present B3LYP/MM and MP2/MM simulations. According to Fig. 1a, the first O_{ox}–O_w peaks are not well separated from the bulk region, indicating that exchange of water molecules between the first hydration shell and the bulk can take place frequently during the simulations. In Fig. 1b, both B3LYP/MM and MP2/MM simulations reveal the first O_{ox}–H_w peaks with a maximum of about 0.2 Å shorter than that of the HF/MM's O_{ox}–H_w peak. In spite of the observed shortening of the $O_{ox}\cdots H_w$ distances, the feature of the first O_{ox}–H_w peaks from both B3LYP/MM and MP2/MM simulations clearly suggests less possibility of finding $O_{ox}\cdots H_w$ hydrogen bond interactions on top of the H_3O^+ ion. This provides information that the H_3O^+ ion is not strongly shared in a local tetrahedral network of water.

The characteristics of hydrogen bonds between the H_3O^+ ion and its nearest-neighbor water molecules can be interpreted from the H_{ox}–O_w and H_{ox}–H_w RDFs, as shown in Fig. 1c and d, respectively. As compared to the previous HF/MM work,[30] both B3LYP/MM and MP2/MM simulations reveal significantly sharper first H_{ox}–O_w and H_{ox}–H_w peaks with a maximum exhibited at the shorter $H_{ox}\cdots O_w$ and $H_{ox}\cdots H_w$ distances, which are consistent with the resulting O_{ox}–O_w and O_{ox}–H_w RDFs. In this respect, the observed differences between the present B3LYP/MM and MP2/MM simulations and the previous HF/MM results could be attributed to the inclusion of the electron correlation effects at the B3LYP and MP2 levels of accuracy, which is reflected in strengthening of the H_3O^+–water hydrogen bond interactions. According to the B3LYP/MM results, however, it should be realized that the DFT methods usually do account for an unknown (uncontrollable) amount of electron correlation, *i.e.*, as a consequence of the semiempirical character of the exchange–correlation functional.[42] On the other hand, the MP2/MM results would be the most suitable benchmark in discussing the effects of electron correlation. Recently, a MP2/MM simulation of pure water has also reported the influence of electron correlation in tightening the structure of the water's first coordination shell.[48] This clearly indicates the important treatment of electron correlation in describing both the H_3O^+–water and water–water interactions. In Fig. 1c, the integrations up to the first minimum of the H_{ox}–O_w RDFs yield one (*i.e.*, 0.98 and 1.01 for the B3LYP/MM and MP2/MM simulations, respectively) well-defined hydrogen bond between each hydrogen atom of H_3O^+ and its nearest-neighbor water molecules.

To provide more detailed analysis on the H_3O^+–water hydrogen bonds, the probability distributions of the O_{ox}–$H_{ox}\cdots O_w$ angle (γ) and of angle θ (defined as an angle between the intramolecular O–H vector and the water dipole vector), calculated up to the first minimum of the H_{ox}–O_w RDFs, are plotted in Fig. 2a and b, respectively. According to the distributions of the O_{ox}–$H_{ox}\cdots O_w$ angle (Fig. 2a), the results obtained by the B3LYP/MM and MP2/MM simulations, as well as by the HF/MM model,[30] apparently show that the first shell water molecules form almost linear hydrogen bonds with each of the oxonium hydrogens. However, a further difference between the present B3LYP/MM and MP2/MM simulations and the previous HF/MM study is observed in the distributions of the θ angle. As can be seen in Fig. 2b, the B3LYP/MM and MP2/MM simulations, although predicting a clear dipole-oriented arrangement of nearest-neighbor water

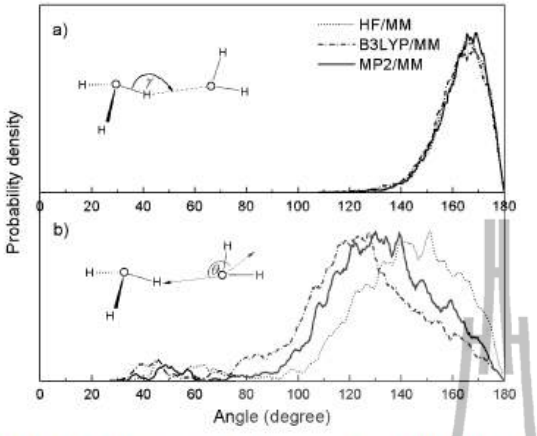

Fig. 2 Distributions of (a) O_{ox}–$H_{ox}\cdots O_w$ angle (γ) and (b) angle θ (defined as an angle between the intramolecular O–H vector and the water dipole vector), calculated up to first minimum of the H_{ox}–O_w RDFs.

molecules toward the H_3O^+ ion similar to that found in the HF/MM study, indicate less influence of the ion on the orientations of its nearest-neighbor water molecules. This suggests that, besides the relatively strong $H_{ox}\cdots O_w$ hydrogen bonds, water molecules in the first hydration shell of H_3O^+ could be somewhat oriented with respect to the influence of other nearest-neighbor water molecules, either those inside the first hydration shell or those in the bulk region.

The intramolecular geometry of the H_3O^+ ion and of its surrounding water molecules can be described by the distributions of their O–H bond lengths and H–O–H bond angles, as depicted in Fig. 3a and b, respectively. As compared to the previous HF/MM results, the inclusion of electron correlation through the B3LYP/MM and MP2/MM models leads to significant elongation of O–H bond lengths as well as to slight broader H–O–H angles of the H_3O^+ ion and the first shell water molecules. Overall, the distributions of the bond length and bond angle of H_3O^+ are broader than those of the first shell water molecules, as a consequence of the partial formation of $H_5O_2^+$ in which the intramolecular O_{ox}–H_{ox} bond is fully extended with respect to the arrangement of strong O_{ox}–$H_{ox}\cdots O_w$ hydrogen bond interactions. This implies that the inclusion of electron correlation effects with respect to the B3LYP/MM and MP2/MM models may result in a more frequent $H_5O_2^+$ formation. To clarify this point, the probability distributions of the *longest* intramolecular O_{ox}–H_{ox} bond distance (*i.e.*, obtained by choosing the longest O_{ox}–H_{ox} bond in each analyzed configuration) are plotted in Fig. 4, together with the *shortest* intermolecular $H_{ox}\cdots O_w$ distance. In the gas phase, it has been demonstrated that the $H_5O_2^+$ complex is considered to be 'formed' when the $O_{ox}\cdots O_w$ distance (*e.g.*, the summation of O_{ox}–H_{ox} and $H_{ox}\cdots O_w$ distances in the symmetrical $H_2O\cdots H^+\cdots OH_2$ formation) in the original $H_9O_4^+$ complex is smaller than 2.4 Å.[8] In the condensed phase, however, the equilibrium $O_{ox}\cdots O_w$ distance could be slightly larger. As can be seen in Fig. 4, the distributions of the *longest* intramolecular O_{ox}–H_{ox} bond length of H_3O^+ as

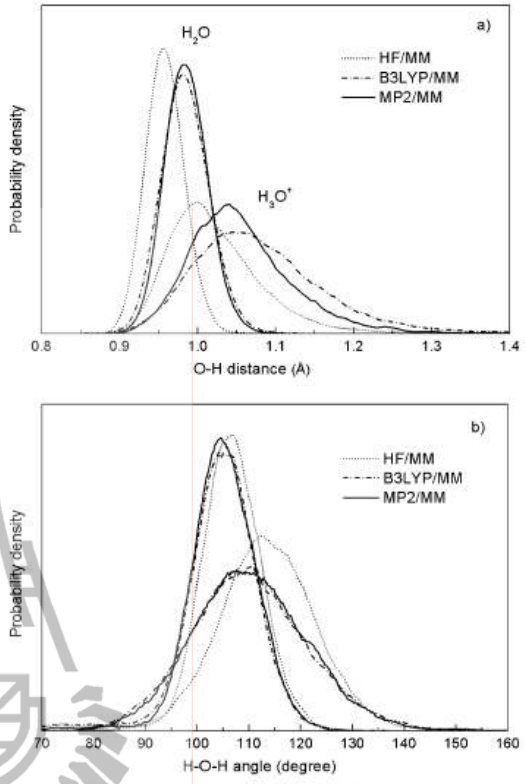

Fig. 3 Distributions of (a) O–H bond lengths and (b) H–O–H angles of H_3O^+.

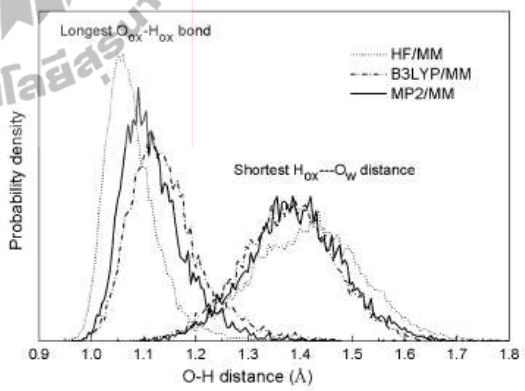

Fig. 4 Distributions of the longest intramolecular O_{ox}–H_{ox} bond length and of the shortest intermolecular $H_{ox}\cdots O_w$ distance, as obtained from the HF/MM,[30] B3LYP/MM and MP2/MM MD simulations.

obtained by both B3LYP/MM and MP2/MM simulations are shifted towards the corresponding $O_{ox}\cdots O_w$ distance of the symmetrical $H_5O_2^+$ ion, compared to the HF/MM results. In combination with the distributions of the *shortest* intermolecular $H_{ox}\cdots O_w$ distance with a maximum around 1.4 Å and a range down to about 1.1 Å, this corresponds to a

higher possibility of finding the $H_5O_2^+$ complex in aqueous solution. With regard to the present B3LYP/MM and MP2/MM simulations, since the use of the restricted QM region allows the proton to oscillate only between the H_3O^+ ion and its surrounding water molecules, it should be noted that no actual PT has occurred during the simulations. Instead, the simulation results can provide data with respect to the structure and dynamics of the hydrated H_3O^+ complex at the state "before" and "after" the actual PT process, rather than visualize the pathway of the PT mechanism.

The process of water exchange at each of the oxonium hydrogens can be visualized by the plots of the $H_{ox}\cdots O_w$ distances against the simulation time, as shown in Fig. 5 and 6 for the MP2/MM and B3LYP/MM simulations, respectively. In addition, the distributions of the intramolecular O_{ox}–H_{ox}

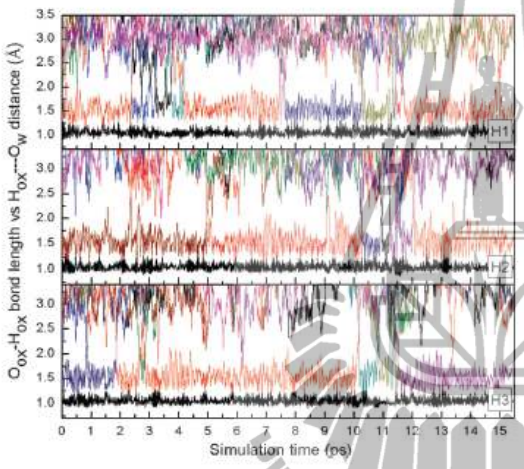

Fig. 5 Time dependence of intramolecular O_{ox}–H_{ox} bond lengths (black line) and $H_{ox}\cdots O_w$ distances, as obtained from the MP2/MM MD simulation.

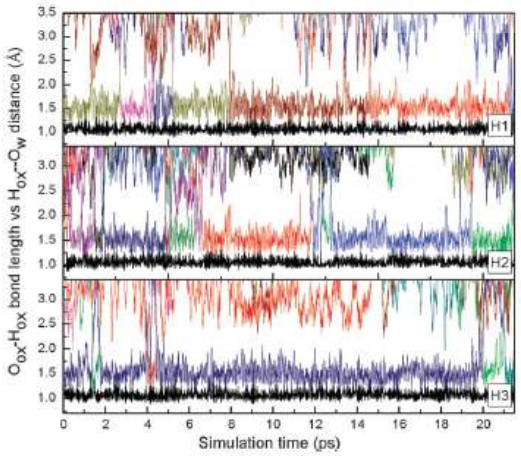

Fig. 6 Time dependence of intramolecular O_{ox}–H_{ox} bond lengths (black line) and $H_{ox}\cdots O_w$ distances, as obtained from the B3LYP/MM MD simulation.

bonds are also plotted in order to provide information on the frequency of the $H_5O_2^+$ formation. In aqueous solution, it is well-established that the $H_9O_4^+$ and $H_5O_2^+$ complexes are the most important species, and that the PT process is an extremely fast dynamics process (*e.g.*, the interconversion period between the $H_9O_4^+$ and $H_5O_2^+$ structures is found to be less than 100 fs[3]), with the $H_5O_2^+$ form being the most important transition state complex. On the basis of both B3LYP/MM and MP2/MM simulations, the $H_9O_4^+$ complex is apparently found to be the most prevalent species in aqueous solution, followed by smaller proportions of $H_5O_2^+$ and $H_7O_3^+$ (*i.e.*, a complex in which two of the $O_{ox}\cdots O_w$ distances of the original $H_9O_4^+$ are $\leq$2.5 Å). In fact, the formation of the $H_5O_2^+$ and $H_7O_3^+$ complexes could be regarded as the fluctuation of the $H_9O_4^+$ structure, *i.e.*, a small shift of the hydrogen atoms of H_3O^+ along their O_{ox}–H_{ox} bonds transiently converts the symmetrical $H_9O_4^+$ complex into either $H_7O_3^+$ or $H_5O_2^+$ complexes, and *vice versa*.

According to Fig. 5 and 6, several water exchange processes were observed during the MP2/MM and B3LYP/MM simulations. The rate of water exchange processes at each of the oxonium hydrogens was evaluated through the mean residence time (MRT) of the water molecules. In this work, the MRT data were calculated using the "direct" method,[49] as the product of the average number of water molecules in the first shell with the duration of the MD simulation, divided by the observed number of exchange events lasting for a given time interval t^*. In general, it has been demonstrated that a t^* value of 0.0 ps is suitable for the estimation of hydrogen bond lifetimes, and a value of 0.5 ps is considered as a good measure for water exchange processes.[49] The calculated MRT data with respect to t^* values of 0.0 and 0.5 ps are summarized in Table 1, together with the corresponding data obtained from the previous HF/MM study[17] and the MRT data for pure water derived by the similar QM/MM scheme.[48,50]

By means of the MP2/MM simulation, the MRT values at each of the oxonium hydrogens for both $t^* = 0.0$ and 0.5 ps are of the same order of magnitude as for pure water.[48] This clearly indicates fast dynamics of water molecules surrounding the H_3O^+ ion. According to the MP2/MM data in Table 1, the slightly observed different MRT values at each of the oxonium hydrogens could be attributed partly to the limitation of the MP2/MM simulation time, as well as to the imbalance of their H_3O^+–water hydrogen bond strengths, *i.e.*, as a consequence of the temporary formation of $H_5O_2^+$ (or $H_7O_3^+$) complexes. As one can see in Table 1, the corresponding MRT data obtained from the previous HF/MM study show good agreement with the present MP2/MM results. This provides information that the neglect of electron correlation effects at the HF level of accuracy appears to have small influence on the dynamics properties of the H_3O^+ hydrate.

In the course of the B3LYP/MM simulation, however, it is found that one nearest-neighbor water molecule spends more than 15 ps long lasting with one hydrogen atom of H_3O^+ (*e.g.*, H3 in Fig. 6). Consequently, this leads to an extremely slow exchange process of water molecules, *i.e.*, the MRT value on this site is about 3.5 times higher than that of the other hydrogen atoms of H_3O^+. According to the plots of the time dependence of the O_{ox}–H_{ox} bond lengths and

Table 1 Mean residence times of water molecules in the bulk and in the first hydration shell of H_3O^+ hydrogens, as obtained from the HF/MM,[30] B3LYP/MM and MP2/MM MD simulations

			$t^* = 0$ ps		$t^* = 0.5$ ps	
QM/MM Model	CN	t_{sim}	$N_{ex}^{0.0}$	$\tau^{0.0}$	$N_{ex}^{0.5}$	$\tau^{0.5}$
MP2/MM						
H1	1.01	15.8	63	0.25	11	1.45
H2	1.01	15.8	50	0.32	6	2.65
H3	1.01	15.8	54	0.30	8	2.00
Pure H_2O[48]	4.60	5.0	—	0.28	—	2.45
B3LYP/MM						
H1	0.98	21.6	71	0.30	10	2.12
H2	0.97	21.6	123	0.17	11	1.91
H3	0.98	21.6	46	0.46	3	7.08
Pure H_2O[48]	4.20	30.0	—	1.07	—	7.84
HF/MM						
H1[30]	1.0	20.0	65	0.31	8	2.50
H2[30]	1.0	20.0	113	0.18	11	1.82
H3[30]	1.0	20.0	47	0.42	8	2.50
Pure H_2O[48]	4.20	40.0	—	0.33	—	1.51
Pure H_2O[50]	4.60	12.0	292	0.20	31	1.80

$H_{ox}\cdots O_w$ distances in Fig. 6, in particular for the trajectories between 4 and 20 ps, the average $O_{ox}\cdots O_w$ distance with respect to the O_{ox}–$H3_{ox}\cdots O_w$ bond is found to be relatively shorter than the $O_{ox}\cdots O_w$ distances along the O_{ox}–$H1_{ox}\cdots O_w$ and O_{ox}–$H2_{ox}\cdots O_w$ bonds. In addition, there are many situations in which the intramolecular O_{ox}–$H3_{ox}$ and the intermolecular $H3_{ox}\cdots O_w$ distances are equal. This suggests that the symmetric $H_5O_2^+$ structure could be formed frequently in aqueous solution, *i.e.*, the strongest O_{ox}–$H3_{ox}\cdots O_w$ bond in the $H_9O_4^+$ complex can transiently convert back and forth into the $H_5O_2^+$ formation. Under this circumstance, it could be demonstrated that the B3LYP/MM simulation predicts the $H_5O_2^+$ complex which is relatively too stable to represent a transition state complex in the PT process. The artificially slow water exchange processes predicted by the B3LYP method have also been found in the B3LYP/MM simulation of pure water.[48] Recently, it has been demonstrated that the performance of the CP-MD scheme with simple DFT functionals, such as BLYP and PBE, could not provide reasonable properties of the solvent water itself, *i.e.*, predicting a glassy state rather than a liquid at room temperature and up to 400 K.[35,36] In this context, since the interconversion between $H_9O_4^+$ and $H_5O_2^+$ complexes is coupled to hydrogen bond dynamics of water molecules in the second hydration or in the bulk, the B3LYP/MM results clearly indicate the deficiency of the B3LYP method in describing the mechanism of PT in water.

4. Conclusion

The role of electron correlation effects in the structure and dynamics of the hydrated H_3O^+ ion has been investigated by means of combined B3LYP/MM and MP2/MM MD simulations. In comparison to the previously published HF/MM data, the inclusion of electron correlation effects with respect to the B3YLP/MM and MP2/MM simulations results in stronger H_3O^+–water hydrogen bond interactions as well as in a slightly greater compactness of the H_3O^+ hydrate. In terms of the B3LYP/MM simulation, however, the overestimation of the H_3O^+–water hydrogen bond strength is recognizable, which leads to an artificial slow dynamic nature of some first shell water molecules, and thus to a too long-living $H_5O_2^+$ complex. With regard to the reported tendency of the DFT methods to predict too rigid ion solvation complexes, as well as wrong dynamics of the liquid water, it is worth noting that the DFT methods should be used with special caution, especially for the description of such hydrogen bond systems.

Acknowledgements

This work was supported by the Thailand Research Fund (TRF), under the Royal Golden Jubilee PhD Program (Contract Number PHD/0185/2548). A.T. also acknowledges support by the Synchrotron Light Research Institute (SLRI), Nakhon Ratchasima, Thailand.

References

1 B. E. Conway, in *Modern Aspects of Electrochemistry*, Butterworths, London, 1964.
2 P. Kebarle, *Annu. Rev. Phys. Chem.*, 1977, **28**, 445.
3 S. Woutersen and H. J. Bakker, *Phys. Rev. Lett.*, 2006, **96**, 138305.
4 A. Botti, F. Bruni, S. Imberti, M. A. Ricci and A. K. Soper, *J. Mol. Liq.*, 2005, **117**, 77.
5 E. Kochanski, *J. Am. Chem. Soc.*, 1985, **107**, 7869.
6 G. Karlström, *J. Phys. Chem.*, 1988, **92**, 1318.
7 D. Q. Wei and D. R. Salahub, *J. Chem. Phys.*, 1994, **101**, 7633.
8 N. Agmon, *Chem. Phys. Lett.*, 1995, **244**, 456.
9 M. E. Tuckerman, K. Laasonen, M. Sprik and M. Parrinello, *J. Chem. Phys.*, 1995, **103**, 150.
10 M. E. Tuckerman, K. Laasonen, M. Sprik and M. Parrinello, *J. Phys. Chem.*, 1995, **99**, 5749.
11 J. Lobaugh and G. A. Vote, *J. Chem. Phys.*, 1996, **104**, 2056.
12 M. E. Tuckerman, D. Marx, M. L. Klein and M. Parrinello, *Science*, 1997, **275**, 817.
13 R. Vuilleumier and D. Borgis, *J. Mol. Struct.*, 1997, **436**, 555.
14 R. Vuilleumier and D. Borgis, *Chem. Phys. Lett.*, 1998, **284**, 71.
15 R. Vuilleumier and D. Borgis, *J. Phys. Chem. B*, 1998, **102**, 4261.
16 D. E. Sagnella and M. E. Tuckerman, *J. Chem. Phys.*, 1998, **108**, 2073.
17 U. W. Schmitt and G. A. Vote, *J. Phys. Chem. B*, 1998, **102**, 5547.
18 U. W. Schmitt and G. A. Vote, *J. Chem. Phys.*, 1999, **111**, 9361.
19 D. Marx, M. E. Tuckerman, J. G. Hutter and M. Parrinello, *Nature*, 1999, **397**, 601.
20 R. Vuilleumier and D. Borgis, *J. Chem. Phys.*, 1999, **111**, 4251.
21 E. Brodskaya, A. P. Lyubartsev and A. Laaksonen, *J. Phys. Chem. B*, 2002, **106**, 6479.
22 T. J. F. Day, A. V. Soudackov, M. Čuma, U. W. Schmitt and G. A. Vote, *J. Chem. Phys.*, 2002, **117**, 5839.
23 J. Kim, U. W. Schmitt, J. A. Gruetzmacher, G. A. Vote and N. E. Scherer, *J. Chem. Phys.*, 2002, **116**, 737.
24 J. M. Hermida-Ramón and G. Karlström, *J. Mol. Struct.*, 2004, **712**, 167.
25 H. Lapid, N. Agmon, M. K. Petersen and G. A. Voth, *J. Chem. Phys.*, 2005, **122**, 14506.
26 F. Wang and G. A. Vote, *J. Chem. Phys.*, 2005, **122**, 144105.
27 T. James and D. J. Wales, *J. Chem. Phys.*, 2005, **122**, 134306.
28 G. Brancato and M. E. Tuckerman, *J. Chem. Phys.*, 2005, **122**, 224507.
29 G. A. Voth, *Acc. Chem. Res.*, 2006, **39**, 143.
30 P. Intrarathep, A. Tongraar and K. Sagarik, *J. Comput. Chem.*, 2006, **27**, 1723.
31 C. J. D. von Grotthuss, *Ann. Chim. (Paris)*, 1806, **LVIII**, 54.
32 T. C. Berkelbach, H.-S. Lee and M. E. Tuckerman, *Phys. Rev. Lett.*, 2009, **103**, 238302.
33 O. Markovitch and N. Agmon, *J. Phys. Chem. A*, 2007, **111**, 2253.
34 J. X. Grossman, E. Schwegler, E. W. Draeger, F. Gygi and G. Galli, *J. Chem. Phys.*, 2004, **120**, 300.
35 S. Yoo, X. C. Zeng and S. S. Xantheas, *J. Chem. Phys.*, 2009, **130**, 221102.

36 J. Schmidt, J. V. Vondele, I.-F. W. Kuo, D. Sebastiani, J. I. Siepmann, J. Hutter and C. J. Mundy, *J. Phys. Chem. B*, 2009, **113**, 11959.
37 T. Kerdcharoen, K. R. Liedl and B. M. Rode, *Chem. Phys.*, 1996, **211**, 313.
38 B. M. Rode, C. F. Schwenk and A. Tongraar, *J. Mol. Liq.*, 2004, **110**, 105.
39 B. M. Rode, C. F. Schwenk, T. S. Hofer and B. R. Randolf, *Coord. Chem. Rev.*, 2005, **249**, 2993.
40 T. H. Dunning Jr and P. J. Hay, in *Modern Theoretical Chemistry, III*, ed. H. F. Schaefer, Plenum, New York, 1976.
41 M. J. Frisch, G. W. Trucks, H. B. Schlegel, G. E. Scuseria, M. A. Robb, J. R. Cheeseman, J. A. Montgomery, T. Vreven, K. N. Kudin, J. C. Burant, J. M. Millam, S. S. Iyengar, J. Tomasi, V. Barone, B. Mennucci, M. Cossi, G. Scalmani, N. Rega, G. A. Peterson, H. Nakatsuji, M. Hada, M. Ehara, K. Toyota, R. Fukuda, J. Hasegawa, M. Ishida, T. Nakajima, Y. Honda, O. Kitao, H. Nakai, M. Klene, X. Li, J. E. Knox, H. P. Hratchian, J. B. Cross, V. Bakken, C. Adamo, J. Jaramillo, R. Gomperts, R. E. Stratmann, O. Yazyev, A. J. Austin, R. Cammi, C. Pomelli, J. W. Ochterski, P. Y. Ayala, K. Morokuma, G. A. Voth, P. Salvador, J. J. Dannenberg, V. G. Zakrzewski, S. Dapprich, A. D. Daniels, M. C. Strain, O. Farkas, D. K. Malick, A. D. Rabuck, K. Raghavachari, J. B. Foresman, J. V. Ortiz, Q. Cui, A. G. Baboul, S. Clifford, J. Cioslowski, B. B. Stefanov, G. Liu, A. Liashenko, P. Piskorz, I. Komaromi, R. L. Martin, D. J. Fox, T. Keith, M. A. Al-Laham, C. Y. Peng, A. Nanayakkara, M. Challacombe, P. M. W. Gill, B. Johnson, W. Chen, M. W. Wong, C. Gonzalez and J. A. Pople, *GAUSSIAN 03 (Revision D.1)*, Gaussian, Inc., Wallingford, CT, 2005.
42 A. D. Becke, *J. Chem. Phys.*, 1993, **98**, 5648.
43 F. H. Stillinger and A. Rahman, *J. Chem. Phys.*, 1978, **68**, 666.
44 P. Bopp, G. Jancsó and K. Heinzinger, *Chem. Phys. Lett.*, 1983, **98**, 129.
45 B. R. Brooks, R. E. Bruccoleri, B. D. Olafson, D. J. States, S. Swaminathan and M. Karplus, *J. Comput. Chem.*, 1983, **4**, 187.
46 H. J. C. Berendsen, J. P. M. Postma, W. F. van Gunsteren, A. DiNola and J. R. Haak, *J. Phys. Chem.*, 1984, **81**, 3684.
47 D. J. Adams, E. H. Adams and G. J. Hills, *Mol. Phys.*, 1979, **38**, 387.
48 D. Xenides, B. R. Randolf and B. M. Rode, *J. Chem. Phys.*, 2005, **122**, 174506.
49 T. S. Hofer, H. T. Tran, C. F. Schwenk and B. M. Rode, *J. Comput. Chem.*, 2004, **25**, 211.
50 A. Tongraar and B. M. Rode, *Chem. Phys. Lett.*, 2004, **385**, 378.

CURRICULUM VITAE

MR. THANAWAT SOMTUA

Education Background:

2006 B.Sc. Second Class Honor (Chemistry), Ubon Ratchathani University, Ubon Ratchathani, Thailand

2006-2011 Ph.D. (Chemistry), Suranaree University of Technology, Nakhon Ratchasima, Thailand

Experience:

2006-2007 Teaching Assistant, School of Chemistry, Institute of Science, Suranaree University of Technology, Nakhon Ratchasima, Thailand

Grants and Fellowships:

2006-2011 The Royal Golden Jubilee (RGJ) Ph.D. Scholarship from Thailand Research Found (TRF)

2006-2007 SUT Teaching Assistantship